Author:
Landon, Emma N U

Title:
Palaeobiology and Preservation of the Ediacaran Weng'an Biota

PALAEOBIOLOGY AND PRESERVATION OF THE EDIACARAN WENG'AN BIOTA

by

Emma Nkaepe Ulaeto Landon

A dissertation submitted to the University of Bristol in accordance with the requirements for the award of the degree of Doctor of Philosophy in the Faculty of Science

School of Earth Sciences

University of Bristol

March 2021

Word count: 25072

Abstract

The Weng'an site of exceptional preservation from the 609 Ma Doushantuo Formation of South China provides a unique window on marine diversity prior to the emergence of unequivocal animal fossils, as it dates to the period in which animals are estimated to have emerged based on molecular clock analyses. The biota preserves a variety of forms, including putative animal embryos and putative florideophyte algae, however these fossils have proven difficult to interpret and their affinities remain uncertain.

The aims of this thesis were to develop a better understanding of the taphonomy of the various components of the biota and how their taphonomy can elucidate or obscure details of their biology.

I have described a new component of the biota, a spore-producing eukaryote that represents part of a vegetative phase of a developmental cycle, adding to a growing body of evidence that this was a common strategy in Ediacaran acritarchs as a response to the environment in which they lived.

I have undertaken a critical evaluation of the Weng'an algae and their taxonomy and phylogenetic interpretations, and found that several of the algal taxa represent different stages of a single life cycle. Furthermore, the algae of the Weng'an biota are total-group Rhodopyta, and cannot definitively be placed within crown-Florideophyceae, calling into question several molecular divergence time analyses that have used them for calibrations.

Finally, I have evaluated the animal embryo interpretation of the Weng'an embryoids, comparing their taphonomy to that of living embryos and unequivocal fossil embryos with a similar diagenetic history. I found that the differing decay and preservation pathways of embryos at different developmental stages means that an animal interpretation for the Weng'an embryoids cannot be ruled out, despite their preservation being fundamentally different to unequivocal animal embryos in terms of structures preserved.

This thesis adds to evidence that the Weng'an fossils were adapted for variable marine conditions, and shows that those elements of the biota that are widely used as calibrations in molecular divergence time analyses (in particular the embryos and the algae) are used erroneously, as the fossils cannot be definitively placed in the clades whose emergence they are used to date.

Acknowledgements

I would like to thank my supervisors for their constant support and guidance during my PhD: Professor Philip Donoghue for his invaluable support, feedback and encouragement, Professor Zongjun Yin for his help with specimen collection and fieldwork, and Dr John Cunningham, for all his help in the tomography lab and at the beamline.

Additionally I would like to thank Dr Thomas Davies for his help in the tomography lab, and in finding places for me to store my many, many rocks!

I would also like to thank Dr Federica Marone at the TOMCAT beamline of the Swiss Light Source (SLS) at the Paul Scherrer Institute in Switzerland for her technical support and advice during scanning sessions, as well as Dr Kelly Vargas, Dr Martin Rücklin and Dr Duncan Murdock for their help and company during all those beamline night shifts!

Finally, I would like to thank the members of my various D&D groups - I would not have survived this without you! In particular, my thanks go to Ben Griffin for being a wonderful and imaginative DM and providing the Waterdeep crew with an awesome sandbox to play in, and my eternal thanks to those who put up with me as a DM: to Anna Williams, Tom Kettlety, Gareth Coleman and Ellen Macdonald, I am endlessly grateful for your constant friendship and support, and also your boundless enthusiasm for the puzzle filled dungeon crawls I send you on!

Author's Declaration

I declare that the work in this dissertation was carried out in accordance with the requirements of the University's *Regulations and Code of Practice for Research Degree Programmes* and that it has not been submitted for any other academic award. Except where indicated by specific reference in the text, the work is the candidate's own work. Work done in collaboration with, or with the assistance of, others, is indicated as such. Any views expressed in the dissertation are those of the author.

SIGNED: .... DATE: ....

Table of Contents

List of Tables and Illustrative Materials

Chapter 1: Introduction

1.1 Overview

The fossil record was once interpreted as showing a Cambrian origin of animals (Budd, 2013), and it is clear from sites of exceptional preservation such as the Burgess Shale and the Chengjiang biota that the majority of animal phyla had been established by the Early Cambrian. These Cambrian assemblages contain stem and crown members of extant metazoan phyla, as well as sponges, ctenophores, and cnidarians. In addition to body fossils, Cambrian strata also record abundant trace fossil taxa, with complex, branching trails and deep burrows (Jensen 2003), showing the complex behavioural ecology of the organisms that made them. The Precambrian, by contrast, was once considered to have been devoid of life, however a wealth of research has shown that Proterozoic age rocks preserve a wide variety of fossils, particularly in the Late Neoproterozoic.

Most of these fossils are microfossils, but rocks of the Ediacaran Period (terminal Neoproterozoic) preserve a great many macrofossil forms, grouped into three different assemblages: the Avalon-type assemblage, the Ediacara-type assemblage and the Nama-type assemblage. Organisms found in these assemblages include forms such as *Charnia, Dickinsonia* and *Kimberella*, and they bear very little resemblance to the Cambrian biotas that came after them. Their affinities have been difficult to constrain, though *Dickinsonia* has been definitively placed within the Metazoa, as have the frond-like taxa *Charnia* and *Arborea* (Dunn et al 2019; Dunn et al. 2021; Hoekzema et al. 2017). Most of the Ediacaran organisms were sessile, although

9

some (such as the aforementioned *Dickinsonia* and *Kimberella*) were capable of movement. Ediacaran trace fossils are far lower in abundance than Cambrian ones, and are morphologically much simpler, consisting of horizontal, unbranched trails or shallow burrows (Jensen 2003).

Evidence from molecular clocks and biomarker analysis (Love et al. 2009; Budd, 2013) suggests a Cryogenian origin of animals - long before the late Ediacaran. This indirect evidence has been called into question however. Budd and Mann (2020), show that some types of molecular clock systematically overestimate clade ages in studies of large clades (such as bilaterians) and suggest that the size of this effect accounts for the discrepancy between clock estimates and the fossil record. Evidence from biomarker analysis has also come under fire. Nettersheim et al. (2019) show that precursors to biomarkers considered diagnostic of sponges are biosynthesised by members of the Rhizaria (heterotrophic protists such as foraminifera) which have an extensive fossil record that may extend as far back as 740 MA, just prior to the Cryogenian, when these biomarkers first appear in sediments (Nettersheim et al. 2019; Porter et al. 2003).

The Weng'an site of exceptional preservation within the 609 Ma Doushantuo Formation offers an opportunity to clarify this obvious dichotomy between molecular clocks and the fossil record, as animal embryos are claimed to be among the microfossils preserved in the deposit, which is early Ediacaran in age - much older than any of the macrofossil assemblages. If the Weng'an embryo fossils *are* animal embryos, it would support molecular clock estimates of a Cryogenian origin of animals. However, the fossils have proven difficult to interpret and their affinities are the subject of much debate, and so far none of the putative embryos have been found to be

definitively metazoan, calling into question their use as a calibration point for metazoan divergence.

The Kuanchuanpu biota, dating to the Meishucunian Stage of the Early Cambrian, also includes exceptionally preserved embryos, and unlike in Weng'an, these embryos are unequivocally metazoans (Steiner et al. 2004b, 2014; Donoghue et al. 2006; Dong et al. 2013, 2016; Duan et al. 2017). As the Kuanchuanpu Formation and the Doushantuo Formation are part of the same sedimentary sequence, and have a similar diagenetic history, the Kuanchuanpu provides an obvious basis for comparison when considering the affinities of the Weng'an putative embryos, and how their taphonomy affects what we can decipher of their biology.

The putative algae of the Weng'an biota present a different problem – they are a hugely varied polyphyletic group with a long geologic record, but their fossil record is poorly understood, and we lack an interpretative framework for understanding their taphonomy. Consequently, there is a tendency among researchers to place problematic taxa into the so-called 'algal wastebasket', and many putative fossil algae are likely not algae at all. Given the age of these Doushantuo fossils, and the fact that many characteristics considered diagnostic of extant algae are rarely preserved in the fossil record (e.g. pit connections and pit plugs that form in rhodophyte cell walls during cytokinesis, and are unique to that group), there is a distinct possibility that the Doushantuo algae have been misidentified.

This too has implications for molecular clock calibrations - in particular, the Weng'an algae, which are currently considered to be crown group Rhodophytes of the class Florideophyceae, are

often used to calibrate the Bangiales-Florideophyceae divergence (e.g. Yoon et al. 2004, 2006, 2010; Yang et al. 2016; Parfrey et al. 2011; Eme et al. 2014; Sharpe et al. 2015). However, the uncertainty of their possession of certain definitive Florideophyte features calls their florideophyte affinity into question, and thus any molecular divergence time analyses that use them as a calibration on the basis of that affinity.

The overarching aim of this project is to develop a better understanding of the taxonomy, systematics and taphonomy of the various components of the Weng'an biota and how their taphonomy can elucidate the details of their biology or obscure them.

1.2 Introduction to the Doushantuo Formation

The Doushantuo Formation is host to the Weng'an Biota, the embryo and algal components of which are the main focus of this thesis. The formation is one of the most studied Ediacaran stratigraphic units, due to its exceptionally preserved fossil record. There is still a great deal of uncertainty with regards to the formation's depositional and diagenetic history however, owing to the poor exposure of the formation itself, and South China's complex tectonic history (Jiang et al., 2011).

1.2.1 Doushantuo Stratigraphy and Sedimentology

The base of the formation records the termination of the Marinoan Glaciation at 635 Ma (Condon et al. 2005). Various attempts have been made to constrain the age of the Weng'an Biota using Pb-Pb geochronometry, producing ages ranging from 572 ± 36 Ma (Chen Y. et al. 2009) to 599 Ma $\pm$ 4 Ma (Barfod et al. 2002). However, current consensus places the age of the

biota at 609 ± 5 Ma, on the basis of a SIMS zircon U-Pb age for a tuffaceous bed directly above the Doushantuo Upper Phosphorite (unit 4a and 4b in Figure 1.1) (Zhou et al. 2017).

The formation is the oldest phosphorite deposit in S. China, and the single most important, as it accounts for more than two thirds of China's high grade phosphorite reserves (Li, 1986). It is, consequently, of great economic importance, and has been quarried extensively, particularly in the Weng'an area. The Doushantuo Formation is 40-300m thick and outcrops discontinuously over the entire Yangtze block. Complete sequences can generally only be observed in quarries (Figure 1.2) and road cuts (Jiang et al., 2011).

The formation was deposited as part of the Yangtze Craton, on a passive continental margin (Muscente et al., 2015). The depositional environment was a rimmed carbonate shelf (Jiang et al., 2011), which was subject to a series of transgressive-regressive cycles. The phosphorite itself likely formed in deeper waters on the lower shelf, whereas the grainstones were deposited in higher energy, shallower conditions (Jiang et al. 2011). There is also evidence of subaerial exposure (Jiang et al. 2011).

At Weng'an, the Doushantuo Formation is 40-50m thick, and consists of five units – the cap carbonate, the lower phosphorite, the middle dolomite, the upper phosphorite and the upper dolomite (Figure 1.1). The cap carbonate is the most continuous of the units, and is widely used as a marker bed to correlate the Doushantuo Formation across the Yangtze platform. The fossils come from the upper phosphorite (called the Weng'an Member in some publications), which is

divided into two facies – the black facies (4a in Figure 1.1) and the grey facies (4b in Figure 1.1). The grey facies is capped by a karstic surface.

Fossils extracted through acid digestion (using 8–10% acetic acid) are derived solely from the grey facies. The black facies cannot be processed this way, as the fossils are preserved as phosphorite bioclasts within a phosphorite matrix, whereas the grey facies consists of phosphorite bioclasts within a dolomite matrix. Fossils from the black facies have so far only been analysed as 2D slices in thin sections, rather than in both 3D and 2D as is possible with the fossils extracted from the grey facies.
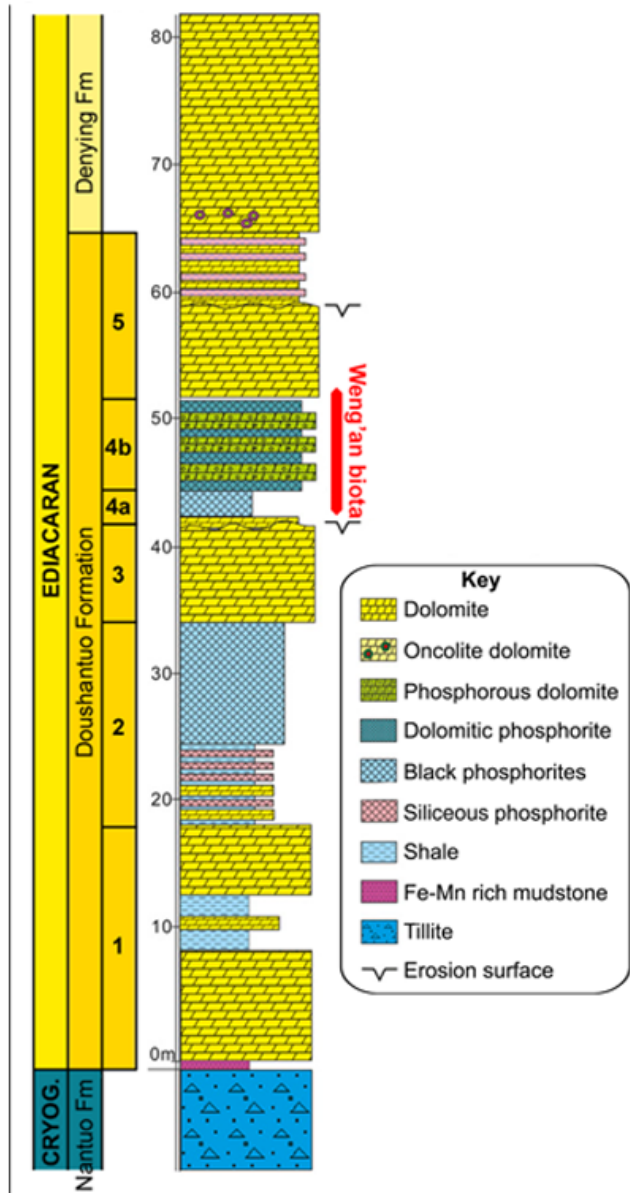
Figure 1.1. Stratigraphic column of the Doushantuo Formation in the Weng'an area, indicating

Units 1-5 of the Doushantuo Formation and the occurrence of the Weng'an Biota. Modified from

Cunningham et al. (2017b).
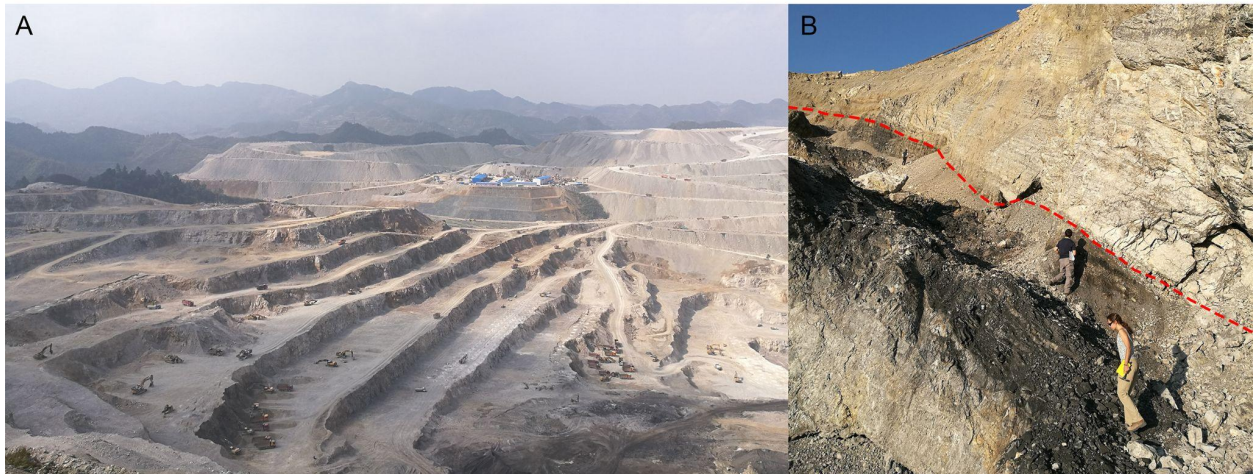
Figure 1.2. Photographs of Nanbao Quarry, in Guizhou Province, South China. This is one of the quarries that the Weng'an fossils are primarily collected from. (A) Overview photograph of the quarry. (B) Outcrop of the Upper Phosphorite, showing the black facies, unit 4a (below the red dotted line) and the grey facies, unit 4b (above the red dotted line).

1.2.2 Doushantuo Taphonomy

The Doushantuo fossils are preserved as bioclasts, and make up the bulk of the clasts that comprise the grainstones of the upper phosphorite (Xiao and Knoll 1999). In parts of both the grey and black facies, the microfossils are so abundant that the grainstones resemble oolites, and a fist sized hand sample yields a few hundred fossils. The bioclasts are not preserved in situ, but were transported post-phosphatisation along with other intraclasts before being cemented to form the upper phosphorite (Xiao and Knoll 1999; Xiao and Knoll 2000), and as a consequence are not representative of a life assemblage.

The Doushantuo fossils preserve both internal and external morphology. The most exceptional specimens preserve subcellular structures, including nuclei in some cases (Yin et al. 2017; Sun et al. 2020). Such specimens are the exception rather than the norm, however. The majority of specimens recovered, while preserving surface features well, are either hollow or contain only void fill that does not replicate original biological structures. The fossils are preserved in two different fluorapatite phases: a cryptocrystalline phase which replicates original biological structure, and a void filling phase with a geoidal texture and relatively large (greater than 1μm) crystals (Cunningham et al. 2012a). This latter phase, a product of diagenesis (changes in a sediment after deposition during the process of lithification), can complicate interpretations of the biology of the microfossils, as it introduces artefacts that have no connection to that biology, but can look deceptively biological (see discussion of *Vernanimalcula* in 1.2.3.6).

1.2.3 Doushantuo Fossils

The first microfossils from the Doushantuo were described as cellularly preserved algae, and assigned to the Rhodophyta (Zhu et al. 1984; Zhu and Wang 1984; Zhao 1986). This was followed by Chen M. et al. (1986), who described the first acanthomorphic acritarch (*Meghystrichosphaeridium wenganensis*) and the first spheroidal microfossil (*Megasphaera inornata*). Fossilised animal embryos were first reported in 1998, by two independent research groups (Li et al., 1998; Xiao et al., 1998) and the debate on their phylogenetic affinities has been ongoing ever since.

The majority of the microfossils recovered from the Doushantuo at Weng'an through acid digestion are spheroidal embryo-like microfossils such as *Megasphaera* (Figure 1.3A-K). The Weng-an biota also includes a variety of acanthomorphic acritarchs (Figure 1.3L) and microalgae (Figure M), as well as a number of branching tube-shaped microfossils (Figure 1.3N). The embryo-like fossils and the acritarchs range in size from 100 to 500 μm. The algae fossils can get as large as 2 mm, as can the tubular fossils, and they are the largest organisms in the biota.

1.2.3.1 Embryoids

The embryo-like fossils are the most hotly debated fossils in the Weng'an biota, a debate mostly centred on the spheroidal microfossil *Megasphaera* (Xiao et al., 2014a). I refer to them here and later in the thesis as embryoids in order to distinguish them from the Cambrian Kuanchuanpu embryo fossils (which are unequivocally embryos, unlike the Weng'an embryoids) discussed later in section 1.3 of this chapter, and in chapter 4 of the thesis.

Megasphaera

There are two species of *Megasphaera*, *Megasphaera inornata* (Figure 1.3A) and *M. ornata*, the former consisting of one cell enclosed in a smooth envelope (Li et al., 1998) and the latter consisting of one cell enclosed in an ornamented envelope (Xiao and Knoll, 2000). *Megasphaera* underwent palintomy (a process by which a parental cell undergoes repeated cell divisions without any overall size increase) to generate morphotypes previously described as *Parapandorina* (Figure 1.3B) and *Megaclonophycus* (Figure 1.3C; Xiao and Knoll, 2000). The current consensus is that *Megasphaera* is the embryo of a multicellular eukaryote (Xiao et al. 2014a). It has been previously interpreted as a giant sulphur bacteria (Bailey et al., 2007) on the basis of its similarity in size and morphology to the extant giant sulphur bacterium *Thiomargarita*, but this has since been refuted by Cunningham et al. (2012b), who ran a series of decay experiments on *Thiomargarita* and concluded that none of the key structures present in *Megasphaera* were compatible with the features exhibited by *Thiomargarita* as it decays. These structures are compatible with features exhibited by animal embryos as they decay (Raff et al. 2006), however an animal affinity for *Megasphaera* is still difficult to ascertain. The *Megaclonophycus*-stage embryoids show no evidence of blastulation (the process by which an embryo develops into a blastula - a hollow sphere of cells known as blastomeres that surround a fluid-filled cavity known as the blastocoel) or of gastrulation (an early phase in the embryonic development of most animals in which the single layered blastula is reorganised into a multilayered structure called a gastrula), both processes that occur in modern animal embryos with >100 cells, and *Megaclonophycus* contains hundreds to thousands of cells (Hagadorn et al. 2006).

Tianzhushania

The embryoid *Tianzhushania* (Figure 1.3D) was originally described as an acanthomorphic acritarch (Yin and Li, 1978). However, it is multicellular, and contains a cleavage sequence similar to *Megaspahera* (Yin et al. 2007), and has consequently been reinterpreted as a diapause egg cyst (Yin et al. 2007). It has been suggested that *Tianzhushania* should be synonymised with *Megasphaera* (Yin et al. 2003, 2004), but the two taxa are very different in terms of their envelope ornamentation, and are still considered separate (Xiao et al. 2014b).

Helicoforamina

This embryoid has a similar cleavage sequence to *Megasphaera* and *Tianzhushania*, developing through one-, four-, and eight-cell stages to stages with hundreds of cells (Yin et al. 2020). It differs in the ornamentation of its envelope, which consists of a dextrally spiralling helical groove (Figure 1.3E). It is interpreted as a developmental stage of a total group holozoan (Yin et al. 2020), as the cellular structures it preserves are not enough to state whether it is metazoan or non-metazoan.

Spiralicellula

This embryoid has a similar developmental sequence to *Megasphaera,* undergoing palintomic cell division, but is distinct in that its internal bodies are coiled helicospirally (Figure 1.3F; Huldtgren et al. 2011). This spiral shape is incompatible with a metazoan interpretation, and *Spiralicellula* has been assigned to the non-metazoan Holozoa (Huldtgren et al. 2011).

Caveasphaera

Caveasphaera (Figure 1.3G) is considered to fall within total group Holozoa (Yin et al. 2019), and is characterised by internal ridges that form a spherical body, either a hollow cage or a solid sphere, enclosed by a smooth envelope. These differing internal morphologies reflect different developmental stages, with the hollow cage representing the early stage, which then develops into the larger solid stage, suggesting it underwent a process similar to gastrulation (Yin et al. 2019). As with *Helicoforamina,* it has yet to be determined whether *Caveasphaera* is a metazoan or not (Yin et al. 2019; Yin et al. 2020).

'Polar-lobe' embryoids

Some Weng'an embryoids have been described as showing evidence of polar lobes, an extrusion of cytoplasm formed immediately before the first cleavage in some annelids and molluscs (Figure 1.3H-I; Chen J. et al. 2006; Yin et al. 2013). The evidence for this interpretation rests on the presence of connection necks (which connect the polar lobe cytoplasm to the nucleated cytoplasm of the cell from which it formed) between the putative polar lobes and the blastomeres. However, subsequent studies have shown that this is likely both a taphonomic artefact and a diagenetic one and is not indicative of a bilaterian affinity, as decay often makes cell boundaries indistinct, and diagenetic cements coalescing neighbouring cells can result in structures similar to a connection neck (Cunningham et al. 2012a, 2017b). The mineralisation of the putative connection necks shows a geometry typical of diagenetic crusts (Figure 1.3I; figure 1 in Bengtson and Budd 2004).

Teloblastic embryoids

Chen J. et al. (2009a) reported embryoid fossils that showed evidence of several modern embryonic features (Figure 1.3J), including macromeres and micromeres (large and small blastomeres, respectively, that are formed by unequal cell division during the early embryonic development of many animals, such as molluscs). However, as with the 'polar-lobe' embryos, these features are taphonomic artefacts, and could equally be interpreted as belonging to a continuum of cell sizes (Cunningham et al. 2012a, 2017b). In specimens described as showing duet cleavage (in which the embryo produces two primary macromeres, the first daughters of which are orthogonally arranged pairs of micromeres), there is very little difference in size between the proposed macromeres and micromeres (Figure 1.3J).

Black facies embryoids

A number of embryoids are known only from thin sections of black facies material, and have variously been described as cnidarian embryos (Chen J. et al. 2000, 2002) and gastrula-stage embryos of bilaterians (Figure 1.3K; Chen J. et al. 2000). However, the biological features on which these assignations depend are considered misinterpretations of diagenetic artefacts, and it is more likely that these black facies embryos are deformed cysts (Cunningham et al. 2017b; Xiao et al. 2014a).

1.2.3.2 Acritarchs

Acanthomorphic acritarchs (Figure 1.3L) are abundant in the Weng'an biota with over 40 distinct species (Xiao et al. 2014b). Several of the Weng'an acanthomorphic taxa are multicellular, e.g. *Tianzhushania*, which may represent animal diapause eggs (Yin et al., 2007). The acritarchs have

been widely studied both in thin section and in 3D, and the assemblage has significant taxonomic overlap with Ediacaran successions in Australia and Siberia, allowing a possible biostratigraphic correlation of the lower-middle Ediacaran between those locations and S. China (Xiao et al. 2014b).

1.2.3.3 Multicellular algae

The algae from the Weng'an biota are currently considered some of the earliest florideophyte red algae (Xiao et al., 2004; Xiao et al., 2014a). Six genera are currently recognised: *Thallophyca, Paramecia, Wengania, Thallophycoides, Gremiphyca* and *Archaeophycus. Thallophyca* (Figure 1.3M) and *Paramecia* possess pseudoparenchyma, cortex-medulla differentiation and specialised reproductive structures, and have been compared to corallinalean florideophytes (Xiao et al., 2014a). *Archaeophycus* has been tentatively assigned to the bangiophyceae, on the basis of its tetrad cell packets that resemble the carposporangia of the extant bangiophyte *Porphyra*.

1.2.3.4 Putative lichen

Yuan et al. (2005) described three specimens of lichen-like fossils, consisting of coccoidal cell clusters interpreted as either cyanobacteria or algae, and thin filaments interpreted as fungal hyphae (Figure 1.3N). Yuan et al. (2005) noted that the coccoidal cells are very similar histologically to the co-occuring alga *Thallophyca*, differing only in the presence of the putative fungal hyphae. The hyphae are not distributed evenly throughout the specimens, which has called into question the validity of the lichen interpretation - Lücking and Nelsen (2018) consider it more likely that the filaments represent saprophytic or parasitic fungi, rather than a symbiont.

The specimens are only known from thin section, and consequently the three-dimensional structure of the putative algal-fungal association cannot be reconstructed.

1.2.3.5 Tubular microfossils

Five species of tubular microfossils have been recognised from the Weng'an biota: *Ramitubus increscens, R. decrescens, Sinocyclocyclicus guizhouensis* (Figure 1.3O)*, Quadratitubus orbigoniatus*, and *Crassitubus costatus* (Xiao et al., 2014a). They have been interpreted as stem cnidarians on the basis of their tubular morphology and their closely spaced cross walls (Li et al., 1997; Liu et al., 2008; Xiao et al., 2000), however subsequent studies have shown that none of these taxa were biomineralised (Cunningham et al. 2015; Sun et al. 2019), and their cross walls only superficially resemble the tabulae of tabulate corals (Cunningham et al. 2015). *Sinocyclocyclicus, Quadratitubus and Crassitubus* are more likely cyanobacteria, on the basis of their blunt apical terminations, smooth enveloping sheath, and their alternating complete and incomplete cross walls, suggestive of a pattern of intercalary growth via binary cell division (Sun et al. 2019). *Ramitubus* differs from the other tubular taxa in that it exhibits dichotomous branching and growth by terminal addition, neither of which are compatible with a cyanobacterial interpretation, but are compatible with an algal interpretation (Cunningham et al. 2015; Sun et al. 2019).

1.2.3.6 Putative adult forms

Vernanimalcula

First described by Chen J. et al. in 2004, *Vernanimalcula guizhouena* (Figure 1.3P) was interpreted as a bilaterian animal - the oldest putative bilaterian, in fact. However, structures that

are key to *Vernanimalcula's* bilaterian affinity have since been revealed as diagenetic artefacts that do not replicate biological tissues in any way (Bengtson and Budd, 2004; Cunningham et al. 2012a; Bengtson et al. 2012). In particular, structures that Chen J. et al. (2004) interpret as layered tissues exhibit a morphology characteristic of multiple generations of void filling diagenetic mineralisation (Bengtson and Budd, 2004; Bengtson et al. 2012), and putative cell boundaries within these layers are instead cracks in the diagenetic crust. Notably, these cracks often propagate across the boundaries between layers, which is not compatible with a cell boundary interpretation (Bengtson and Budd 2004; Bengtson et al. 2012). Additionally, Bengston et al. (2012) show that Weng'an acritarchs and embryoids can exhibit *Vernanimalcula*-like morphology when thin sectioned, depending on orientation (figure 4 in Bengston et al. 2012), suggesting that specimens attributed to *Vernanimalcula* are instead acritarchs or cysts that are heavily decayed and overprinted with successive phases of diagenetic cement (Bengtson and Budd, 2004; Cunningham et al. 2012a; Bengtson et al. 2012).

Eocyathispongia

Described by Yin et al. in 2015, *Eocyathispongia qiania* (Figure 1.3Q) is the only fossil in the Weng'an biota to display features that could be described as poriferan. It consists of a tubular form which wraps around itself and possesses orifices for inflow and outflow of water, and is densely covered with a layer of cells that resemble sponge pinacocytes (flattened cells that comprise the outer surface of a sponge). However, it lacks certain sponge apomorphies, namely pores and spicules (Cunningham et al. 2017b). It is known from only one specimen, and so far no others have been found.
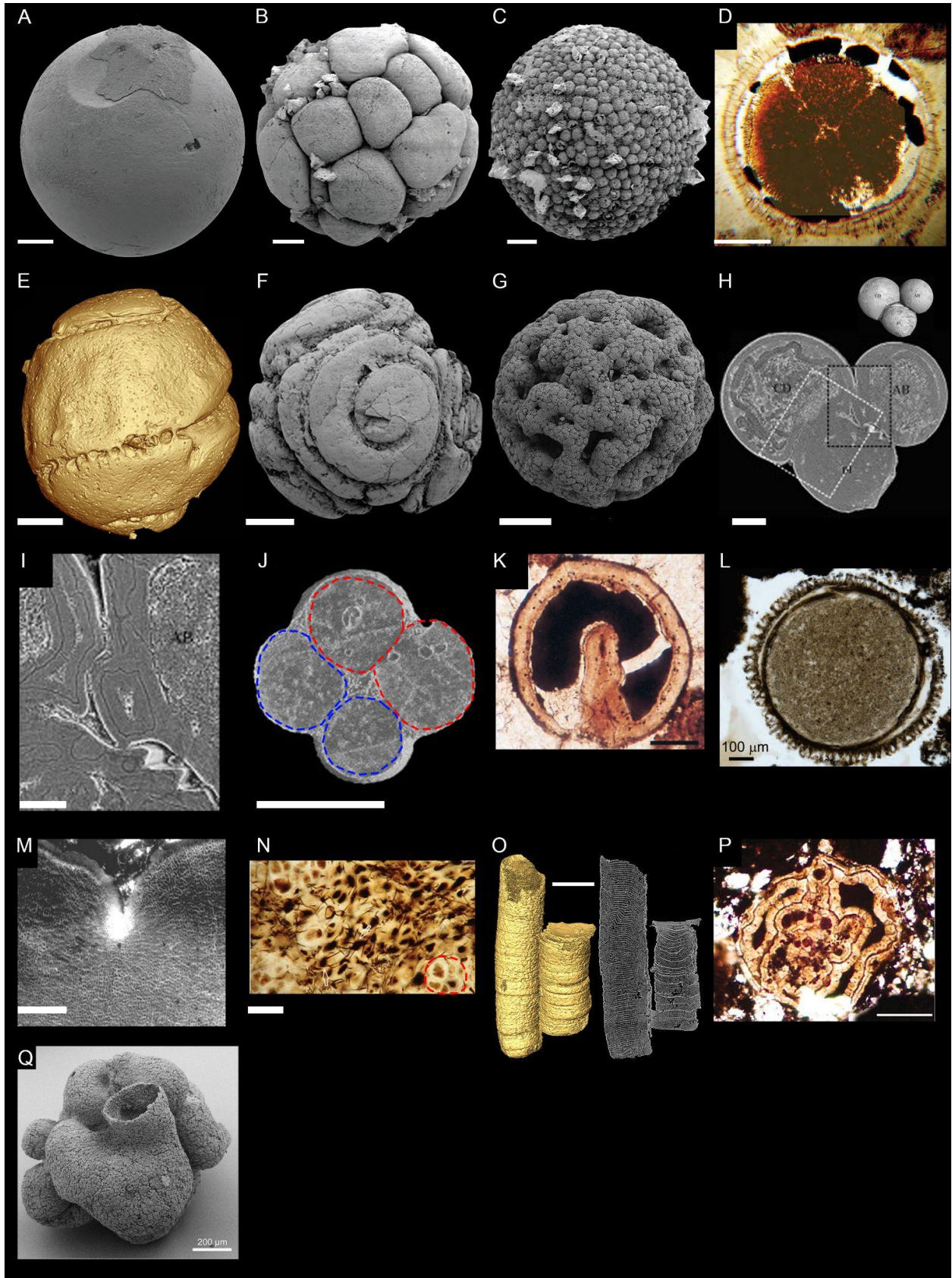
Figure 1.3. Fossils of the Weng'an Biota. (A) *Megasphaera.* Image from Xiao et al. 2014a. Scale bar is 100 μm. (B) *Parapandorina.* Image from Xiao et al. 2014a. Scale bar is 100 μm. (C) *Megaclonophycus.* Image from Xiao et al. 2014a. Scale bar is 100 μm. (D) *Tianzhushania spinosa,* containing an eight-cell embryoid. Image from Yin et al. 2007. Scale bar is 163 μm. (E) *Helicoforamina.* Image from Yin et al. 2020. Scale bar is 140 μm. (F) *Spiralicellula.* Image from Yin et al. 2020. Scale bar is 190 μm. (G) *Caveasphaera.* Image from Yin et al. 2019. Scale bar is 95 μm. (H-I) "Polar lobe embryo". Images from Yin et al. 2013. (I) is a virtual slice through the embryo (3D morphology shown on top right), (I) is a magnification of the area outlined with a black dashed rectangle in (H). Abbreviations: pl = polar lobe, AB = AB blastomere, CD = CD blastomere. Scale bar is 100 μm for (H) and 45 μm for (I). (J) "Teloblastic embryo" showing putative macromeres (red dashed lines) and micromeres (blue dashed lines). Image from Chen J. et al. 2009a. Scale bar is 500 μm. (K) Black facies embryoid. Image from Chen J. et al. (2000). Scale bar is 50 μm. (L) *Asterocapsoides robustus.* Image from Xiao et al. 2014b. Scale bar is 100 μm. (M) *Thallophyca corrugata.* Image from Xiao et al. 2004. Scale bar is 100 μm. (N) Unnamed lichen showing algal/cyanobacterial cells (red dashed outline) and associated dark filaments. Arrows indicate terminal structures connected to multiple filaments. Image from Yuan et al. (2005). Scale bar is 20 μm. (O) *Sinocyclocyclicus.* On the left is a surface render showing external morphology, on the right is an orthoslice showing the internal morphology. Images from Cunningham et al (2017b). Scale bar is 180 μm. (P) *Vernanimalcula.* Image from Chen J. et al. 2004. Scale bar is 40 μm. (Q) *Eocyathispongia.* Image from Yin et al. 2015. Scale bar is 200 μm.

Embryoids	Features				
	Cleavage stages	**Palintomy**	**Gastrula**	**Macromeres and micromeres**	**Polar lobes**
Megasphaera	Present	Present	Absent	Absent	Absent
Tianzhushania	Present	Present	Absent	Absent	Absent
Helicoforamina	Present	Present	Absent	Absent	Absent
Caveasphaera	Absent	Absent	Potentially present	Absent	Absent
Spiralicellula	Present	Present	Absent	Absent	Absent
"Polar-lobe" embryos	Present	Present	Absent	Absent	Disputed
"Teloblastic" embryos	Present	Present	Absent	Disputed	Absent
Black facies embryos	Present	Present	Disputed	Absent	Absent
Algae	**Pseudoparenchyma**		**Cortex-medulla differentiation**	**Specialised reproductive structures**	
Thallophyca	Present		Present	Present	
Paramecia	Present		Present	Present	
Wengania	Present		Absent	Absent	
Gremiphyca	Present		Absent	Absent	
Thallophycoides	Present		Absent	Absent	
Archaeophycus	Present		Absent	Present	
Putative lichens	**Algal component**		**Fungal component**		
Unnamed taxon	Present		Present; unclear if symbiotic, saprophytic or parasitic		
Tubular microfossils	**Cross walls**	**Smooth sheath**	**Intercalary growth**	**Dichotomous branching**	**Growth by terminal addition**
Ramitubus	Present	Absent	Absent	Present	Present
Sinocyclocyclicus	Present	Present	Present	Absent	Absent
Quadratitubus	Present	Present	Present	Absent	Absent
Crassitubus	Present	Present	Present	Absent	Absent
Putative bilaterians	**Layered Tissues**		**Cell boundaries**	**Digestive tract**	
Vernanimalcula	Disputed		Disputed	Disputed	

Putative sponges	Pinacocytes	Spicules	Pores
Eocyathispongia	Potentially present	Absent	Absent

Table 1.1. Summary of the taxa present in the Weng'an biota and their diagnostic features.

Features listed as 'disputed' indicates these are argued to be diagenetic artefacts.

1.3 Introduction to the Kuanchuanpu Formation

The Kuanchuanpu Formation contains the Kuanchuanpu Biota, which contains exceptionally preserved cnidarian embryo fossils. The Kuanchuanpu embryos are preserved as phosphatic bioclasts, similarly to the Weng'an putative embryos. The Kuanchuanpu Formation and the Doushantuo Formation are part of the same sedimentary sequence and have a similar diagenetic history, providing a basis for comparative taphonomy between the Weng'an putative embryos and the Kuanchuanpu embryos when trying to constrain the Weng'an embryos' affinity.

1.3.1 Kuanchuanpu Stratigraphy and Sedimentology

The Kuanchuanpu Formation is approximately 55m thick at its most complete section (near Kuanchuanpu in Ningqiang County, Southwest Shaanxi Province), and outcrops in the northernmost part of the Yangtze Platform (Steiner et al. 2004a; 2014). The Formation was deposited as part of a shallow carbonate shelf during the Meishucunian Stage (dated to 535 Ma by Zhu et al. 2009) of the Early Cambrian (Steiner et al. 2014), and disconformably overlies the Neoproterozoic Dengying Formation (Steiner et al. 2004a) which, in turn, overlies the Doushantuo Formation.

The formation consists mainly of limestones and phosphatic limestones with thick interlayers of cherts and some shales, with the uppermost 10m consisting of clastic limestones, with breccia beds and conglomerates (Figure 1.4; Steiner et al. 2004a). Most of the embryo fossils come from the Shizonggou Section, a 15m thick horizon approximately 35m above the Dengying (Figure 1.4; Steiner et al. 2004a).
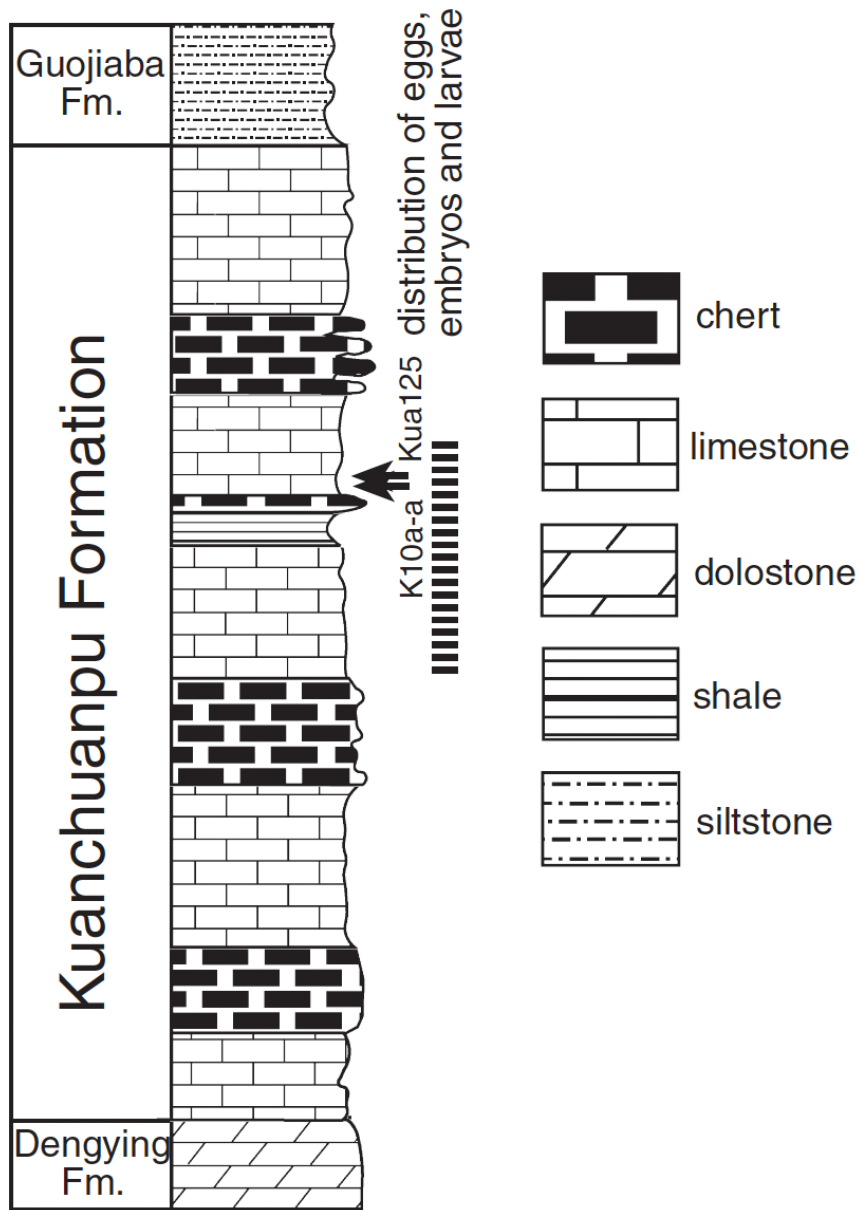
Figure 1.4. Stratigraphic column of the Shizhonggou Section of the Kuanchuanpu Formation. Stippled pattern and arrows indicate the distribution of fossils within the section. Modified from Steiner et al. (2014).

1.3.2 Kuanchuanpu Taphonomy

The Kuanchuanpu fossils occur as phosphatic bioclasts within phosphatic limestone, having been transported post-phosphatisation and deposited to make up the Kuanchuanpu phosphorites (Bottjer et al. 2020). As with the Doushantuo fossils, they have been size sorted, and do not represent a life assemblage.

The Kuanchuanpu fossils generally only preserve external morphology, though some exceptions with internal morphology preserved do exist (Dong et al. 2013; 2016). The fossils are phosphatized, and generally preserved in three distinct mineral phases. The first is void filling, with large, blocky crystals 5-10μm across. The second is a smaller square-shaped phase which surrounds the void fill, and in the embryos aligns along the blastomere edges. The final phase consists of small crystals (less than 2μm across) which are located along putative cell boundaries, between the bands of square-shaped crystals.

1.3.3 Kuanchuanpu Fossils

The Kuanchuanpu Formation preserves a variety of embryo, egg and larval microfossils, as well as a wide array of small shelly fossils (SSFs). The SSF assemblages have been used to divide the formation into a series of biostratigraphic zones, and the embryo microfossils occur in the *Anabarites trisulcatus - Protohertzina anabarica* zone - the oldest zone in the Kuanchuanpu, dated to 537-532 Ma (Duan et al. 2017; Steiner et al. 2004a).

1.3.3.1 Embryos

The embryos were first identified as such by Bengtson and Yue (1997). There are several species of embryo within the biota, all assigned to cnidaria, which include *Olivooides multisulcatus* (Qian, 1977), *O. mirabilis* (Yue in Xing et al. 1984), *Quadrapyrgites quadratacris* (Li, 1984), *Sinaster petalon* (Wang et al. 2017), *Hanagyroia orientalis* (Wang et al. 2020), *Qinscyphus necopinus* (juvenile first described by Liu et al. 2017; embryo first described by Shao et al. 2018) and *Pseudooides prima* (Qian, 1977). The biota also preserves a great many cleavage embryos associated with both *Olivooides* and *Pseudooides*, as well as a number of unnamed taxa (Han et al. 2013, 2016; Xian et al. 2019). Unlike in the Doushantuo, the Kuanchuanpu preserves nearly complete developmental sequences of both *Olivooides* and *Pseudooides*, from late embryonic stages to hatched larvae, and several ontogenetic stages of those larvae (Yue and Bengtson, 1999; Dong et al. 2013; Duan et al. 2017; Steiner et al. 2004b, 2014).

1.3.3.2 Other fossils

The biota also includes a number of meiofaunal adult organisms, including *Saccorhytus,* a putative deuterostome (Han et al. 2017), *Eopriapulites*, a priapulid-like scalidophoran (Liu et al. 2014) and *Eokinorhyncus*, an armoured kinorhynch-like scalidophoran (Zhang et al. 2015).

1.4 Thesis Outline

Despite the sizeable body of previous work, the affinities of the Doushantuo fossils are still very uncertain – because many of the putative animal fossils are preserved only as embryos, and we have no constraint on the nature of the organisms they would eventually have developed into

(Cunningham et al. 2017b). The Weng'an algae are similarly problematic, being known exclusively based on histology, with little reference to their broader anatomy, and only one of the Weng'an algal taxa is known definitively from three-dimensional material. As well as this, many of the features that are diagnostic of red algae (such as pit connections and pit plugs) are only rarely preserved in the fossil record. There is evidence that pit plugs can be preserved in the right conditions (e.g. *Rafatazmia,* first described by Bengtson et al. (2017)) but the Weng'an algae do not show evidence of possessing such features. The diagnostic features that they do potentially show (such as reproductive structures known as carposporangia (Xiao et al. 2004) which are unique to the florideophyceae), are difficult to interpret.

In this thesis I explore the taphonomy and affinities of these and other components of the Weng'an Biota, outlined below.

1.4.1 Chapter Summaries

Chapter 2: Cellular preservation of excysting developmental stages of new eukaryotes from the early Ediacaran Weng'an Biota

A description of a new taxon from the Doushantuo formation, an enigmatic Doushantuo acritarch that produced spores. The aim of this chapter was to describe this fossil and determine what it may have been and what it can tell us about the nature of the environment in which it lived. This was published in Paleoworld in December 2019.

Chapter 3: Systematics, developmental biology and phylogenetic significance of red algae (Rhodophyta) from the Ediacaran Weng'an Biota

An investigation of the diversity and taxonomy of Weng'an fossils currently attributed to algae. These fossils are known almost exclusively from thin section and, consequently only their histology has been given consideration, with little reference to their broader morphology and anatomy. The degree to which morphology and histology covary has been unclear. Consequently, my aim in this chapter was to test whether the existing taxonomic concepts and phylogenetic interpretations of the Weng'an algae are valid when their internal and external anatomy are considered together. I obtained a large suite of algae specimens preserved three dimensionally which encompass the range of morphologies found in the Doushantuo algae and studied them using synchrotron tomography, allowing me to reconcile external morphology, histology and their variation. The results of this suggest that there is continuous variation in both internal and external structure between subsets of existing taxa, reflecting developmental variation. Using these data, I revise the taxonomy of the fossils and test hypotheses on their affinity.

Chapter 4: Experimental and comparative taphonomy of Weng'an embryoids and Kuanchuanpu animal embryos

Here, my aim was to determine whether comparative taphonomy, combined with experimental taphonomy, can elucidate the affinities of the Weng'an embryoid fossils. I use a combination of SRXTM, EPMA and BSE, to study the taphonomy of the animal embryos of the Kuanchuanpu Formation, and compare that with an earlier study of Doushantuo taphonomy using the same methods (Cunningham et al. 2012a). I also compare both the Weng'an embryoids and Kuanchuanpu embryos with decay experiments performed on early-stage and late-stage cleavage embryos of modern animals, to test whether their decay pathways are the same, and whether this can be used to clarify the affinities of the Weng'an embryoids.

Chapter 2: Cellular preservation of excysting developmental stages of new eukaryotes from the early Ediacaran Weng'an Biota

Project design: E. Landon, P. Donoghue, Z. Yin; Materials: E. Landon, Z. Yin; Data collection: E. Landon, W. Sun; Analysis: E. Landon, with contributions from W. Sun, P. Liu, X. Shang; Interpretation: E. Landon with contributions from P. Donoghue, Z. Yin; Writing: E. Landon wrote the text to which P. Donoghue and Z. Yin contributed edits.

2.1 Abstract

The Ediacaran Weng'an Biota provides a unique window on marine diversity during the interval in which the fundamental animal body plans were being established. Here we describe a previously unreported component of the assemblage, millimeter-scale encysted spheres that exhibit a characteristic but simple slit-shaped excystment mechanism (*Sporosphaera guizhouensis* n. gen. n. sp.), reminiscent of acritarchs. The cysts contain a large inner body or numerous small discrete membrane-bounded bodies. It is possible that the inner bodies represent disaggregated cells of a multicellular body, like an embryo, but there is no evidence to support this interpretation and the occurrence of the excystment structure is not readily compatible with an embryo interpretation. Rather, we interpret the encysted organisms as multicellular stages

within the lifecycle of otherwise probably unicellular eukaryotes. The developmental mode exhibited by *Sporosphaera*, incorporating a resting stage, implies an adaptation to adverse environmental conditions. This parallels the appearance of Large Ornamented Ediacaran Microfossils (LOEMs) which have been interpreted as diapause stages in the embryology of early animals. *Sporosphaera* is distinct from LOEMs by ornamentation instead of size, which may implicate that not all LOEMs are animal embryos, if any.

2.2 Introduction

The 609 million-year-old Weng'an Biota (Zhou et al., 2017) is among the most exquisite of fossil lagerstätte (Xiao et al., 2014a, Cunningham et al., 2017b), preserving in calcium phosphate the three-dimensional remains of unicellular and multicellular organisms to a subcellular (Hagadorn et al., 2006) and even organelle level of fidelity (Yin et al., 2017). However, the great significance of the exceptionally preserved Weng'an biota is rooted in its temporal context, by providing a unique window to look at marine biodiversity long before the appearance of uncontroversial animal fossils but within the interval of geological time in which the fundamental lineages of bilaterian phyla were estimated to have diverged base on molecular clocks (dos Reis et al., 2015, Cunningham et al., 2017a).

The Weng'an Biota is dominated by millimeter to submillimeter scale embryo-like remains attributed to *Megasphaera*, *Parapandorina*, *Megaclonophycus*, and *Tianzhushania*. They have been the focus of research because of their debated animal affinity (Xiao et al., 1998, Xiao et al., 2007, Hagadorn et al., 2006, Bailey et al., 2007, Chen L. et al., 2014, Zhang and Pratt, 2014, Yin

et al., 2016), leaving the remaining fossils in the Weng'an biota largely understudied. Here we describe a previously unreported component of the Weng'an Biota encompassing millimeter-scale encysted spheres that exhibit a characteristic but simple slit-shaped excystment mechanism, reminiscent of acritarch cysts, with evidence of a multicellular structure. We establish a new genus and species, *Sporosphaera guizhouensis* n. gen. n. sp. based on the specimens presented herein and explore the taphonomy, biology, affinity, evolutionary and environmental implications of these fossils.

2.3 Materials and Methods

The specimens were recovered from the Upper Phosphorites of the Doushantuo Formation in the '54 Quarry', Weng'an County, Guizhou Province, Southwest China (Cunningham et al., 2017b). Rock samples were subjected to dissolution in 8–10% acetic acid, dissolving the calcium carbonate cement and matrix to leave an insoluble residue of phosphates, silicates and pyrite. The residue was washed through a number of sieves to sort it for ease of picking, then allowed to dry before the fossils were picked out of the residue manually under a binocular stereomicroscope. The fossils were sufficiently abundant in the samples that most of the residue consisted of fossils, the majority *Megasphaera, Parapandorina* and *Megaclonophycus*. 37 'cyst with slit' specimens were recovered, of which 21 (chosen randomly) were subjected to microtomography at the TOMCAT (X02DA) beamline of the Swiss Light Source (SLS), Paul Scherrer Institute (Villigen, Switzerland) or the BM5 beamline of the European Synchrotron Radiation Facility (ESRF, Grenoble, France). X-Ray projections were obtained at 1501 or 1800 stepwise increments through a 180° rotation of the specimen, at beam energies ranging from

19–21 KeV, exposure times of 110–1000 milliseconds and using scintillators composed of lutetium, aluminium and garnet. The X-Ray projections were rearranged into dark- and flatfield-corrected sinograms, after which they were reconstructed using a gridding procedure and a highly optimized routine based on the Fourier transform method (Marone et al., 2010). The resulting datasets of reconstructed tomographic slices have a voxel resolution of 0.74 μm (10× objective) and 0.36 μm (20× objective) at SLS, or 0.75 μm (10× objective) at ESRF. The studied specimens are deposited in the Nanjing Institute of Geology and Palaeontology, Chinese Academy of Sciences. Following best practice for digital morphology (Davies et al., 2017), our tomographic datasets and models are available from https://doi.org/10.5523/bris.3sxs2in77ois323881yvhxwa71.

2.4 Results

2.4.1 External morphology

The fossils are all spheroidal, approximately 1 mm in diameter, smooth, unornamented and otherwise featureless apart from a shallow ambital slit that varies between 50–60 μm in depth and 158–445 μm in width, representing half to two-thirds of the circumference at its greatest extent (Fig. 2.1, Fig. 2.2, Fig. 2.3). The radial angle relative to the margins of the slit varies between 7.4° (Fig. 2.1) and 46.7° (Fig. 2.2) in different specimens. The slits with small radial angles look like narrow, arcuate troughs when observed from the surface (Fig. 2.1A-G, K-Q, T, V), while those with broader radial angles are rounded in outline, and the resulting trough does not extend far (no more than 60 μm in depth) with a rounded base (Fig. 2.2A-C, F-H). In some specimens, the original cyst walls are not preserved, or were lost through laboratory processing

(Fig. 2.2A-C, F-H), and so there is no preserved structure at the slit margins. In contrast, the specimen with the broadest slit (Fig. 2.2K-N) preserves the slit margins of the cyst curled inward (Fig. 2.2K, L) and a crescentic mass of small spheres, cemented by a phosphatic matrix, protruding from the slit (Fig. 2.2K-N). A number of these small spheres appear to have been preserved while being released to the external environment (Fig. 2.2L, M). The retention of the crescentic mass of small spheres with this specimen suggests that it may have possessed an outer envelope that has not been preserved, preventing the release of the small spheres.

2.4.2 Internal structure

 Specimens can be attributed to three broad categories of internal preservation. In general, most specimens preserve no discernable biological structure (Fig. 2.3) (this was the case in 15 of the 21 scanned specimens) and most of the interior volume of the fossils is comprised of a granular matrix (grains approximately 2 μm in diameter), permeated with micrometer scale pores and cross-cut by fine cracks (Fig. 2.3A-C), or internally they exhibit anastomosing layers of void-filling linings (e.g., Fig. 2.3D-F). The specimens are principally composed of calcium phosphate, but there is some subtle variation in composition as reflected by differences in contrast and, therefore, X-ray attenuation, which reflects the atomic number of the material. Some voids are filled with a high contrast, low attenuation phase of calcite or dolomite.

More rarely, distinct intracellular structures are preserved that vary in size and number (Figs. 2.1E-H, O-R, T-W, 2 C, H, L, M). A few specimens contain only one large intracellular structure (LIS) (e.g., Fig. 2.2A-J). Some of these are irregular but the most distinct is approximately spherical (Fig. 2.2C-E, H-J; shortest diameter 265.4 μm, longest diameter 290.6 μm). The LIS is

either filled with void-filling cement (Fig. 2.2C-E) or else exhibits a distinct outer fine-grained

mantle and void-filling core (Fig. 2.2H-J). In such circumstances, the rest of the fossil is

comprised of a porous mineral phase in which the texture is dominated by small voids or dark

mineral microspheres, all of approximately the same diameter (~2 μm) (Fig. 2.2I, J). The LIS is

slightly off-center in one specimen (Fig. 2.2H-J), and it is about 30% of the diameter of the

whole specimen. It has a distinct mineralogy, with an outer dense layer, approximately half its

radius (some pores) and an equally distinct bright, low-attenuating core that may be a void-fill

(Fig. 2.2H-J). Another specimen also includes an LIS of approximately the same relative

volume, but it is positioned off-center and is distinguished by more void-filling cement (Fig.

2.2C-E). The surrounding mineral is more compact, with fewer, larger pores associated with

secondary void-filling mineralization (Fig. 2.2D, E).

A number of specimens (Fig. 2.1) preserve numerous (20–60) small spheroidal intracellular

structures (SIS) disseminated discretely throughout their interior, ranging in size from 25 to 121

μm in diameter, with a membrane thickness of 3.9 to 5.3 μm. The SIS membrane itself has a

distinct, homogeneous fabric and X-Ray attenuation profile while the outer mineral matrix is

more variable (Fig. 2.1H-J, R, S, U, W-Y). The SISs are usually at least partially or else

completely filled with a bright (low attenuation) mineral phase that is largely homogeneous and

appears to represent a late void-filling cement (Fig. 2.1R, S, U, W-Y); this interpretation is

supported by the observation that in some specimens, some SISs are empty (Fig. 2.1I, J, S, X).

High resolution imaging reveals the SIS membranes to have been among the first structures

being mineralized since they have been preserved as a dark mineral phase with a much higher

X-Ray attenuation than the matrix (Fig. 2.1I, J, S, X, Y). Many, but not all of the specimens

preserve evidence of a distinct surface layer as a more highly attenuating mineral phase (e.g.,

Fig. 2.3D-F).
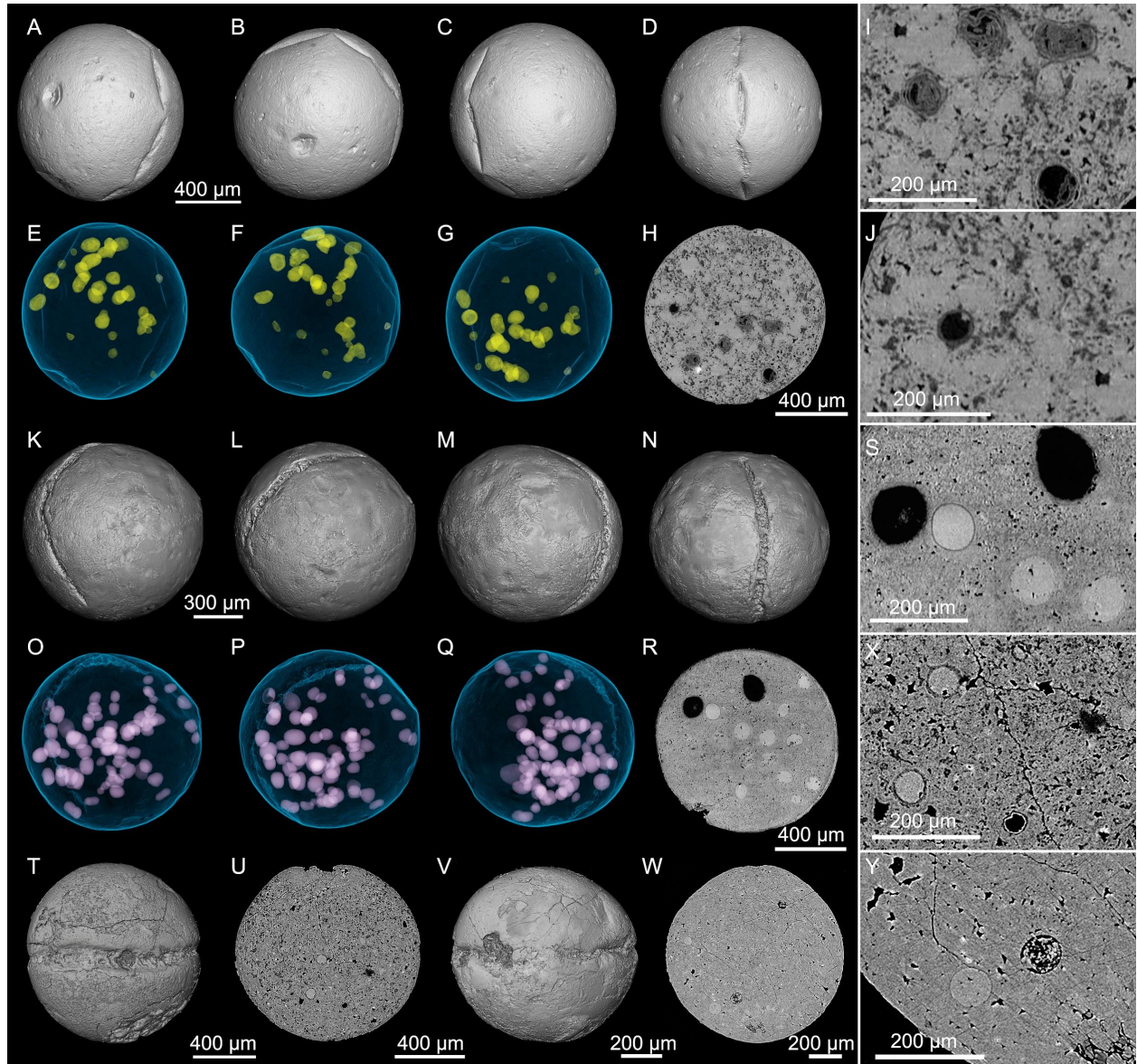
Figure 2.1. Volume renders of *Sporosphaera* fossils with narrow slits. (A–D) 3-D surface renderings of the specimen NIGP 170566 from different view angles, showing the narrow slit. (E–G) Transparent models of (A–C), respectively, showing distribution of small intracellular structures (yellow spheres). (H) An orthoslice of (D), showing inner bodies. (I, J) Close-up views of inner bodies from (H), showing preservation detail. (K–N) 3-D surface renderings of the specimen WA_B3_H03E from different view angles, showing the narrow slit. (O–Q) Transparent models of (K–M), respectively, showing distribution of SISs (pink spheres). (R) An orthoslice of

43

(N). (S) A close-up view of (R), displaying SISs. (T, V) Surface renderings of specimen ZY1216_21 and ZY1709_11. (U, W) Orthoslices of (T, V), respectively. (X, Y) Close-up views of (T, V), respectively, showing the SISs.
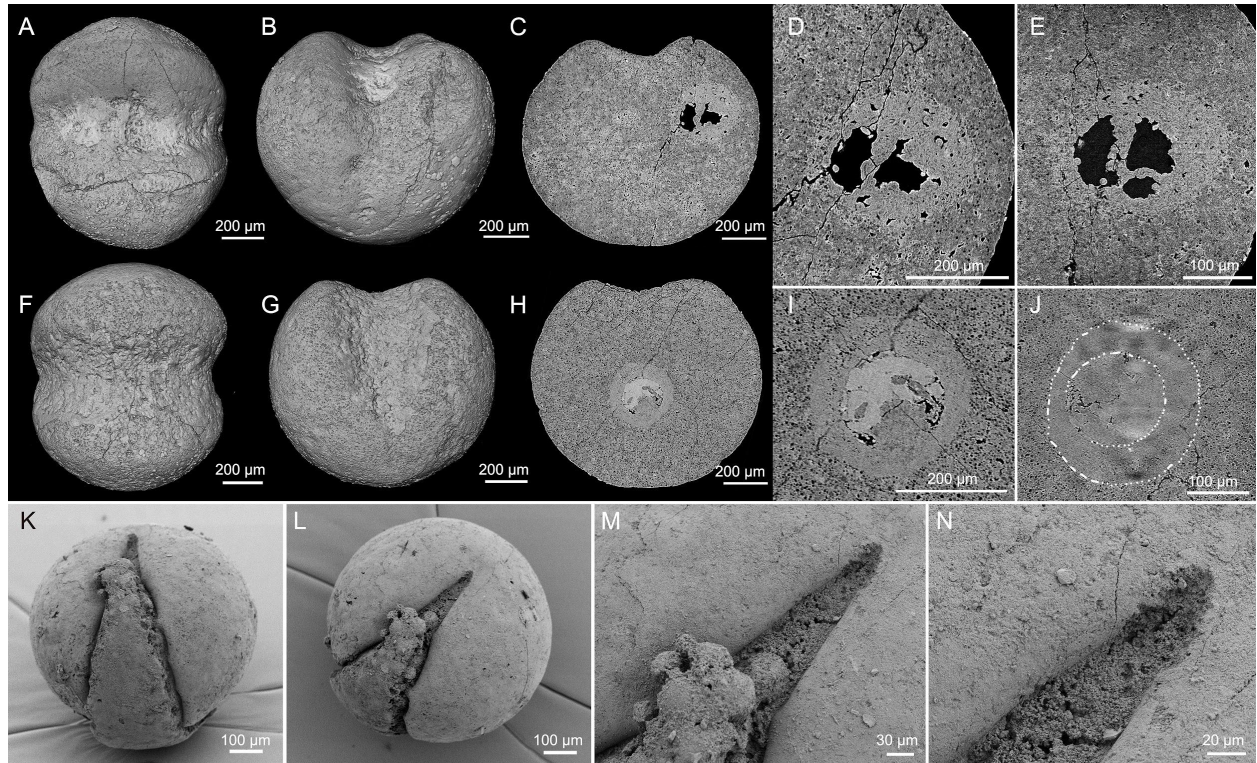
Figure 2.2. Volume renders and SEM images of *Sporosphaera* fossils with broad slits. (A, B) 3-D surface renderings of specimen ZY1216_13. (C) Orthoslice of (B), showing a large intracellular structure. (D, E) Close-up views of the LIS shown in (C) from different depth. (F, G) 3-D surface renderings of specimen ZY1216_20. (H) Orthoslice of (G), showing a large inner body. (I, J) Close-up views of the LIS shown in (H) from different depth; the dotted circles in (J) indicate the boundaries of the mantle and core. (K, L) SEM images of specimen WA_B1_D02. (M, N) Close-up views of the center area in (L), showing details of the SISs and slit margins.
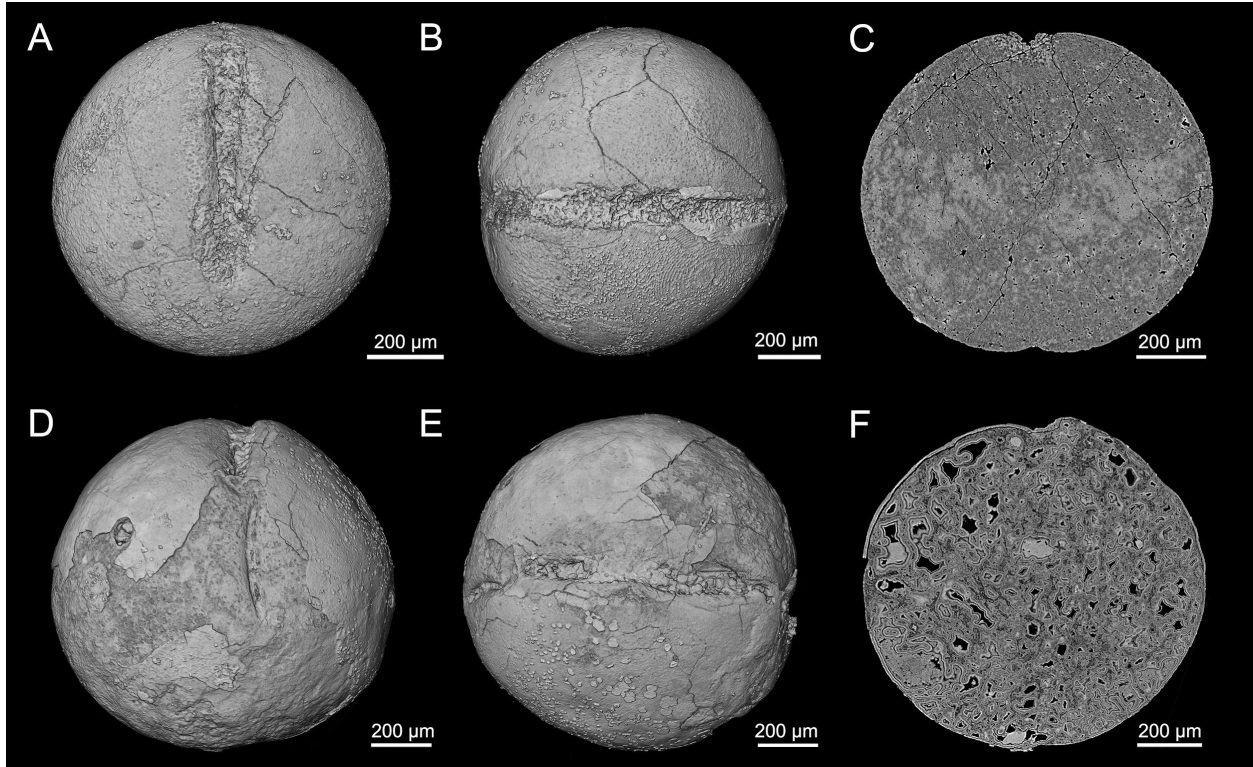
Figure 2.3. Volume renders of *Sporosphaera* specimens without internal biological structures. (A, B) 3-D surface renderings of specimen ZY1709_05. (C) Orthoslices of ZY1709_05, showing internal diagenetic structures. (D, E) 3-D surface renderings of specimen ZY1709_15. (F) Orthoslices of ZY1709_15, showing internal diagenetic structures.

2.5 Discussion

2.5.1 Distinguishing geology from biology

 Differences in the structure of the fossils reflect a combination of geological and biological

factors. Differences in the number of internal structures could reflect differences in the biological

affinity of the fossils, but the consistency in size, shape, and the nature of the slit suggests that

they represent a taxonomically coherent assemblage. The fossils differ principally in the

longitudinal extent and breadth of the slit, which we interpret to reflect developmental

differences. The fossils also differ significantly in terms of their internal structures, which we

interpret principally as a consequence of biostratinomy.

The biostratinomy of the Weng'an Biota has been considered previously (Cunningham et al.,

2012a, Schiffbauer et al., 2012, Yin et al., 2014, Yin et al., 2017), discriminating early phases of

mineralization which preserve biological structure from later void-filling mineralization and late

diagenetic mineral phases. Mineral phases preserving biological structure are invariably

microcrystalline and randomly oriented, reflecting growth on and within an organic template;

later phases unrelated to the original biological structure are usually more coarsely crystalline

and polarized, reflecting centripetal void-filling growth relative to existing mineral substrates

(Cunningham et al., 2012a).

The anastomosing palisade mineral structure of many of the fossils is compatible with

void-filling after most of the original internal biological structure had decayed away. Most of the

fossils otherwise exhibit a structureless and homogeneous interior which reflects mineralization

47

of a structureless, extensively decayed cyst interior (Fig. 2.3). The low contrast, low-attenuation mineral SISs that characterize the mineralization of the interior of some cysts (e.g., Fig. 2.2H-J), is characteristic of mineral-replicated biological structure in other Weng'an fossils (Cunningham et al., 2012a). Their consistent shape and distribution is compatible with preservation of original biological structure, as component cells as in *Megaclonophycus* (Cunningham et al., 2012a), or as small lipid droplets (Hagadorn et al., 2006, Raff et al., 2006). The SISs are invariably enveloped by concentrically arranged layers of a brighter mineral phase (Fig. 2.2I, J; refer to Yin et al., 2017, fig. 1d, h); some of the structures are unmineralized, reflecting non-preservation of structures that remained physically intact while the void-filling process proceeded.

The two classes of larger internal structures exhibit compatible diagenetic records; the membranes of the SISs and the outer layer of the LISs, are both characterized by a dark, low X-Ray attenuation mineral phase, compatible with early mineralization of original unmineralized biological structure, while their lumens are filled with a bright, high low X-Ray attenuation mineral phase, compatible with later void-filling mineralization in Weng'an fossils (Cunningham et al., 2012a). This interpretation is corroborated by the occurrence of empty lumens in subsets of the SISs in some specimens (e.g., Fig. 2.1X, Y). The cyst walls themselves are often characterized by a thin bright, high X-Ray attenuation mineral phase, indicating that the cyst wall itself is preserved through late, void-filling diagenetic mineralization, and that the originally unmineralized cyst wall remained structurally intact while the interior was mineralized, later lost through decay. This mirrors the preservation of cell membranes associated with the embryo-like fossils attributed variably to *Tianzhushania, Megasphaera, Parapandorina*, and *Megaclonophycus* (Cunningham et al., 2012a).

Thus, we discriminate the cyst walls and the large singular and numerous smaller intracellular structures, as original biological structures worthy of interpretation.

2.5.2 Palaeobiology: large, singular intracellular structures

The large, singular intracellular structures of the specimens shown in Fig. 2.2A and F exhibit a strong resemblance, in terms of size and shape, as well as positional and preservational variation, to the 'large intracellular structures' described from the embryo-like fossils *Tianzhushania* and *Spiralicellula*, from the same deposit (Hagadorn et al., 2006, Huldtgren et al., 2011, Schiffbauer et al., 2012, Yin et al., 2017). These structures were originally interpreted as 'nuclei, spindle bundles, or other organelles' (Hagadorn et al., 2006), constrained as nuclei based on consistency of size, shape and topology, subsequently dismissed as degraded cytoplasmic remains (Schiffbauer et al., 2012, Xiao et al., 2012, Xiao et al., 2014a, Pang et al., 2013) based principally on incredulity that nuclei could be fossilized (Pang et al., 2013). The nucleus interpretation of these structures has since been corroborated based on quantitative characterization of the volumetric relationship between the 'large internal structures' and their host cells, across successive rounds of palintomy represented in the fossil assemblage (Yin et al., 2017). The LISs exhibit differences in the predominant mode of preservation in *Sporosphaera* versus *Tianzhushania* and *Spiralicellula*; in the former, the border is characterized by early mineralization of a biological substrate, whereas in the latter, the border is typically characterized by later diagenetic void-filling mineralization (Schiffbauer et al., 2012). However, the LISs exhibit an overlapping range of preservational modes such that in *Sporosphaera* the structure has an irregular border and is characterized by void-filling mineralization (e.g., Fig. 2.2D, E),

49

presumably reflecting preservation of decayed remains; in *Tianzhushania* and *Spiralicellula*, an organic outer membrane can be preserved (Yin et al., 2017). The LISs in *Sporosphaera* also exhibit variation in position within the cyst, mirroring that of the nuclei in *Tianzhushania* and *Spiralicellula* where this might reflect the in vivo position of their nucleus, but also co-varies with the preservational state of the nucleus itself and, therefore, must reflect the role of intracellular degradation. The most poorly preserved LIS in *Sporosphaera* is positioned away from the center of the cyst (Fig. 2.2C).

Based on similarity in preservation, size and position to the large intracellular structures in *Tianzhushania* and *Spiralicellula*, the large, singular intracellular structures in *Sporosphaera* can also be interpreted as preserved nuclei. However, it remains possible that the similarity does not extend beyond size and preservational mode, and they could be the shrunken and decayed remains of a cluster of cells.

2.5.3 Palaeobiology: small intracellular structures

The small intracellular structures in the specimens shown in Fig. 2.1 do not compare well to the larger, singular intracellular structures, either in terms of their preservation or their size, number and position within the cyst. Both the '*Parapandorina*' and '*Megaclonophycus*' stages of *Tianzhushania* preserve structures that are comparable to the SISs; these structures are interpreted as lipid vesicles or yolk granules in '*Parapandorina*' stages (Hagadorn et al., 2006, Cunningham et al., 2012a), and as the component cells in '*Megaclonophycus*' stages (Cunningham et al., 2012a). In both cases, the structures are far more numerous and, consequently, densely packed than are the SISs in *Sporosphaera*. The style of preservation

exhibited by the SISs in *Sporosphaera* is most comparable to that seen in at least some specimens of '*Megaclonophycus*' stages (e.g., Cunningham et al., 2012a), where the membrane is preserved by dark, low attenuation dense mineral phase, indicative of early mineralization, replicating original biological structure. This likely reflects simply that the membranes have a similar preservational style in *Sporosphaera* and '*Megaclonophycus*' stages of *Tianzhushania*, providing support for the interpretation of the SISs in *Sporosphaera* as component cells; it is difficult to conceive a credible alternative biological interpretation.

2.5.4 Development

 The SISs of *Sporosphaera* look very similar to the small cells of '*Megaclonophycus*' stages of *Tianzhushania*. Both *Sporosphaera* and *Tianzhushania* are recovered from the same deposit and share similar morphology and size. These superficial similarities between them may lead to an argument that they represent different development stages of the same taxon or several closely related taxa. However, it is difficult to reconcile *Sporosphaera* with the development pattern of the *Megasphaera–Parapandorina–Megaclonophycus* complex (or *Tianzhushania* complex), because no slit or similar structures have been observed in any *Tianzhushania* specimens, and no evidence indicates that *Sporosphaera* possesses an ornamented envelope similar to that of *Tianzhushania*. Following the interpretation of the SISs in *Sporosphaera* as cells, they might either represent individuals in an essentially unicellular organism, or else the disaggregated cells of a multicellular stage in the lifecycle of an otherwise unicellular or multicellular organism. Diverse unicellular eukaryotes exhibit a multicellular stage in otherwise unicellular organisms, including propagules of mesomycetozoans, sporangia of slime molds, and green algae. Alternatively, taphonomy experiments have shown that multicellular embryos of multicellular

organisms can disaggregate to yield loose assemblages of individual cells (Raff et al., 2006). The comparatively small number of SISs in any one *Sporosphaera* and, critically, their comparatively small collective volume relative to that of the host cyst, speaks against their interpretation as the disaggregated components of a multicellular embryo. The slit in *Sporosphaera* is not incompatible with an embryo-interpretation; for example, animals that mechanically escape their fertilization envelope often leave via a simple slit-shaped rupture. However, this is a feature of embryos comprised of hundreds of cells; animal embryos comprised of small numbers of cells tend to maintain cell adhesion post mortem (Raff et al., 2006) and in most other eukaryotes that have an embryonic stage, the component cells aggregate as a consequence of incomplete cytoplasmic division (Green et al., 1981, Rensing, 2016, Cunningham et al., 2017b), a feature also seen in sponges (Degnan et al., 2015). Neither is seen in *Sporosphaera* and there is no evidence that the cells are ever clustered. Thus, we conclude that these multicelled stages of *Sporosphaera* do not represent embryos but, rather, a stage in the life cycle of component individual unicellular organisms.

Obviously, the extent of the slit, in terms of its width, is not correlated with the number of intracellular structures that the specimen contains, since specimens with both very broad and narrow ambital slits contain numerous small structures. However, the observation that the width and shape of the slit varies from narrow and acute to broad and rounded in different specimens leads to interpretation as polarity in a developmental process, perhaps associated with the progressive maturation and release of the cells. However, it is difficult to rationalize the specimens with single large intracellular structures and broad slits (Fig. 2.2A-J) in this developmental pattern. That said, these two specimens are taphonomic outliers, preserved as

inner casts, suggesting that the original cysts decayed out and the original width of the slits is difficult to constrain. Certainly a pattern of reduction from an encysted mother cell to numerous spores is compatible with vegetative phases in the life cycle of numerous unicellular eukaryotes (Mendoza et al., 2002, Schaap, 2012); no viable interpretation is compatible with a metazoan affinity.

2.5.5 Evolutionary and environmental interpretations

 While the affinity of *Sporosphaera* is difficult to constrain beyond that of a unicellular eukaryote, what can be gleaned of its life cycle, undergoing episodic encystment, is informative on the nature of Ediacaran marine environments. Cohen et al. (2009) have observed that large ornamented Ediacaran 'acritarch' cysts are the recalcitrant remains of metazoan diapause embryos, an adaptation to widespread anoxia of marine bottom conditions. Their argument is based on the observation that such cysts, including *Tianzhushania*, can be demonstrated to have contained embryo-like fossils (Yin et al., 2007), are comparable to modern diapause cysts in terms of their size, shape, ornamentation, and ultrastructure, and disappear from palynological assemblages in association with the oxygenation of continental shelves. It is now known that temporal and spatial variation in the oxygenation of continental shelf bottom waters continued into the Cambrian (Bowyer et al., 2017) and, though the class of large ornamented microfossils interpreted as diapause stages by Cohen et al. (2009) may well be limited to the Ediacaran, this life history strategy continued into the Cambrian (Yin et al., 2018). *Sporosphaera*, too, appears to further nuance this general hypothesis in demonstrating that unornamented equivalents of the large ornamented Ediacaran acritarchs also represent encysted developmental stages, albeit not

of metazoans. This suggests that the prevalence of widespread marine anoxia impacted not only

on the life history strategy of early metazoans, but also on eukaryotes more generally.

Interpretation of LIS	
Nuclei	Interpretation based on similarity of size, shape and structure to previously described preserved nuclei from the Weng'an biota.
Interpretation of SIS	
Lipid granules	Rejected as a viable interpretation as the structures seen in *Sporosphaera* do not compare well to structures previously described as lipid granules in fossils such as *Parapandorina*.
Component cells	Interpretation based on similarity of size, shape and structure to component cells of the fossil *Megaclonophycus*.
Interpretation of overall organism	
Embryo	Rejected as a viable interpretation as the component cells have too small a collective volume relative to the total volume of the fossil and are too loosely packed, with no evidence of having been tightly clustered.
Cyst	Interpretation based on similarity to multicellular spore-producing life phase exhibited by organisms such as mesomycetozoans.

Table 2.1. Summary of the various interpretations of *Sporosphaera* and its components.

The fossils show similarity to features of the *Tianzhushania* complex, but they are clearly distinct (table 2.1 summarises the evidence for different interpretations of their affinity). Some have argued that all of the embryo-like fossils in the Weng'an Biota can effectively be synonymized, but the similarity and differences exhibited by these fossils evidence a greater diversity of embryo-like fossils within the Weng'an Biota. That they are consistently preserved in cysts suggests that they may represent a resting stage within a broader life cycle, perhaps an adaptation for the temporal and spatial variability of Ediacaran shallow marine environments.

2.7 Systematic Palaeontology

Kingdom Eukaryota

Phylum Incertae Sedis

Genus *Sporosphaera* n. gen.

Etymology. The name is derived from Latin and named in reference to the spherical morphology of the fossils, and the ability to produce spores.

Type species. *Sporosphaera guizhouensis* n. gen. n. sp., by monotype.

Diagnosis. As for the type species.

Occurrence. '54 Quarry' in Weng'an County, Guizhou Province, Southwest China; Doushantuo Formation, Upper Phosphorite Member, early Ediacaran.

Sporosphaera guizhouensis n. sp. (Fig. 2.1A-H)

Etymology. Reference to Guizhou Province, where the fossils were found.

Holotype. Reg. no. NIGP 170566 (Fig. 2.1A-H). The holotype has been deposited in the collection of Nanjing Institute of Geology and Palaeontology (NIGP).

Diagnosis. A spheroidal unornamented cyst, 1 mm diameter, with an ambital excystment structure. Contains small, discrete, spheroidal membranes.

Occurrence. '54 Quarry' in Weng'an County, Guizhou Province, Southwest China; Upper Phosphorite Member, Doushantuo Formation, early Ediacaran. More than 500 specimens in total have been discovered.

Description. A spheroidal unornamented cyst, 1 mm diameter, with an ambital excystment structure that varies between 50–60 μm in depth and 158–445 μm in width, representing half to two-thirds of the circumference at its greatest extent. The extreme margins of the excystment structure are rounded in outline and the resulting trough is shallow and has a rounded base. The radial angle relative to the margins of the excystment structure varies between 7.4° and 46.7°.

In general, most of the interior volume of the fossils is comprised of a granular matrix, permeated with micrometer scale pores and cross-cut by fine cracks. Most specimens preserve no discernable biological structure; internally they are homogeneous or exhibit anastomosing layers of void-filling cement. A smaller number of specimens are generally homogeneous but preserve a distinct clotted fabric of high and low attenuating mineral phases at the margins of the slit in the surface of the fossil, and in some this clotted fabric comprises the entire volume of the

specimen. The best-preserved specimens contain between one and forty spheroidal internal structures, which vary between 25 and 290 μm in diameter.

Remarks. The single large inner body preserved in some specimens is reminiscent of the structures interpreted as nuclei in the embryo-like fossils *Tianzhushania* and *Spiralicellula* (Yin et al., 2017). The smaller spheroidal structures disseminated throughout the interior of some other specimens resemble structures in the '*Parapandorina*' stage of *Tianzhushania* that have been interpreted as lipid droplets, possibly yolk granules (Hagadorn et al., 2006, Cunningham et al., 2012a). These structures also bear some resemblance to the '*Megaclonophycus*' stage of the *Tianzhushania* complex, although in '*Megaclonophycus*' stage the structures are interpreted as cells and are much more closely packed than the structures in *Sporosphaera guizhouensis*, which comprise far less of the internal volume and do not touch.

2.8 Acknowledgements

2.9 References

Bailey, J.V., Joye, S.B., Kalanetra, K.M., Flood, B.E., Corsetti, F.A. 2007. Evidence of giant sulphur bacteria in Neoproterozoic phosphorites. Nature 445, 198-201.

Bowyer, F., Wood, R.A., Poulton, S.W. 2017. Controls on the evolution of Ediacaran metazoan ecosystems: a redox perspective. Geobiology 15, 516-551.

Chen, L., Xiao, S., Pang, K., Zhou, C., Yuan, X. 2014. Cell differentiation and germ-soma separation in Ediacaran animal embryo-like fossils. Nature 516, 238-240.

Cohen, P.A., Knoll, A.H., Kodner, R.B. 2009. Large spinose microfossils in Ediacaran rocks as resting stages of early animals. Proceedings of the National Academy of Sciences 106, 6519-6524.

Cunningham, J.A., Thomas, C.-W., Bengtson, S., Kearns, S.L., Xiao, S., Marone, F., Stampanoni, M., Donoghue, P.C.J. 2012a. Distinguishing geology from biology in the Ediacaran Doushantuo biota relaxes constraints on the timing of the origin of bilaterians. Proceedings of the Royal Society B 279, 2369-2376.

Cunningham, J.A., Liu, A.G., Bengtson, S., Donoghue, P.C.J. 2017a. The origin of animals: can molecular clocks and the fossil record be reconciled? Bioessays 39, 1600120.

Cunningham, J.A., Vargas, K., Yin, Z., Bengtson, S., Donoghue, P.C.J. 2017b. The Weng'an

Biota (Doushantuo Formation): an Ediacaran window on soft-bodied and multicellular

microorganisms. Journal of the Geological Society 174, 793-802.

Davies, T. G., Rahman, I. A., Lautenschlager, S., Cunningham, J. A., Asher, R. J., Barrett, P. M.,

Bates, K. T., Bengtson, S., Benson, R. B. J., Boyer, D. M., Braga, J., Bright, J. A., Claessens, L.

P. A. M., Cox, P. G., Dong, X.-P., Evans, A. R., Falkingham, P. L., Friedman, M., Garwood, R.

J., Goswami, A., Hutchinson, J. R., Jeffery, N. S., Johanson, Z., Lebrun, R., Martínez-Pérez, C.,

Marugán-Lobón, J., O'Higgins, P. M., Metscher, B., Orliac, M., Rowe, T. B., Rücklin, M.,

Sánchez-Villagra, M. R., Shubin, N. H., Smith, S. Y., Starck, J. M., Stringer, C., Summers, A. P.,

Sutton, M. D., Walsh, S. A., Weisbecker, V., Witmer, L. M., Wroe, S., Yin, Z., Rayfield, E. J. and

Donoghue, P. C. J. 2017. Open data and digital morphology. Proceedings of the Royal Society B:

Biological Sciences, 284.

Degnan, B.M., Adamska, M., Richards, G.S., Larroux, C., Leininger, S., Bergum, B., Calcino,

A., Taylor, K., Nakanishi, N., Degnan, S.M. 2015. 'Porifera' in Wanninger A. (Ed.) Evolutionary

Developmental Biology of Invertebrates 1: Introduction, Non-Bilateria, Acoelomorpha,

Xenoturbella, Chaetognatha. Springer-Verlag, Wien, pp. 65-106.

dos Reis, M., Thawornwattana, Y., Angelis, K., Telford, M.J., Donoghue, P.C.J., Yang, Z. 2015.

Uncertainty in the timing of origin of animals and the limits of precision in molecular timescales.

Current Biology 25, 1-12.

Green, K.J., Viamontes, G.I., Kirk, D.L. 1981. Mechanism of formation, ultrastructure, and function of the cytoplasmic bridge system during morphogenesis in Volvox. Journal of Cell Biology 91, 756-769.

Hagadorn, J. W., Xiao, S., Donoghue, P. C., Bengtson, S., Gostling, N. J., Pawlowska, M., Raff, E. C., Raff, R. A., Turner, F. R., Chongyu, Y., Zhou, C., Yuan, X., McFeely, M. B., Stampanoni, M., and Nealson, K. H., 2006. Cellular and subcellular structure of Neoproterozoic animal embryos. Science 314, 291-294.

Huldtgren, T., Cunningham, J.A., Yin, C., Stampanoni, M., Marone, F., Donoghue, P.C.J., Bengtson, S. 2011. Fossilized nuclei and germination structures identify Ediacaran "embryos" as encysting protists. Science 334, 1696-1699.

Marone, F., Münch, B., Stampanoni, M., 2010. Fast reconstruction algorithm dealing with tomography artifacts. Proceedings of SPIE 7804, 780410

Mendoza, L., Taylor, J.W., Ajello, L. 2002. The class Mesomycetozoa: a heterogeneous group of microorganisms at the animal-fungal boundary. Annual Review of Microbiology 56, 315-344.

Pang, K., Tang, Q., Schiffbauer, J.D., Yao, J., Yuan, X.L., Wan, B., Chen, L., Ou, Z.J., Xiao, S.H. 2013. The nature and origin of nucleus-like intracellular inclusions in Paleoproterozoic eukaryote microfossils. Geobiology 11, 499-510.

Raff, E.C., Villinski, J.T., Turner, F.R., Donoghue, P.C.J., Raff, R.A. 2006. Experimental taphonomy shows the feasibility of fossil embryos. Proceedings of the National Academy of Science USA 103, 5846-5851.

Rensing, S.A. 2016. (Why) Does evolution favour embryogenesis? Trends in Plant Science 21 (7), 562-573.

Schaap, P. 2012. Evolutionary crossroads in developmental biology: *Dictyostelium discoideum.* Development 138, 387-396.

Schiffbauer, J. D., Xiao, S. H., Sen Sharma, K., and Wang, G., 2012. The origin of intracellular structures in Ediacaran metazoan embryos. Geology 40 (3), 223-226.

Xiao, S., Zhang, Y., and Knoll, A.H. 1998. Three-dimensional preservation of algae and animal embryos in a Neoproterozoic phosphorite. Nature 391, 553-558.

Xiao, S.H., Hagadorn, J.W., Zhou, C.M., Yuan, X.L. 2007. Rare helical spheroidal fossils from the Doushantuo Lagerstatte: Ediacaran animal embryos come of age? Geology 35 (2), 115-118.

Xiao, S.H., Knoll, A.H., Schiffbauer, J.D., Zhou, C.M., Yuan, X.L. 2012. Comment on "Fossilized nuclei and germination structures identify Ediacaran 'animal embryos' as encysting protists". Science 335, 1169-c, 10.1126/science.1218814

Xiao, S., Muscente, A.D., Chen, L., Zhou, C., Schiffbauer, J.D., Wood, A.D., Polys, N.F., Yuan, X. 2014a. The Weng'an biota and the Ediacaran radiation of multicellular eukaryotes. National Science Review 1, 498-520.

Yin, L., Zhu, M., Knoll, A.H., Yuan, X., Zhang, J., Hu, J. 2007. Doushantuo embryos preserved inside diapause egg cysts. Nature 446, 661-663.

Yin, Z.J., Liu, P.J., Li, G., Tafforeau, P., Zhu, M.Y. 2014. Biological and taphonomic implications of Ediacaran fossil embryos undergoing cytokinesis. Gondwana Research 25, 1019-1026.

Yin, Z.J., Zhu, M.Y., Bottjer, D.J., Zhao, F.C., Tafforeau, P. 2016. Meroblastic cleavage identifies some Ediacaran Doushantuo (China) embryo-like fossils as metazoans. Geology 44, 735-738.

Yin, Z., Cunningham, J.A., Vargas, K., Bengtson, S., Zhu, M., Donoghue, P.C.J. 2017. Nuclei and nucleoli in embryo-like fossils from the Ediacaran Weng'an Biota. Precambrian Research 301, 145-151.

Yin, Z., Zhao, D., Pan, B., Zhao, F., Zeng, H. Li, G., Bottjer, D.J., Zhu, M. 2018. Early Cambrian animal diapause embryos revealed by X-ray tomography. Geology 46, 387-390.

Zhang, X.G., Pratt, B.R. 2014. Possible algal origin and life cycle of Ediacaran Doushantuo microfossils with dextral spiral structure. Journal of Paleontology 88, 92-98.

Zhou, C., Li, X., Xiao, S., Lan, Z., Ouyang, Q., Guan, C., Chen, Z. 2017. A new SIMS zircon U–Pb date from the Ediacaran Doushantuo Formation: age constraint on the Weng'an biota. Geological Magazine 154, 1193-1201.

Chapter 3: Systematics, developmental biology and phylogenetic significance of red algae (Rhodophyta) from the Ediacaran Weng'an Biota

Project design: E. Landon, P. Donoghue, Z. Yin; Materials: E. Landon, Z. Yin; Data collection: E. Landon; Analysis: E. Landon; Interpretation: E. Landon with contributions from P. Donoghue; Writing: E. Landon wrote the text to which P. Donoghue contributed edits.

3.1 Introduction

Red algae (Rhodophyta) are one of only five eukaryotic lineages that have independently achieved complex multicellularity (Cock and Collén 2015). Along with green and glaucophyte algae, they are one of the fundamental lineages of Kingdom Plantae (aka Archaeplastida) descended from the primary cyanobacterial endosymbiosis. Red algae are also the source of the plastids, through secondary, tertiary and even quaternary symbioses, found in other photosynthetic eukaryote lineages including alveolates, cryptophytes, haptophytes and stramenopiles (Zimorski et al. 2014). Thus, knowledge of these fundamental events in eukaryote evolutionary history are all inextricably linked with an understanding of the evolutionary history of red algae. Unfortunately, red algae have an appalling fossil record and so attempts to elucidate their evolutionary history have largely been the preserve of molecular phylogenetics and molecular divergence time analyses (e.g. Yoon et al. 2004, 2006; Yang et al. 2016). Molecular clock analyses, in particular, rely on the fossil record for calibration and so those few Proterozoic records of red algae that exist have proven critical to understanding the timescale of red algal

evolution, but also the timing of the symbiosis events in which red algae are implicated (Porter 2020).

The oldest possible records of red algae, *Rafatazmia chitrakootensis* and *Ramathallus lobatus*, are from the Palaeoproterozoic-Mesoproterozoic (~1.6 Ga) Vinhyan Supergroup of central India (Bengtson et al. 2017). The thalloid gestalt and cellular structure of *Ramathallus lobatus* are compatible with a rhodophyte interpretation, but they do not provide for a definitive red alga interpretation. *Rafatazmia* has the more convincing claim on rhodophyte affinity, preserving structures comparable to pit plugs and pyrenoids, though pyrenoids are not specific to red algae and it is difficult to discriminate the putative pit plugs from diagenetic mineralization unrelated to biological structure (Carlisle et al. 2021). Otherwise, *Bangiomorpha pubescens* from the latest Mesoproterozoic (1.03 Ga) Hunting Formation of Arctic Canada (Butterfield, 2000; Gibson et al. 2018) exhibits a number of characteristics, including intercalary spore formation, that compare favourably to members of the paraphyletic Bangiophyaceae. *Bangiomorpha* has been more precisely compared to the bangiophyte *Bangia* (Butterfield 2000), though despite its close resemblance, the shared features including filamentous form, pattern of cell division and sporangium formation, are more widespread among paraphyletic Bangiophyceae (Betts et al. 2018). As such, these characters are best considered rhodophyte symplesiomorphies and Bangiomorpha interpreted as a total-group rhodophyte (Betts et al. 2018; Porter 2020). This leaves rhodophytes from the Ediacaran Weng'an Biota as the oldest possible records of the crown clade since they have been interpreted to encompass both stem- and crown-Florideophyta (Xiao et al. 2004). As such, the Weng'an rhodophytes have been widely used in calibrating molecular divergence time analyses (Yoon et al. 2004, 2006, 2010; Yang et al. 2016; Parfrey et

al. 2011; Eme et al. 2014; Sharpe et al. 2015). Unfortunately they are little studied and, indeed, differences between established taxa have been alternately interpreted as different stages in the life cycle of the same organism (Xiao et al. 2004). Here we attempt to resolve their taxonomy, systematics, and evolutionary history.

3.1.1 History of research into multicellular algae from the Weng'an Biota
Six algal taxa are currently recognised from the Weng'an Biota: *Wengania, Thallophyca, Thallophycoides, Paramecia, Gremiphyca* and *Archaeophycus*.

Wengania (Figure 3.1A), first described by Zhang (1989) was described as spherical, composed of rectangular cells that are on average 6.4µm across. The cells form unbranching filaments aggregated into pseudoparenchyma. Zhang (1989) tentatively assigned *Wengania* to Rhodophyta, on the basis of its similarity to Solenoporaceae, a group of Palaeozoic putative calcareous rhodophytes (though *Wengania* itself was not interpreted as having been calcareous in life). Zhang et al. (1998), in a critical review of the Weng'an algae, concluded that *Wengania* should not be placed in Rhodophyta, noting similarities to peltate parenchymatous green algae. However, more recent reviews by Xiao et al. (2004; 2014a) consider *Wengania* a stem-florideophyte red alga, due to its pseudoparenchymatous construction and evidence of apical growth.

Thallophyca (Figure 3.1B-D) was described by Zhang (1989) as having a sheet-like, nodular thallus differentiated into a cortex and inner medulla (Figure 3.1C). Zhang (1989) described the cortical cells as elongate with an average size of 13.4µm x 2.9µm (length x width), arranged in a

compact layer around the margin of the thallus. The medullary cells are more varied, generally spheroidal, ellipsoidal, or spindle-shaped, arranged in filaments which are aggregated and splay out into what Zhang (1989) described as a 'cell fountain structure'. Zhang (1989) observed two distinct substructures in the medulla region of *Thallophyca*, spheroidal cavities up to 100 μm in diameter, generally situated just beneath the cortex, and 'cell islands', special cell groupings consisting of a variable number of unusual cells that are often larger than the surrounding medullary cells (Figure 3.1D). As with *Wengania,* Zhang (1989) tentatively assigned *Thallophyca* to Rhodophyta on the basis of its 'fountain type' thallus structure which resembles that of some modern rhodophytes. Zhang and Yuan (1996) corroborated the assignment of *Thallophyca* to the rhodophytes, interpreting the cell islands as carposporangia, structures unique to rhodophytes that produce diploid carpospores (resulting from sexual reproduction) which develop into the sporophyte phase of the rhodophyte life cycle. Zhang and Yuan (1996) also compared the dark spheroidal or elongated structures that occur in clusters in the peripheral part of thalli of *Thallophyca* to spermatangia in extant florideophytes, structures that form on male red algal gametophytes, within which the spermatia (male gametes) develop. Zhang et al. (1998) agreed with the reasoning of Zhang and Yuan (1996) in assigning *Thallophyca* to the rhodophytes based on its cortex-medulla differentiation and possession of carpospores and carposporangia. They also compared *Thallophyca* to Solenoporaceae, the same comparison previously drawn for *Wengania* (Zhang, 1989). Xiao et al. (2004; 2014a) interpreted *Thallophyca* as a stem-corallinalean due to its putative pseudoparenchymatous structure, apical growth, and the presence of carpospores and carposporangium.

Thallophycoides (Figure 3.1E, F) was first described by Zhang and Yuan (1992). It was described as having a sheet-like thallus and exhibiting cortex-medulla differentiation, with a cortex consisting of numerous layers of rectangular cells, and a pseudoparenchymatous medulla with spheroidal cells (Figure 3.1F). It resembles *Thallophyca* in general morphology but differs in exhibiting less tissue differentiation and smaller cells (2-3μm in diameter). *Thallophycoides* was assigned to Rhodophyta on the basis of structural similarity to *Thallophyca*, in particular the similar shapes of the cortical and medullary cells in each taxon. In the review undertaken by Zhang et al. (1998), *Thallophycoides* retained its status as a rhodophyte, though it was noted that it does not have any features that would unambiguously place it in this group. Zhang et al. (1998) also observe that *Thallophycoides* does not exhibit any evidence of cortex-medulla differentiation, a departure from the initial description by Zhang and Yuan (1992). They emend the diagnosis of *Thallophycoides* to include *Corticina* (Figure 3.1G, H), an alga described by Zhang and Yuan (1992) with similar features to *Thallophycoides.* As with *Wengania,* Xiao et al. (2004; 2014a) consider it a stem-florideophyte.

Zhang and Yuan (1992) described *Paramecia* (Figure 3.1I-K) as an organism of uncertain affinity, exhibiting tissue differentiation, with a peripheral tissue consisting of fibre-like cells arranged in layers parallel to the surface and an inner region in which the cells branch repeatedly to form a network-like structure (Figure 3.1J, K). Distributed within the peripheral layer are cell islands consisting of multiple cells that are larger and darker than the surrounding tissue (Figure 3.1J, K). Zhang et al. (1998) assigned *Paramecia* to the rhodophytes on the basis of having thallus differentiation similar to carpospore-producing florideophyte red algae, and also suggested that *Paramecia* could be a stem representative of extant Gigartinales and Ceramiales.

68

Xiao et al. (2004; 2014a) instead interpret *Paramecia* as a stem representative of extant Corallinales, as with *Thallophyca.*

Gremiphyca (Figure 3.1L, M) is described by Zhang et al. (1998) as having a nodular thallus with undifferentiated rectangular cells arranged in diverging, closely packed rows. *Gremiphyca* was assigned tentatively to Rhodophyta, though Zhang et al. (1998) acknowledge that it does not exhibit features that make this assignment unambiguous. Xiao et al. (2004; 2014a) interpret *Gremiphyca* as a member of the florideophyte stem, as with *Wengania* and *Thallophycoides.*

Archaeophycus (Figure 3.1N-P) was originally described as *Paratetraphycus,* one of a number of coccoid microfossils first described by Zhang (1985) as a cyanobacterium on the basis of their size and cyanophytic habit of spheroids arranged in planar tetrads (Figure 3.1O, P) and diads. Zhang et al. (1998) reinterpreted *Paratetraphycus* as an alga on the basis of its close resemblance to the tetraspore-producing life stage of the extant bangiophyte *Porphyra*, along with evidence of synchronised cell division which is a property of eukaryotic rather than prokaryotic organisms. Xiao et al. (1998) agreed with this interpretation, this time comparing the tetrads of *Paratetraphycus* to the carposporangia of *Porphyra.* Xiao et al. (2004) in their review of the Weng'an algae, did not consider *Paratetraphycus*, which Dong et al. (2009) later considered indistinguishable from the Cambrian coccoid microfossil *Archaeophycus,* which had been described by Wang et al. (1983) as a cyanobacterium. As a result, Xiao et al. (2004) considered *Paratetraphycus* both a junior synonym of *Archaeophycus* and a cyanobacterium. Xiao et al. (2014a) returned to the algal interpretation of *Archaeophycus*, making comparison to the tetrad

69

cell packets of *Porphyra*, though they accept that this might as readily be interpreted as a cyanobacterium on the basis of the same evidence.

In summary, six taxa of Weng'an algae are currently recognised: *Wengania, Thallophyca, Thallophycoides, Paramecia, Gremiphyca* and *Archaeophycus. Wengania* is distinguished by a spheroidal thallus and rectangular cells that form unbranching filaments that are aggregated into pseudoparenchyma (Zhang 1989). *Gremiphyca* has a similar histology to *Wengania,* with undifferentiated rectangular cells arranged in closely packed rows, but has a nodular rather than spheroidal thallus (Zhang et al. 1998). *Thallophycoides* is also histologically similar to *Wengania,* with rectangular cells forming pseudoparenchyma, but differs from both *Wengania* and *Gremiphyca* in having a sheet like thallus (Zhang and Yuan 1992, Zhang et al. 1998). *Thallophyca* has a more complex histology, with a sheet-like, nodular thallus, and an interior that exhibits cortex medulla differentiation. The medulla region of *Thallophyca* exhibits two distinct substructures - spherical cavities that are situated just below the cortex, and 'cell islands', which are groupings of a number of unusual cells that are larger than the surrounding medullary cells (Zhang 1989). *Paramecia* is similarly complex, with cortex-medulla differentiation and cell islands, however in *Paramecia* the cell islands are distributed within the cortex. There is no description of *Paramecia*'s overall thallus shape.
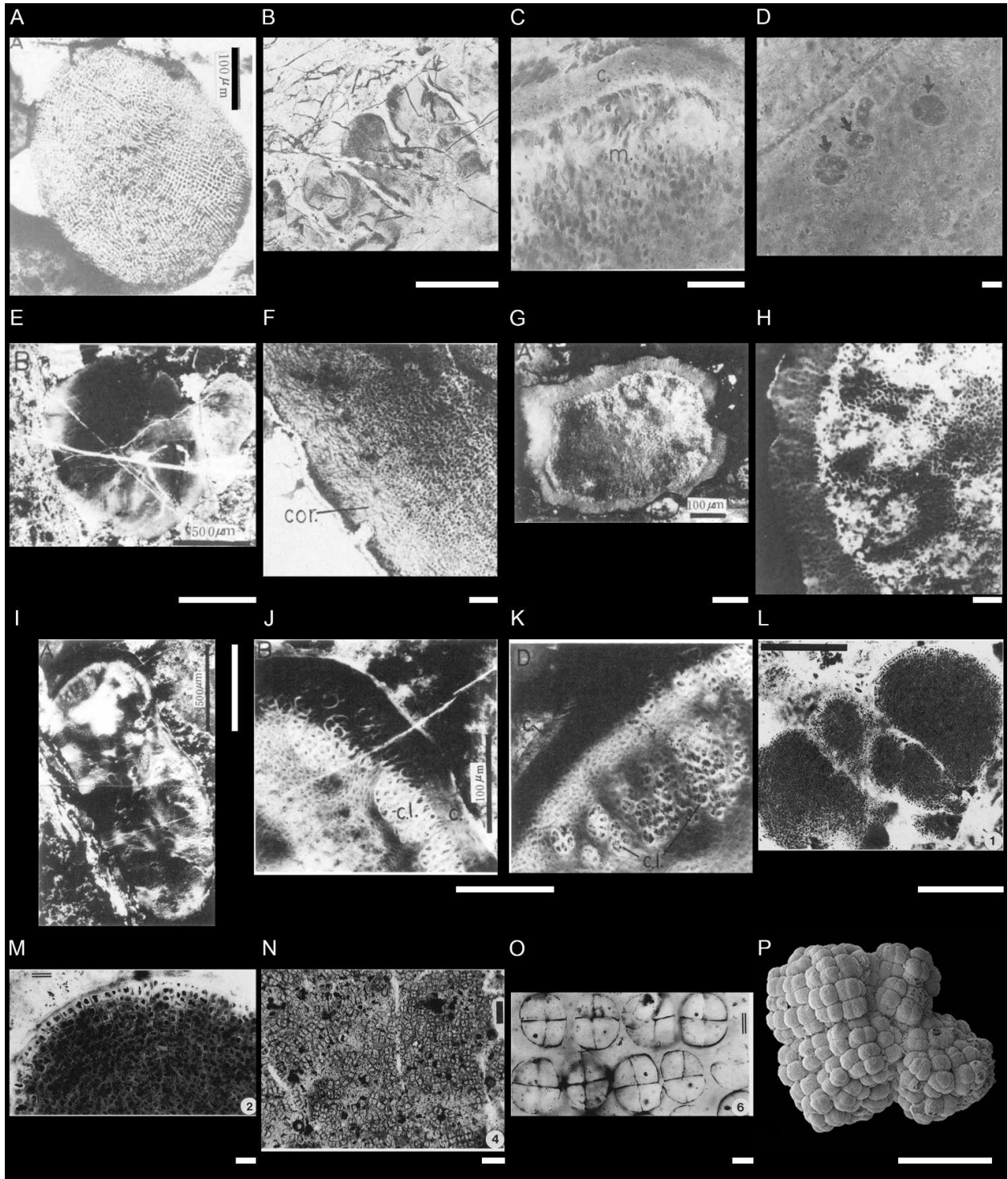
Figure 3.1. Algae from the Weng'an Biota. (A) Holotype of *Wengania globosa.* Image from Zhang (1989). Scale bar is 100 μm. (B-D) *Thallophyca ramosa.* Images from Zhang (1989). (B) Holotype of *Thallophyca ramosa.* Scale bar is 1 mm. (C) close up of cortical and medullary cells

in (B). Scale bar is 50 μm; c. = cortex, m. = medulla. (D) Cell islands in the medulla of *Thallophyca ramosa.* Scale bar is 10 μm. (E-F) *Thallophycoides phloeatus.* Images from Zhang and Yuan (1992). (E) Holotype of *Thallophycoides phloeatus.* Scale bar is 500 μm. (F) Close up of the *Thallophyocides* holotype, showing the cortical (cor.) tissue and the medullary region. Scale bar is 20 μm. (G-H) *Corticina irregularia.* Images from Zhang and Yuan (1992). (G) Holotype of *Corticina irregularia.* Scale bar is 100 μm. (H) Magnified view of a peripheral part of the *Corticina* holotype, showing a dark rim of cortical tissue. Scale bar is 20 μm. (I-K) *Paramecia incognata.* Images from Zhang and Yuan (1992). (I) Holotype of *Paramecia incognata.* Scale bar is 500 μm. (J, K) Magnified views of a peripheral part of the *Paramecia* holotype, showing cortical cells (c.) and cell islands (cl.). Scale bars are 100 μm. (L-M) *Gremiphyca corymbiata.* Images from Zhang et al. (1998). (L) Holotype of *Gremiphyca corymbiata.* Scale bar is 100 μm. (M) Magnified view of the *gremiphyca* holotype. Scale bar is 10 μm. (N-P) *Archaeophycus yunnanensis.* (N) *Archaeophycus* in thin section. Image from Zhang et al. (1998). Scale bar is 100 μm. (O) magnified view of (N), showing tetrad cell packets. Image from Zhang et al. (1998). Scale bar is 10 μm. (P) Scanning electron microscope image of *Archaeophycus.* Image from Cunningham et al. (2017b). Scale bar is 255 μm.

Without doubt, the Weng'an algae are exceptionally preserved, however, they are known almost exclusively based on histology with little reference to their broader morphology and anatomy. Effective tests of their phylogenetic affinities rely on knowledge of their three dimensional structure and, in particular, that of key structures such as carposporangia. Only *Archaeophycus* is known definitively from three-dimensional material, recovered through acid preparation of the host rock. Xiao et al. (2004) present some isolated specimens which they attribute to

Gremiphyca, Paramecia and *Thallophyca*, however, the degree to which morphology and histology covary remains unclear. Thus, with the aim of testing existing taxonomic concepts and phylogenetic interpretations, we obtained a large suite of isolated three dimensional specimens from the Weng'an Biota which encompass the range of morphologies attributed to algae. These were sorted into self-similar morphological groupings, and subjected to histological analysis using synchrotron tomography. Subsequently, we rationalise the variation in external morphology and histology with existing taxonomic concepts, before evaluating phylogenetic interpretations of the fossils. Our results suggest that there is continuous variation in both internal and external structure between subsets of existing taxa indicating that the existing classification of Weng'an algae based on histology is not valid.

3.2 Materials and Methods

An abundant collection of fossilized phosphatised algae was recovered through acetic acid digestion (Jeppsson et al. 1999) of phosphoritic dolomite from the Upper Grey Facies (Unit 4b; Cunningham et al. 2017b) of the Doushantuo Formation at '54' Quarry, Baiyan-Gaoping Anticline, Weng'an County, Guizhou Province, Southwest China. These specimens were sorted into three groupings with similar external morphologies based on lobe number and 67 specimens (23 from group 1, 20 from group 2, and 24 from group 3) were characterised through synchrotron radiation X-Ray Tomographic Microscopy (srXTM) at the X02DA TOMCAT beamline of the Swiss Light Source (SLS; Paul Scherrer Institute, Villigen, Switzerland). srXTM data were obtained using 4X, 10X and 20X objective lenses, yielding reconstructed tomographic data with voxel dimensions of 1.625 μm, 0.65 μm and 0.325 μm, respectively) at energy levels

of 20-27 keV, exposure times of 100-850 ms, and scintillators composed of lutetium, aluminium and garnet. 1501 projections were taken equi-anglularly through 180º of rotation within the beam. Projections were post-processed and rearranged into flat- and dark-field-corrected sinograms, and reconstruction was performed on a 60-core Linux PC farm, using a highly optimized routine based on the Fourier transform method and a regridding procedure (Marone et al. 2017). Slice data were analysed and manipulated using AVIZO 9.7 (www.thermofisher.com). X-Rays from synchrotron light sources are monochromatic and so contrast differences in the ensuing tomographic data reflect the relative densities of the fossil materials they pass through (Margaritondo 2002).

3.3 Results

The Weng'an algae exhibit a range of variation in external morphology, which can be broadly sorted into three morphotypes (Figures 3.2-3.7). These morphotypes represent subdivisions of a spectrum, rather than distinct categories. The morphotypes are described below, and summarised in table 3.1. All of the studied specimens exhibit a granular internal matrix that is often cross-cut by fine cracks (Figures 3.8-3.12). Where there is no cellular preservation, this matrix exhibits some compositional differences in the form of discontinuous patches of variable X-ray attenuation, reflecting differences in mineral chemistry (Cunningham et al. 2012a, 2014) but they are otherwise structureless. However, many specimens preserve some degree of cellular structure, distinguished by both compositional and textural differences.

3.3.1 Morphotype 1

External morphology. Comparatively large (between 0.5mm and 2mm across), smooth-surfaced and irregularly shaped (Figure 3.2A-D). These specimens exhibit a large number of lobes divided by narrow, often deep invaginations. Each major lobe is composed of several smaller lobes that are only partially divided from the main structure, as opposed to being one large smooth structure. Most specimens are convex, without any evidence of a stalk.

Histology. Internally, specimens attributed to this morphotype are composed of cells that vary between 3-10μm along their long axis, and the degree of preservation varies, with cells either preserved throughout the interior (Figure 3.8A, B), or in patches separated by large areas of structureless matrix (Figure 3.8C, D). Some specimens exhibit a thin (3-10μm) structureless outer layer (Figure 3.8E, F). The cells are either preserved empty or infilled by secondary mineralization (diagnosed by contrasting X-ray attenuation), and many specimens exhibit both of these preservational states. In some specimens there is a change from clearly delineated cells to a clotted fabric at the core (Figure 3.8G).

While most specimens exhibit an originally undifferentiated cellular structure, one specimen exhibits differentiation into distinct subunits, each of which contains multiple small vesicle-like structures that exhibit higher X-ray attenuation than the surrounding tissue (Figure 3.8H, I). These structures tend to be larger than the cells in other specimens, ranging between 5-15μm across. Generally, the vesicle-like structures are entirely infilled, but in some cases they consist of only a thin rim of highly attenuating mineral defining an inner void.

3.3.2 Morphotype 2

External Morphology. These specimens are between 0.5-2mm across and are generally smooth-surfaced (Figure 3.3A-D; Figure 3.4A-E), although in a small number of specimens cells can be seen on the exterior (Figure 3.5A-D). The specimens are commonly composed of a few large lobes delimited by a series of narrow, shallow, invaginations. The specimens either show no preferred direction of growth (Figure 3.3A-D; Figure 3.5A-D), with the lobes protruding in all directions, or are convex (Figure 3.4A-E), reflecting growth in one direction. They show no evidence of having a stalk.

Histology. Component cells vary in length between 3-10μm along their long axis and exhibit variable preservation of cellular structure, either continuous throughout the interior (Figure 3.9A, B), or preserved only in patches separated by large areas of structureless mineral (Figure 3.9C-E). In some specimens, the mineral matrix contains clusters of one to three cells disseminated through it (Figure 3.9C-E). Some of these specimens also exhibit a thin (3-10μm), structureless margin between the specimen edge and the interior proper (Figure 3.9A, B), and a change from clearly delineated cells to a clotted fabric at the centre of the alga (Figure 3.9F, G). Some specimens exhibit cortex-medulla differentiation, with a change in cell size and orientation between the periphery and the centre (Figure 3.9H-J).

Some specimens also exhibit cell islands, clusters of cells that are either enclosed within a medulla or cortex but distinct from the surrounding cells (Figure 3.10A), isolated within the matrix and with no distinct cellular cortex (Figure 3.9H-J; Figure 3.10B, C), or tightly clustered into small packages throughout the interior of the specimen (Figure 3.10D, E). The isolated cell

islands frequently have a cortex of smaller and thinner cells surrounding them, separated from the cell island proper by a thin band of mineral matrix (Figure 3.10C).

Specimens attributed to this morphotype may also be internally divided into distinct packages, each of which contains multiple small vesicle-like structures that range in size between 5 and 15μm, that are more highly attenuating than the surrounding material (Figure 3.10F-H). The vesicle-like structures are usually fully infilled but, in some instances, they consist only of a thin rim of bright material surrounding a void.

3.3.3 Morphotype 3

External Morphology. These specimens are between 0.5-2mm across and have no or very few lobes and are irregular in shape (Figure 3.6A-E; Figure 3.7A-D), lacking well developed invaginations. Some specimens have a reniform morphology (Figure 3.7A-D). They show a preferred direction of growth, being elongated along one axis (Figure 3.6; Figure 3.7), with no evidence of a stalk.

Histology. The component cells vary in length between 3-10μm and are preserved either as voids or infilled, either consistently throughout the volume of the specimen (Figure 3.11A, B) or in patches separated by structureless mineral matrix (Figure 3.11C, D), reflecting differential preservation of the original structure. Preservational variation notwithstanding, this morphotype exhibits cortex-medulla differentiation, with a change in the size and orientation of the cells between the periphery and centre (Figure 3.11B, E, F). Peripheral cortical cells are more tightly packed and often more elongate than the medullary cells (Figure 3.11E).

77

Cell islands occur rarely, either isolated within the matrix of otherwise undifferentiated cells (Figure 3.11F; Figure 3.12A, B), or at the margins of the specimen within the cortex (Figure 3.11F). In some specimens the cell islands are surrounded by a halo of smaller and thinner cells (Figure 3.11C, D), which is separated from the cell island proper by a thin band of matrix material. The cell islands that occur within the medulla regions of the specimens are near spherical, with diameters of 60-70μm (Figure 3.11C, D, F-H; Figure 3.12A-I). Those that occur in the cortical region are in most cases elongated (Figure 3.11A), measuring up to 200μm along the long axis and 100μm along the short axis at its greatest extent. The cell islands are distinguished from the matrix by their darker colour. In some cases the cells that comprise the cell island are contained within a dark rim (Figure 3.12A, B), and in some cases appear to nucleate around a core of paler matrix material (Figure 3.11F-H). The cell islands are generally one solid mass of cells all through. Rarely, the cell islands are instead cup shaped, consisting of a mass of cells surrounding a matrix-infilled void (Figure 3.12C-I). In the centre of the cup, a mass of cells protrude from its base into the void fill (Figure 3.12H). The cell islands resemble those described by Zhang (1989) and Xiao et al. (2004) in that they are darker and larger than the vegetative cells and can occur within the medulla and the cortex.

Features	Morphotype		
External morphology	1	2	3
Multilobate	✓	✓	✕
Minor lobes	✓	✕	✕
Deep invaginations	✓	✕	✕
Shallow invaginations	✕	✓	✕
Histology			
Cortex-medulla differentiation	✕	(✓)	✓
Divided into subunits	(✓)	(✓)	✕
Cell islands	✕	(✓)	(✓)

Table 3.1. Summary of major features of algal morphotypes. ✓ indicates all examined specimens possess this feature, (✓) indicates some examined specimens possess this feature, ✕ indicates no examined specimens possess this feature.
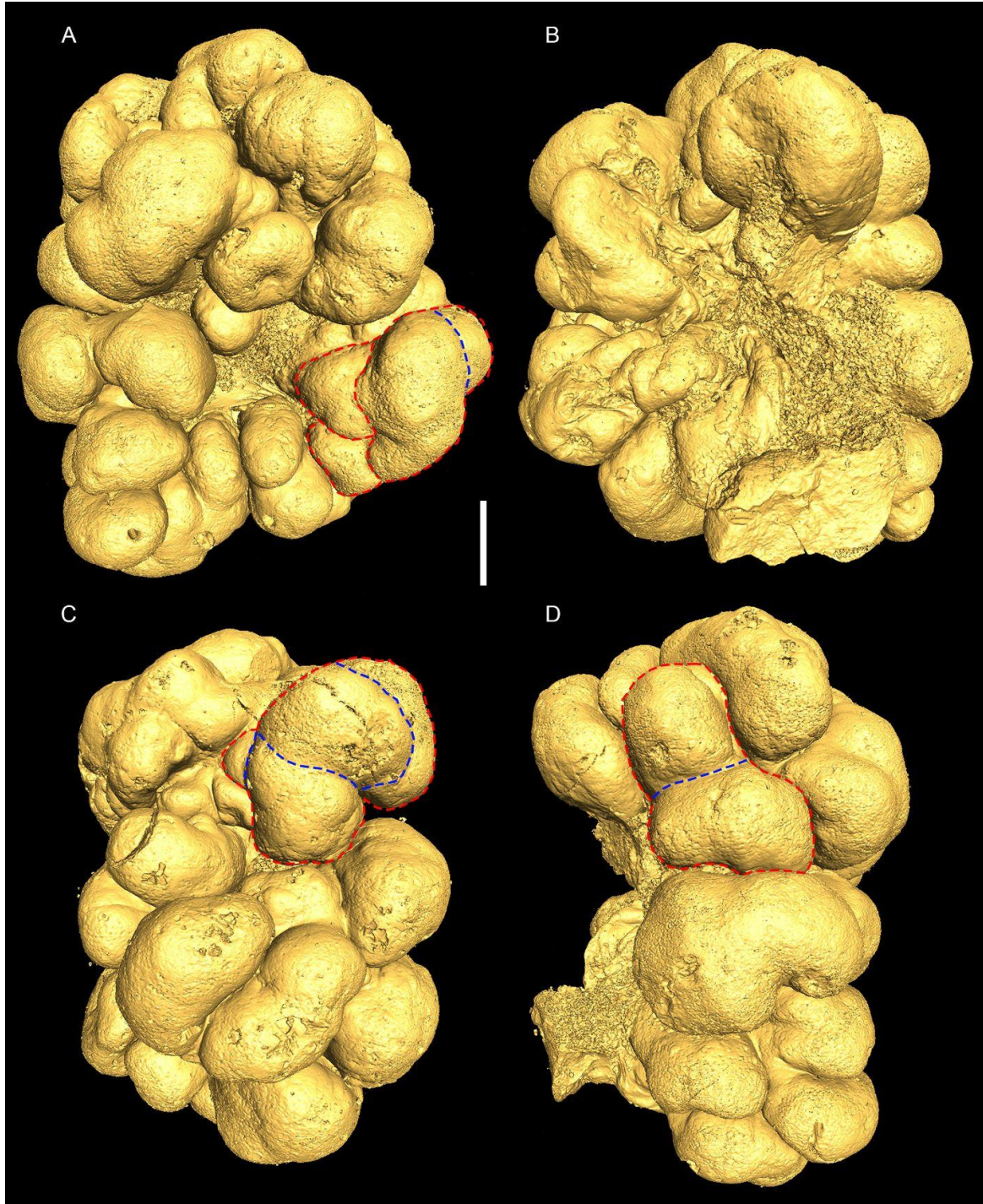
Figure 3.2. Isosurfaces showing morphotype 1 external morphology. Red dashed lines indicate

boundaries between major lobes, blue dashed lines indicate boundaries between minor lobes.

(A-D) 3D surface renderings of the specimen ZY1701_10 from different view angles.

80

Figure 3.3. Isosurfaces showing morphotype 2 external morphology. Red dashed lines indicate boundaries between major lobes, blue dashed lines indicate boundaries between minor lobes. (A-D) 3D surface renderings of the specimen ZY1804_07 from different view angles. Scale bar is 500 μm.
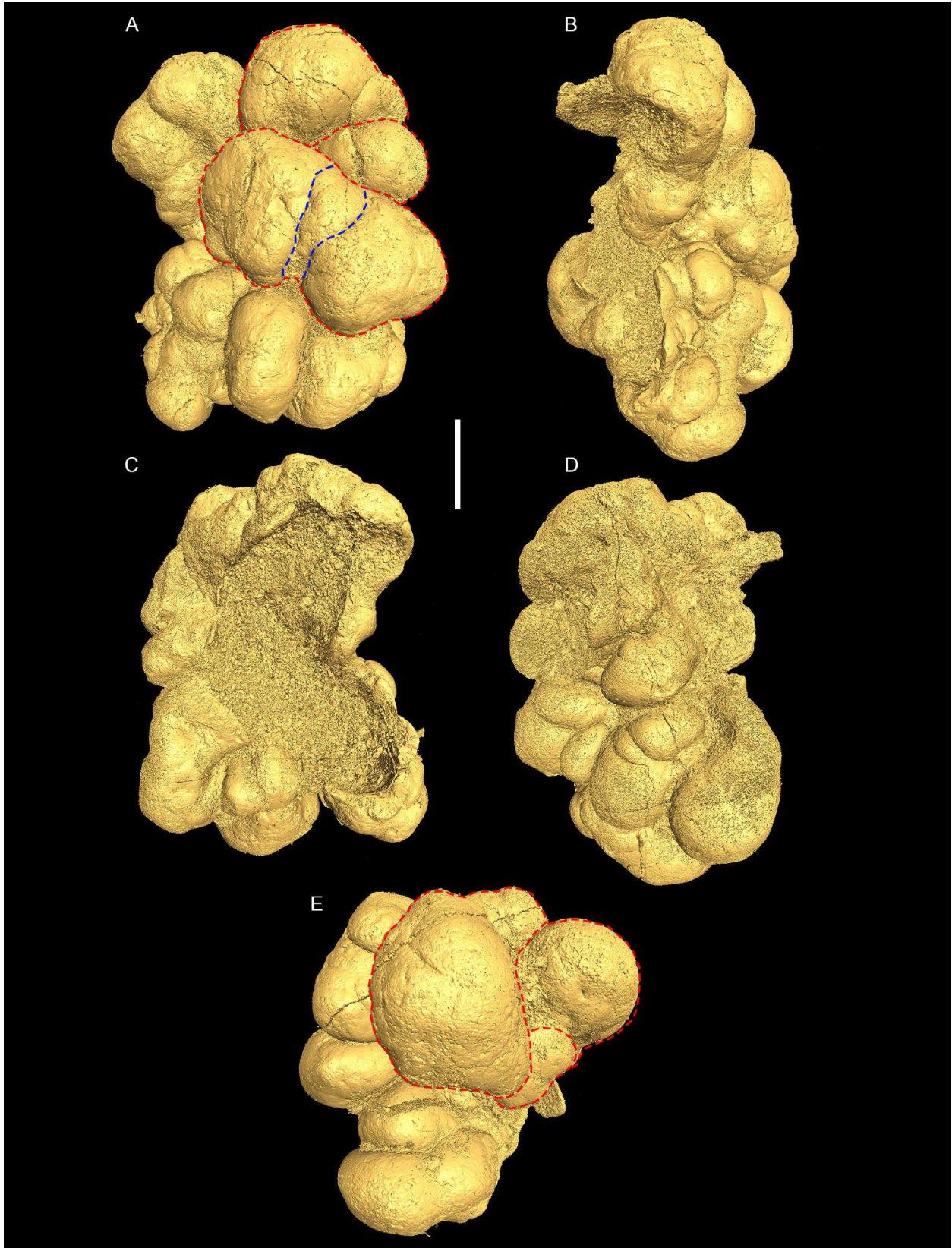
Figure 3.4. Isosurfaces showing morphotype 2 external morphology. Red dashed lines indicate boundaries between major lobes, blue dashed lines indicate boundaries between minor lobes. (A-E) 3D surface renderings of the specimen ZY1701_05r from different view angles.
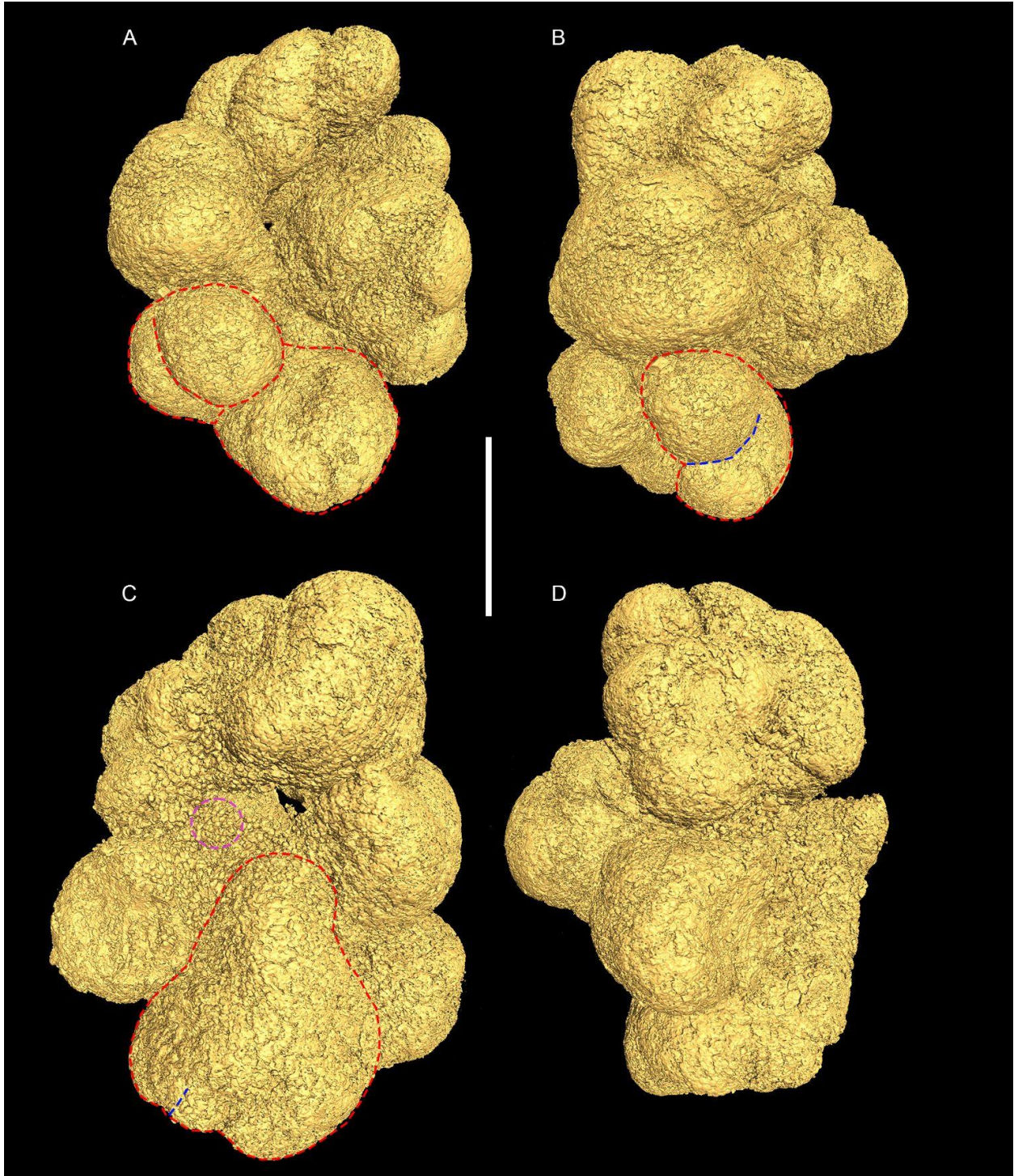
Figure 3.5. Isosurfaces showing morphotype 2 external morphology. Red dashed lines indicate boundaries between major lobes, blue dashed lines indicate boundaries between minor lobes. (A-D) 3D surface renderings of the specimen ZY1811_06 from different view angles. The pink

circle in (H) highlights a region where cells can be observed on the surface of the specimen. Scale bars are 500 μm.

Figure 3.6. Isosurfaces showing morphotype 3 external morphology. (A-E) surface renderings of the specimen ZY1701_06 from different view angles.

Figure 3.7. Isosurfaces showing morphotype 3 external morphology. (A-D) 3D surface renderings of the specimen ZY1216_11 from different view angles. Scale bars are 500 μm.
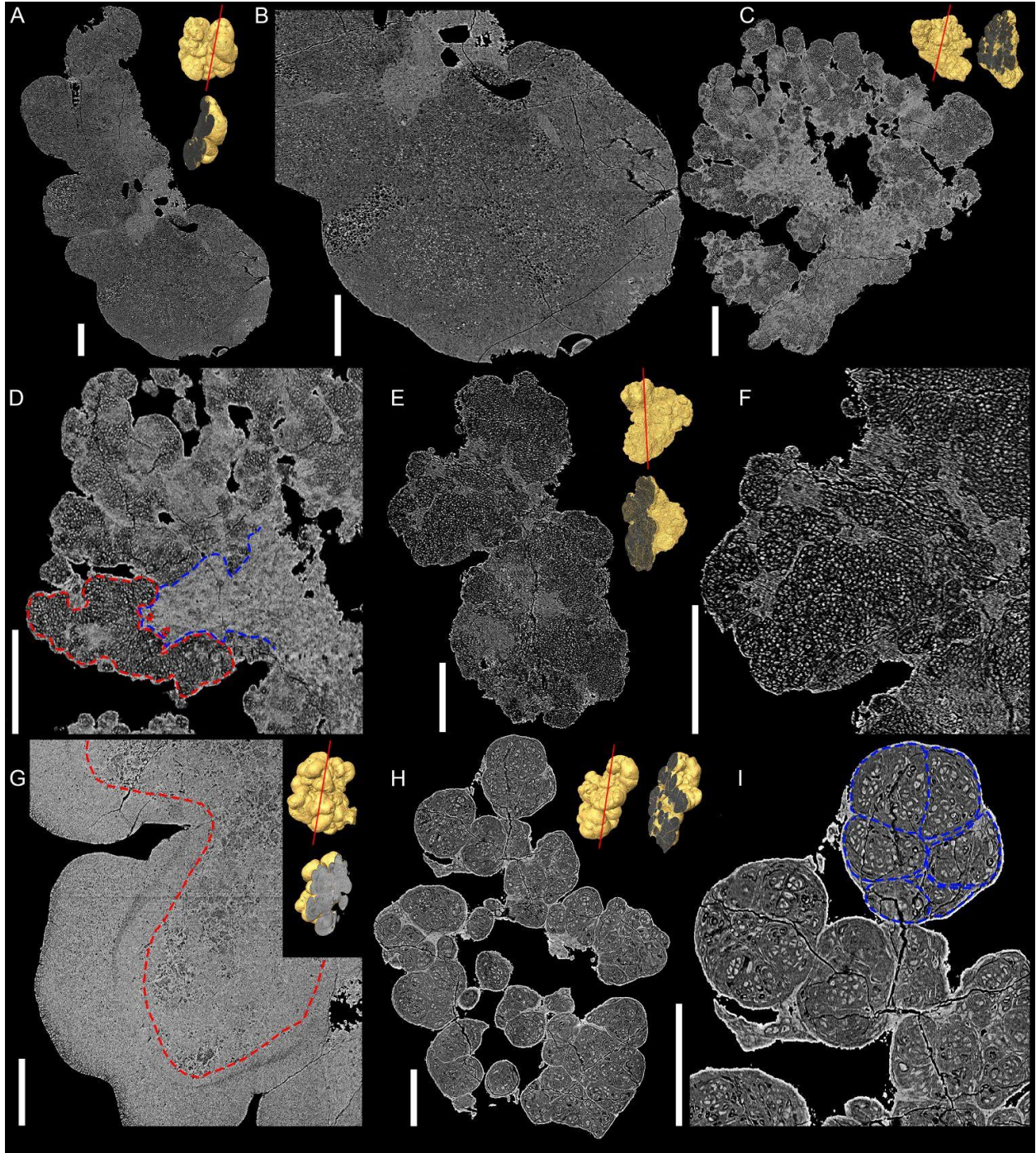
Figure 3.8. Orthoslices showing histology of morphotype 1. (A) Orthoslice of the specimen ZY1701_07, showing cells preserved throughout the interior of the specimen. (B) close-up of (A). (C) Orthoslice of the specimen ZY1811_02, showing patchy preservation of cells. (D) close-up of (C). The red dashed lines outline a region where cells are preserved, the blue dashed

line outlines a region where cells are not preserved and only matrix can be observed. (E) Orthoslice of the specimen ZY1804_08, showing patchy preservation of cells and a thin margin. (F) close-up of (E). (G) Orthoslice of the specimen ZY1701_10, showing a clotted fabric at the centre of the specimen, on the right of the red dashed line. (H) Orthoslice of the specimen ZY1701_04 showing division into distinct subunits. (I) Close-up of (H). The blue dashed lines indicate subunits within one lobe of the specimen. The pale grey blebs within each subunit are the vesicle-like structures. Scale bars are 200 μm.
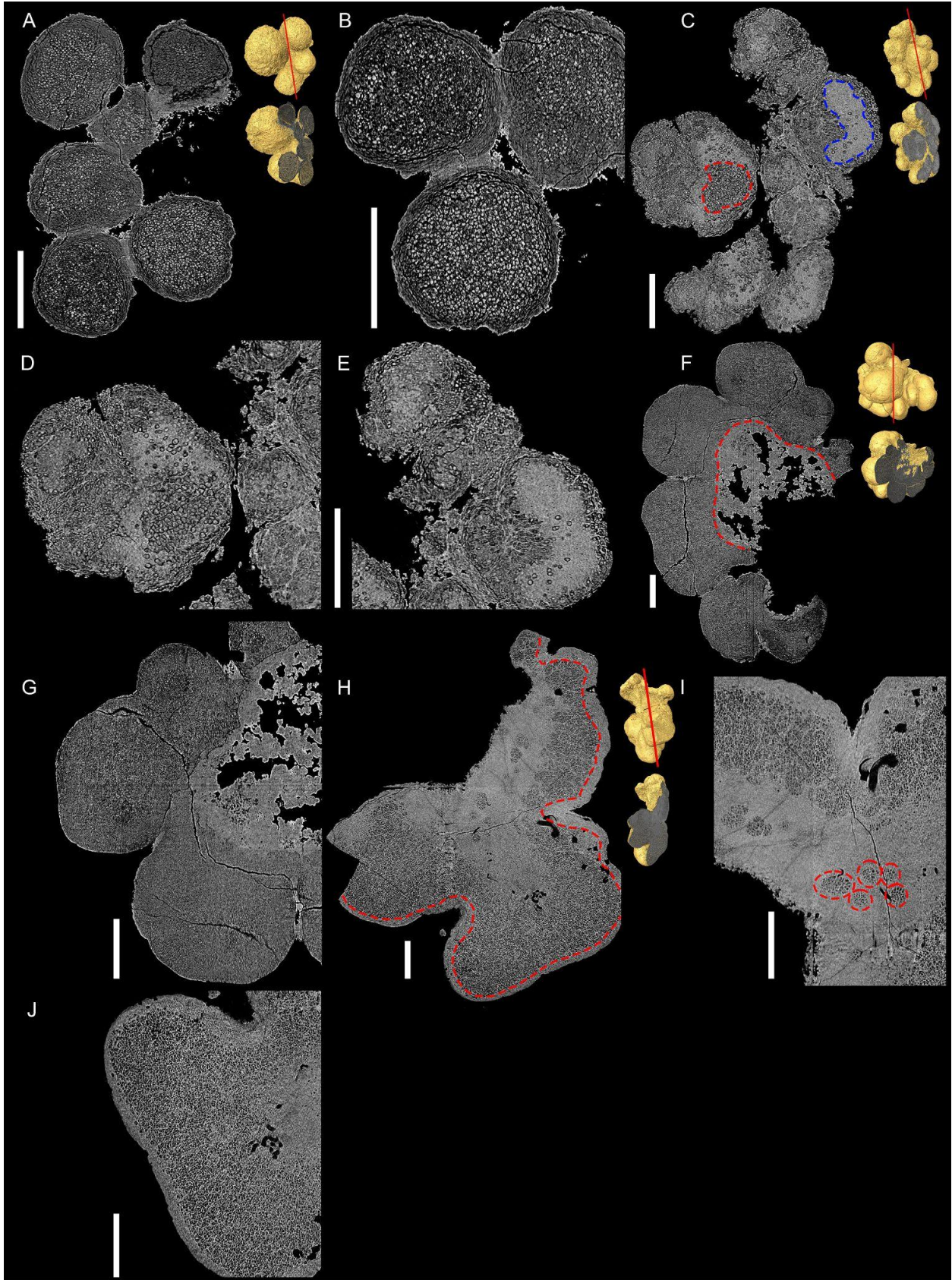
Figure 3.9. Orthoslices showing histology of morphotype 2. (A) Orthoslice of the specimen ZY1804_07. (B) Close-up of (A), showing infilled cells and thin margin. (C) Orthoslice of the specimen ZY1811_06. The red dashed line indicates a region of cellular preservation, and the blue dashed line highlights a region of structureless matrix (with a few isolated cells). (D and E) close-ups of (C), showing patchy distribution of cells and cells isolated within structureless matrix. (F, G) Orthoslices of the specimen ZY1701_05r, showing a clotted fabric at the centre of the specimen, on the right of the red dashed line. (H) Orthoslice of the specimen ZY1811_08. The red dashed line indicates the boundary between the cortex and medulla. (I and J) close-ups of (H), showing cell islands (highlighted by red circles) (I) and cortex-medulla differentiation (I, J). Scale bars are 200 μm.
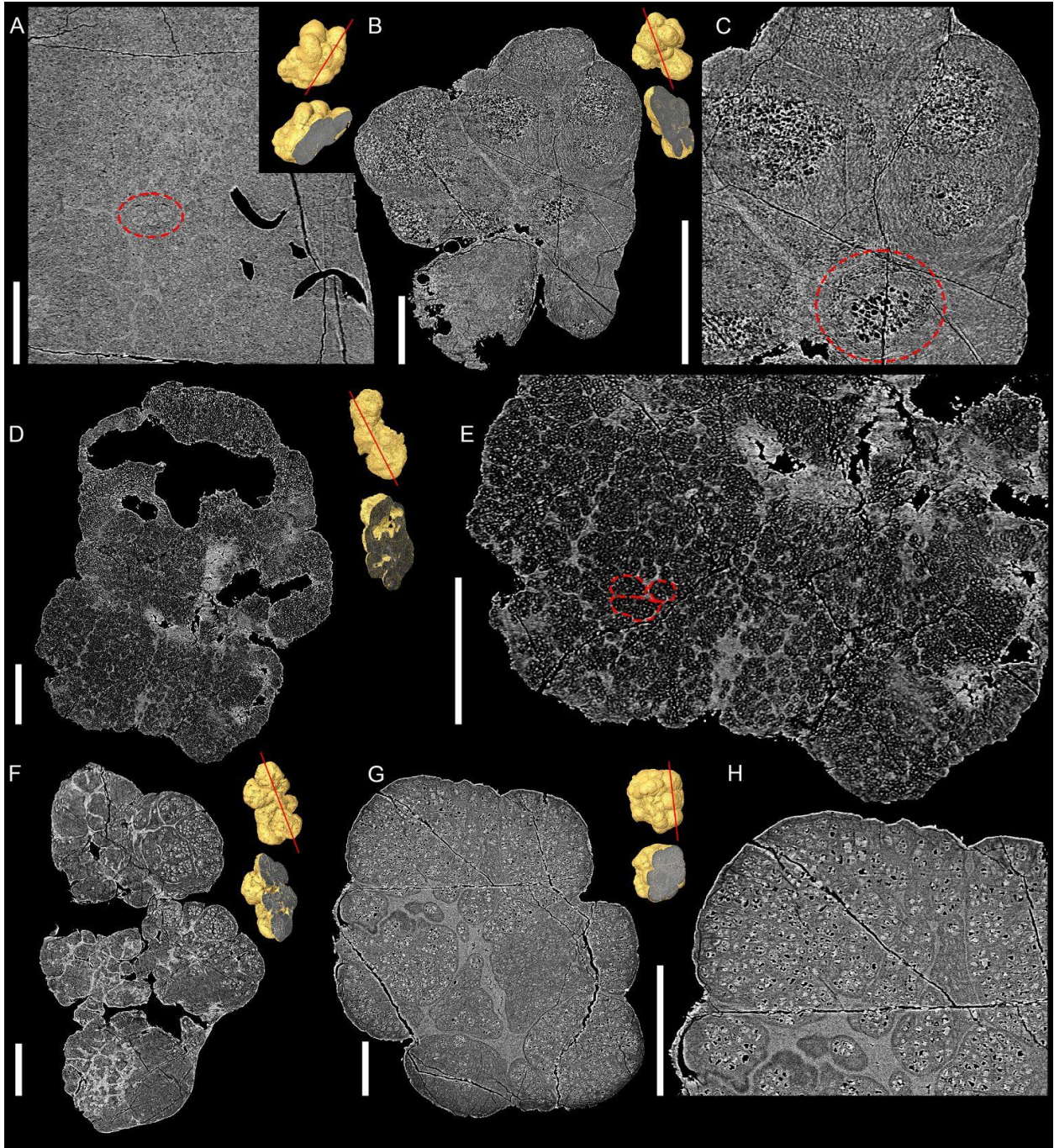
Figure 3.10. Orthoslices showing histology of morphotype 2. (A) Orthoslice of specimen ZY1216_04, showing cell islands surrounded by vegetative cells (red circle). (B) Orthoslice of specimen ZY1811_07. (C) Close-up of (B), showing cell islands surrounded by a halo of smaller cells (red circle). (D) Orthoslice of specimen ZY1804_15. (E) close-up of (D), showing tightly

clustered cell islands (examples highlighted by red circles). (F) Orthoslice of specimen ZY1811_10. (G) Orthoslice of specimen ZY1216_22. (H) close-up of (G) showing division into subunits and vesicle-like structures. Scale bars are 200 μm.
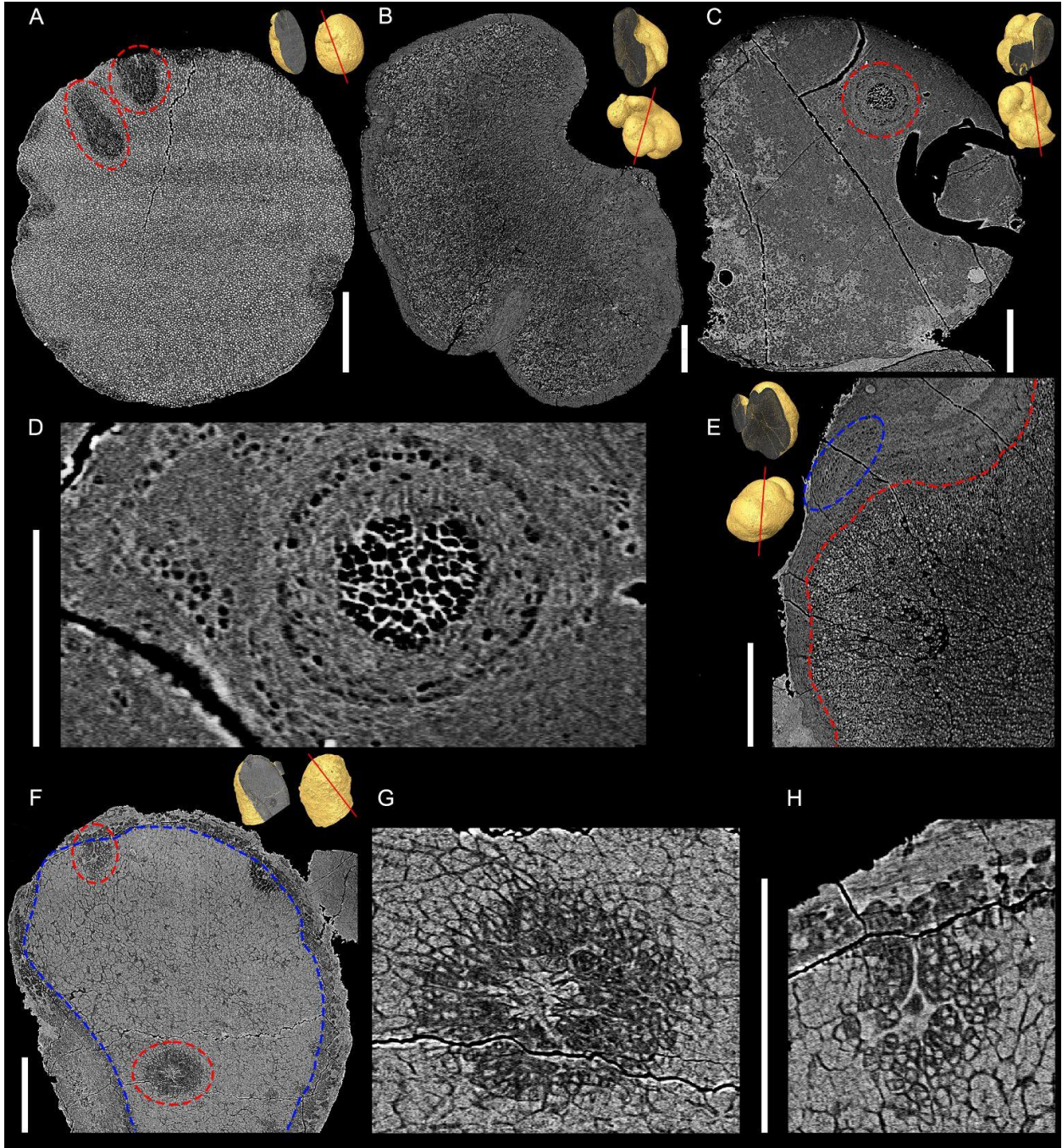
Figure 3.11. Orthoslices showing histology of morphotype 3. (A) Orthoslice of specimen JC_55d, showing elongate cell islands at the margin of the specimen (indicated in red). (B) Orthoslice of the larger alga in specimen ZY1701_06. (C) Orthoslice of the smaller alga in specimen ZY1701_06. (D) close-up of (C) showing the cell island and its halo of smaller cells

(red circle). (E) close-up of (B) showing cortex-medulla differentiation (boundary shown by red dashed line). The blue ellipse highlights an area where the elongated shape of the cortical cells can be clearly seen. (F) Orthoslice of specimen JC_62d, showing cell islands (red circles) and cortex-medulla differentiation (boundary indicated by blue dashed line). (G) close up of (F) showing the cell island in the medullary region. (H) close up of (F) showing the cell cell island just underneath the cortical region. Scale bars are 200 μm.
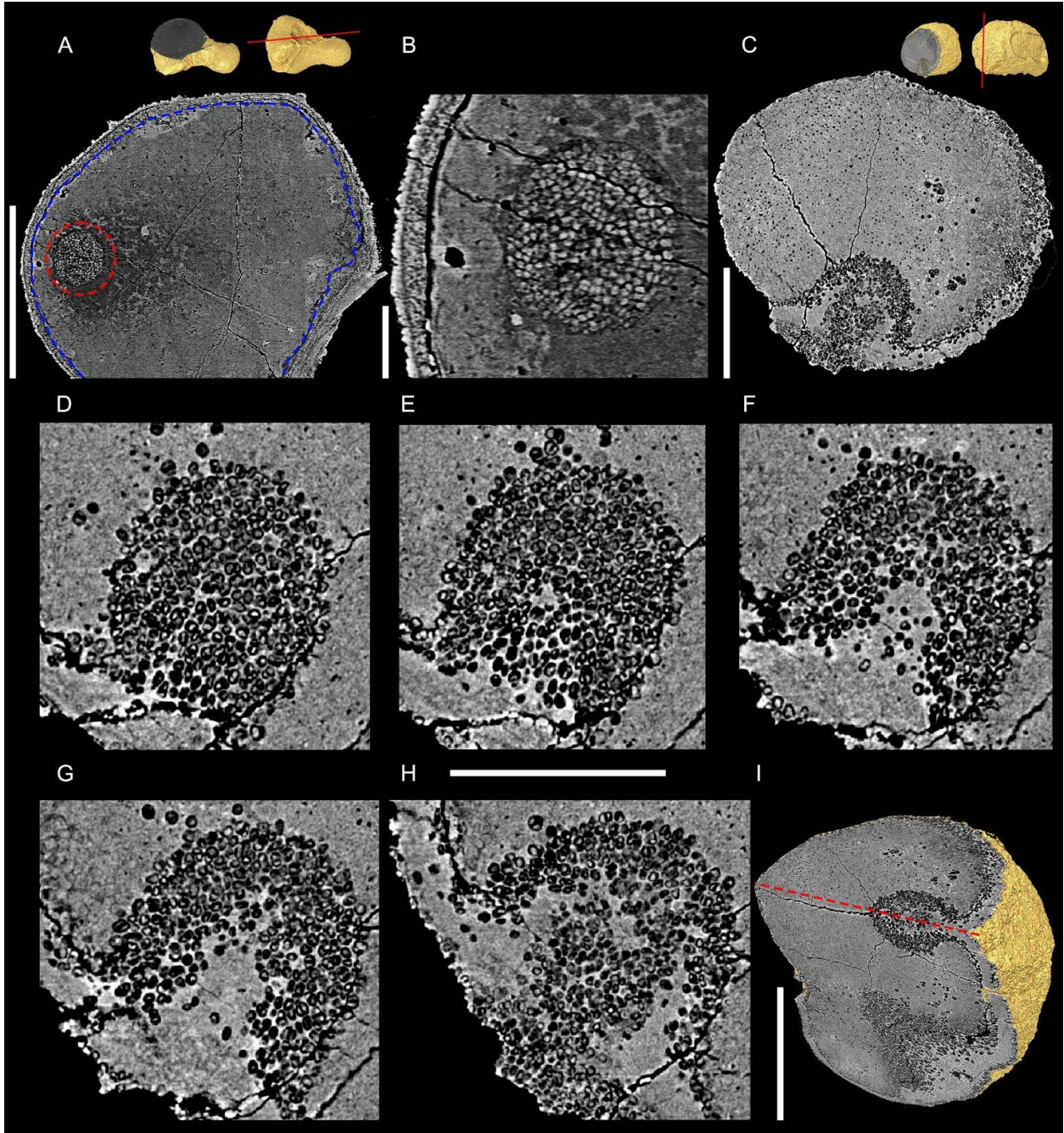
Figure 3.12. Orthoslices showing histology of morphotype 3. (A) Orthoslice of specimen JC_58f, showing a cell island (red circle) and cortex-medulla differentiation (boundary indicated by blue dashed line. (B) close up of (A), showing the cell island. (C) Orthoslice of specimen JC_56f showing a cup shaped cell island with a mass of cells protruding from its base at the centre. (D-H) Close ups of (C), showing the cell island. (I) Intersecting orthoslices of (C), clipping an

isosurface. The red dashed line indicates the line of intersection. (A, C, I) Scale bar is 200 μm;

(B) Scale bar is 20 μm; (D-H) scale bar is 10 μm.

3.4 Discussion

3.4.1 Taxonomic implications

The three different morphotypes show a great deal of similarity in terms of both their external morphology and their histology. Each morphotype differs externally in the number and size of lobes and can be roughly sorted on that basis, but histologically they intergrade with one another.

None of the morphotypes show any evidence of any sort of attachment structure. The multilobate specimens (morphotypes 1 and 2) tend not to show any preferred orientation of growth, with their lobes protruding in all directions, where the specimens with few or no lobes (morphotype 3) had a preferred axis of growth. In terms of their histology, morphotype 1 is the only morphotype that shows no evidence of either cortex-medulla differentiation or cell islands. Both morphotype 2 and morphotype 3 exhibit the same range of histologies, with cortex-medulla differentiation and cell islands. Both of these morphotypes also include specimens that have neither cortex-medulla differentiation nor cell islands, as with the histologies demonstrated by morphotype 1. Morphotype 1 and 2 also include specimens that histologically are very distinct from all the other specimens in the sample, being divided into distinct irregularly shaped subunits containing a number of vesicle-like structures (Figure 3.8H-I; Figure 3.10F-H).

If histology and external morphology are considered separately, most of the specimens can be assigned readily to existing taxa. On the basis of external morphology, morphotypes 1 and 2 can be assigned to *Gremiphyca* and *Thallophycoides*, and morphotype 3 to *Paramecia* following the classification laid out by Xiao et al. (2004). However, on the basis of histology, the specimens

99

that lack cortex-medulla differentiation and cell islands are attributable to *Wengania*, *Gremiphyca* and *Thallophycoides*, all of which have a very similar histology, while the specimens that possess cortex-medulla differentiation and cell islands can be attributed to *Thallophyca* and *Paramecia*. The exceptions to this are the specimens with an internal arrangement into distinct subunits, which cannot be attributed to any currently existing taxa on the basis of histology, but can still be assigned to *Gremiphyca* or *Thallophycoides* on the basis of external morphology. Clearly, when histology and external morphology are considered together, these taxonomic assignments are not compatible.

Although none of the specimens we examined match *Wengania* in both histology and external morphology, many of the cell islands present in specimens of Morphotype 2 and 3 are otherwise indistinguishable in terms of size and shape from free-living specimens previously attributed to *Wengania*. This is not the case for all specimens that possess cell islands. Several are more elongate than free-living *Wengania* (Figure 3.11A), and the cell island in specimen JC_56f (Figure 3.12C-I), does not preserve a uniform mass of cells throughout the cell island, but rather a cup shaped structure with a mass of cells in the centre, surrounded by void fill.

Given the above, *Thallophyca, Paramecia, Thallophycoides, Gremiphyca* and *Wengania* should be synonymised, in which case, *Thallophyca* is the senior synonym, on the basis of being the first described in Zhang (1989), in which *Thallophyca* and *Wengania* were both introduced. The specimens that form internal subunits are a distinct taxon and should be treated separately.

It is clear that both internal and external anatomy should be used together when possible for determining the taxonomic criteria for the Weng'an algae, as we see here that one histologically distinct taxon would be assigned to a completely different taxon if only its external morphology was considered. However, if as we suggest below in section 3.4.2, and as has been previously discussed by Xiao et al. 2004, certain of the Weng'an algae are different parts of one life cycle, their histology changes during the course of their life history, making its taxonomic utility less reliable on its own.

3.4.2 Developmental biology

Xiao et al. (2004) have previously suggested that some of the Weng'an taxa are different parts of one life cycle rather than separate taxa. In particular, they suggest that *Wengania* may be a juvenile form of either *Gremiphyca* or *Thallophycoides*, on the basis of similar cell size and organisation. The cell islands found in *Thallophyca* and *Paramecia* are also held up as evidence for a potentially multiphasic life cycle, interpreted as cystocarps with enclosed carpospores (Zhang and Yuan, 1996; Xiao et al. 1998; Zhang et al. 1998), structures which are borne on female gametophytes in extant florideophyceaen rhodophytes, and are unique to Rhodophyta.

Extant Florideophyceae have a triphasic life cycle, consisting of a haploid sexual phase (the gametophyte), a diploid phase that develops directly on the female gametophyte (the carposporophyte), and a free-living diploid phase bearing the meiospores that will go on to produce the gametophytes (the tetrasporophyte) (Figure 3.13A). The carposporophyte and surrounding gametophytic tissues that become modified to support the developing carpospores are collectively known as the cystocarp (Hommersand and Fredericq, 1990; Figure 3.13B).

Within the cystocarp, the carposporangia form on filaments called gonimoblasts, produced as a result of fertilisation.
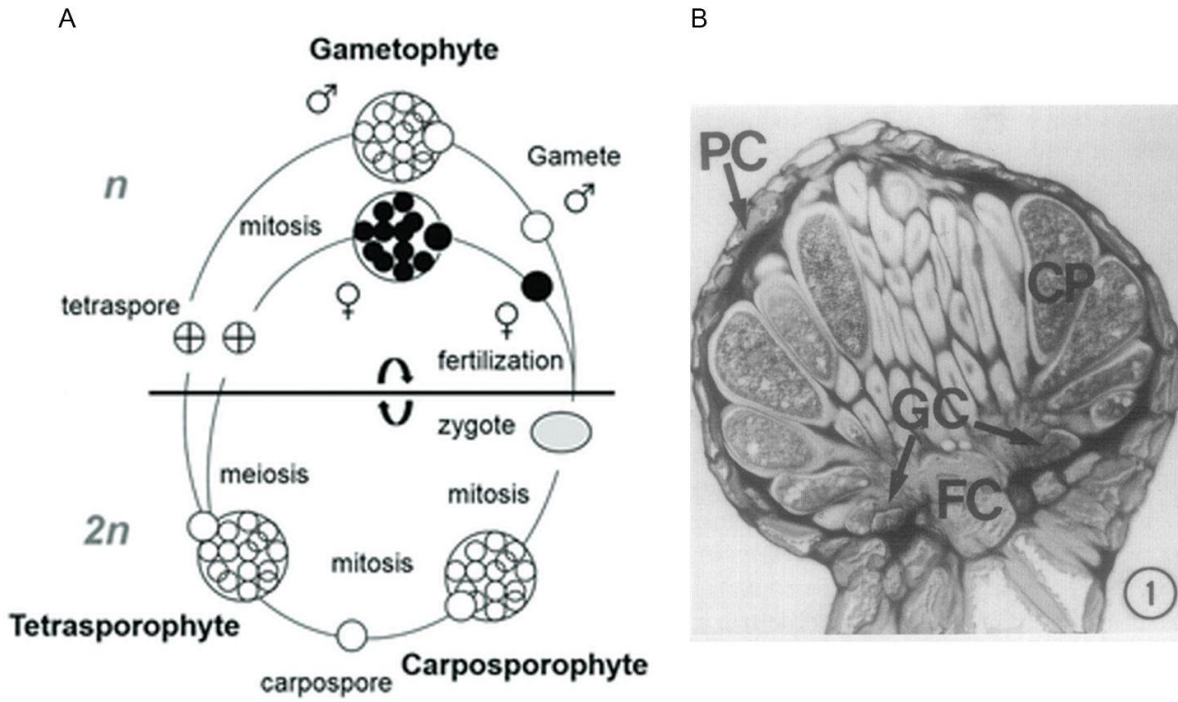
Figure 3.13. (A) Generalised life cycle of the Florideophyceae. The horizontal line separates the haploid (n) from the diploid (2n) phases. Modified from de Bettignies et al. (2018). (B) Developing cystocarp of the red alga *Polysiphonia.* The pericarp (PC) encloses the developing carposporophyte, which includes the fusion cell (FC), gonimoblast cells (GC) and carpospores (CP). Magnification x 400. Image from Weatherbee (1980).

Although the cell islands seen in *Paramecia* and *Thallophyca* are interpreted as carposporangia, they do not show any evidence of the structures associated with carposporangia in extant Florideophyceae. In particular, there is no evidence for the presence of gonimoblasts on which the carposporangia form, nor is there evidence of a cystocarp. Instead the cell islands are scattered among the (presumably) vegetative cells of the thallus (Figure 3.10D-E; Figure 3.11F-G), distinguished by size and mineral density but not by any unique structure. This is reminiscent of zygotosporangia (Figure 3.14A, B), the equivalent of carposporangia in Bangiophyceae, which have a biphasic life cycle that does not involve a carposporophyte (Figure 3.14C). Instead, Bangiophyceae alternate between a haploid gametophyte phase and a diploid sporophyte phase, often called the conchocelis phase (West and Hommersand, 1981). However, modern bangiophytes produce zygotosporangia in great quantity along the thallus periphery, whereas the Weng'an algae possess comparatively few cell islands, only one or two in some specimens.
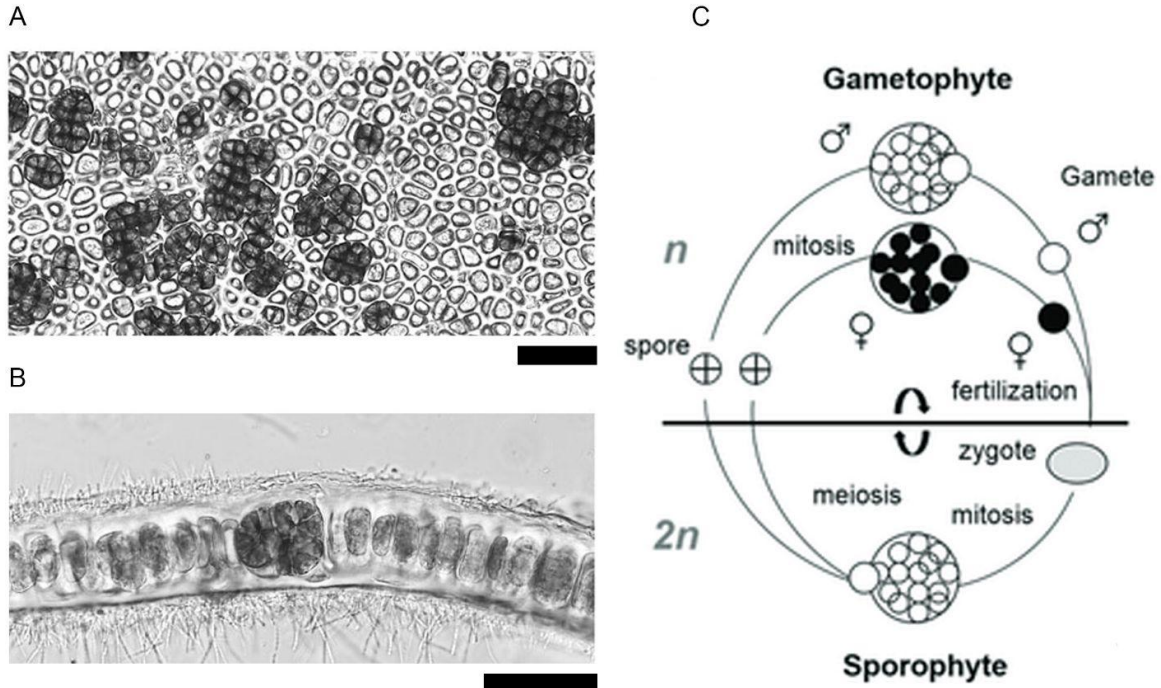
Figure 3.14. (A) Zygotosporangial region of a *Pyropia* thallus. The large dark cells are the zygotosporangia, surrounded by smaller vegetative cells. Image from Harden et al. (2016). Scale bar is 50 μm. (B) Cross section of *Pyropia* zygotosporangium and vegetative cells. Image from Harden et al. (2016). Scale bar is 50 μm. (C) Generalised life cycle of the Bangiophyceae. The horizontal line separates the haploid (n) from the diploid (2n) phases. Modified from de Bettignies et al. (2018).

The cell islands could alternatively be interpreted as tumours, which have been observed in red algae as a response to pathogens (Tsekos, 1982). However, tumours generally consist of cells that are irregularly sized and shaped, and the cell cluster that makes up a tumour generally has poorly defined boundaries (e.g figure 1a, b, d in Tsekos 1982), unlike the cell islands in the Weng'an algae, in which the cells are uniformly sized and shaped and there is a clear boundary between the cell islands and the surrounding vegetative tissue.

The cell islands could also be interpreted as conceptacles, reproductive structures found in brown algae and some red algae, and many of the cell islands do have a conceptacle-like shape, enclosing the putative sporangia. However, conceptacles form at the margins of the thallus, which we only observe in the cell island in some specimens (e.g. Figure 3.11A, F; Figure 3.12C-I), however in many specimens the cell islands are embedded in the medullary regions of the thallus, which is not compatible with a conceptacle interpretation.

Another interpretation is that the cell islands represent clusters of algal cells within a lichen thallus. However, none of the specimens have any structures within their thalli that could be interpreted as fungal hyphae, making a lichen affinity unlikely.

The cell islands within *Paramecia* and *Thallophyca* also bear a resemblance to *Wengania*, in both shape and cell organisation, and they fall within the size range exhibited by specimens of *Wengania*. An alternate hypothesis, therefore, is that rather than being sporangia, the cell islands have budded from the parent in their entirety, to form free-living *Wengania*, which then go on to develop into a *Thallophyca*/*Paramecia* adult form, making these taxa different parts of one life

cycle. *Gremiphyca* and *Thallophycoides* are also compatible with this life cycle, exhibiting a more lobate morphology than *Wengania,* but not yet exhibiting the daughter cell islands that characterise *Thallophyca* and *Paramecia.* This method of reproduction, by which cell clusters are ejected from the parent organism, has been described in other fossil remains from the same deposit (Cunningham et al. 2016), who noted that the cell clusters are similar to multicellular propagules released by extant red algae such as *Gracilaria* and *Hildenbrandia*. The fossil described by Cunningham et al. (2016) also shows evidence of scars left behind when the cell clusters are ejected, which is not a feature that we have seen on any of the algal fossils. Cunningham et al. (2016) note that the cell islands within the fossil they describe could instead be exogenous organisms that are parasitic, and the exit scars are rather entrance scars. This interpretation could also be true of the cell islands in the algae, and it cannot be conclusively ruled out.

Of those specimens that show no cell islands, most exhibit vegetative cells only. Some specimens (e.g. Figure 3.10D-E) contain structures that could be interpreted as endosporangia or monosporangia. Monosporangia are present in both Bangiophyceae and Florideophyceae, while endosporangia occur only in the Bangiophyceae. These structures produce monospores as a result of mitosis, which then give rise to either gametophyte or sporophyte clones depending on which generation produced the initial monospore. Monosporangia produce spores either singly or in packets of up to 16 spores, whereas endosporangia form irregular clusters of spores of indefinite number (Guiry 1990).

We therefore propose a life cycle for *Thallophyca* in which the alga starts out as a free living *Wengania*-type juvenile, develops into the more lobate *Gremiphyca/Thallophycoides* form, and then develops daughter *Wengania*-type cell islands, which grow within the thallus before being ejected from the parent to grow to adulthood (Figure 3.15). We cannot determine whether the daughter cell islands are produced through asexual or sexual reproduction, but it is possible that *Thallophyca* had a multiphasic life cycle somewhat similar to extant red algae, with a gametophytic phase and a sporophytic phase, given it produced the daughter cell islands and there is evidence of possible monospores as well.
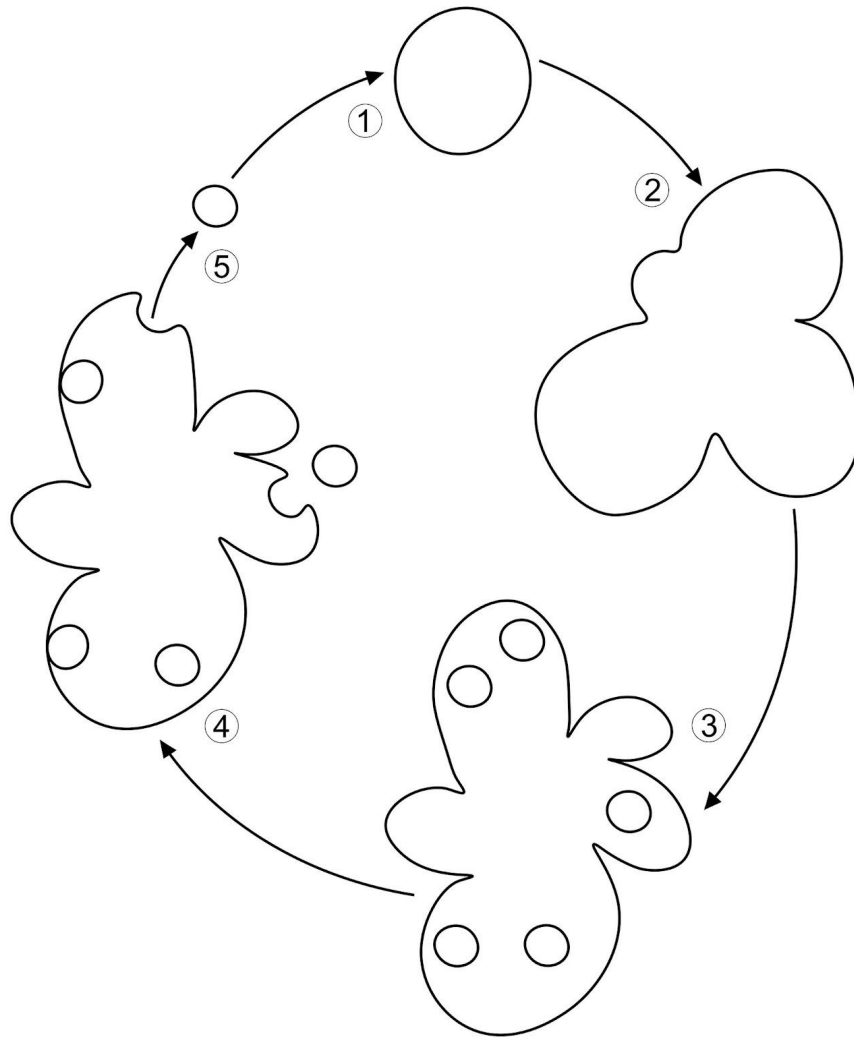
Figure 3.15. Hypothesised life-cycle for *Thallophyca*. (1) *Wengania*-type juvenile. (2) *Gremiphyca/Thallophycoides*-type juvenile. (3) *Paramecia/Thallophyca*-type adult, with *Wengania*-type cell islands. (4, 5) cell islands are released to become free-living *Wengania*-type juveniles.

3.4.3 Phylogenetic affinity

In an attempt to constrain the affinity of the Weng'an algae we used the character matrix from Gabrielson et al. (1985) together with the topology from Yoon et al. (2006) and Le Gall and Saunders (2007) in an attempt to resolve the pattern of character evolution in Rhodophyta under a parsimony ACCTRAN model in Mesquite (Maddison and Maddison, 2019) (Figure 3.16). The matrix from Gabrielson et al. (1985) is reasonably comprehensive, although several new florideophyte orders have since been erected and Bangiophyaceae is now recognised as paraphyletic with respect to Florideophyaceae. Consequently, some orders have been moved to new classes and in some cases renamed. Notably, the matrix omits the order Cyanidiales, instead considering it part of Porphyridiales. However, in subsequent studies (Saunders and Hommersand, 2004; Yoon et al. 2006) which recognise Cyanidiales, this group consistently resolves as a sister to the rest of the red algae. Of the groups included in Gabrielson et al. (1985), Porpyridiales is the only group that is not monophyletic.

Of the characters used in Gabrielson et al. (1985), the only ones that the Weng'an algae definitively possess are multicellularity, organised thalli, and sporangia. Many of the characters cannot be observed in the fossils, such as which pigment proteins they use, and the presence and nature of organelles. The three characters that are observable in all of the Weng'an algae are primitive to Rhodophyta, as all rhodophyte groups except Porphyridiales are multicellular, with organised thalli, and produce sporangia. This analysis consequently can only be used to place the Weng'an algae in total-group Rhodophyta.

109

A

Porphyridiales
ⓑ Rhodochaetales
ⓒ Compsopogonales
ⓓ Erythropeltidales
Bangiales
Hildenbrandiales
ⓘ Palmariales
ⓚ ⓜ Acrochaetiales
Nemaliales
ⓙ Batrachospermales
Corallinales
ⓝ Bonnemaisoniales
ⓢ ⓣ Gigartinales
ⓠ Rhodymeniales
ⓡ Gelidiales
ⓟ Ceramiales

ⓐ GAIN: multicellularity; organised thalli; pseudofilamentous construction; diffuse growth; pit connections; sporangia; filamentous thallus organisation

ⓑ LOSS: multicellularity; organised thalli; pit connections; sporangia

ⓒ GAIN: filamentous construction; apical growth, sexual reproduction; filamentous spermatangial/carposporangial structure; oblique spermatangial division; macroscopic female gametophyte; isomorphic life history

ⓓ LOSS: pit connections

ⓔ GAIN: filamentous construction; apical growth; cellulose; pit plugs; one-layer plug caps; sexual reproduction; oblique spermatangial division; macroscopic female gametophyte; heteromorphic life history

ⓕ GAIN: parenchymatous spermatangial/carposporangial structure

ⓖ GAIN: cruciately dividing tetrasporangia; pseudoparenchymatous thallus organisation

ⓗ GAIN: zonately dividing tetrasporangia
LOSS: sexual reproduction

ⓘ GAIN: two-layer plug caps; morphologically differentiated carpogonium; morphologically differentiated carpogonial branch; filamentous gonimoblast; filamentous spermatangial/ carposporangial structure; isomorphic life history
LOSS: one-layer plug caps

ⓙ LOSS: tetrasporangia

ⓚ LOSS: morphologically differentiated carpogonial branch

ⓛ GAIN: microscopic female gametophyte
LOSS: macroscopic female gametophyte; heteromorphic life history

ⓜ GAIN: filamentous thallus organisation
LOSS: pseudoparenchymatous thallus organisation

ⓝ GAIN: zonately dividing tetrasporangia; calcite
LOSS: cruciately dividing tetrasporangia; heteromorphic life history

ⓞ GAIN: auxiliary cell
LOSS: plug caps

ⓟ LOSS: heteromorphic life history

ⓠ LOSS: heteromorphic life history

ⓡ GAIN: one-layer plug caps; transverse spermatangial division
LOSS: morphologically differentiated carpogonial branch; auxiliary cell

ⓢ LOSS: auxiliary cell

ⓣ GAIN: zonately dividing tetrasporangia

Figure 3.16. (A) Rhodophyte character acquisitions and losses. (B) Parenchymatous gametophyte of *Porphyra olivii*. Image from Brodie et al. (2007). Scale bar is 2 cm. (C)

Filamentous tetrasporophyte of *Polysiphonia sabulosia.* Image from Kim and Kim (2014). Scale

bar is 2cm. (D) *Palmaria palmata,* pit plug with plug cap (Ca) composed of inner (1) and outer

(2) layers. The cell membrane (P) is continuous along the edges of the plug core (Co).

Magnification x 93,000. Image from Pueschel and Cole (1982). (E) Tetrasporangia in

Polysiphonia amplacapilli. Arrowhead shows two tetrasporangia in a segment. Scale bar is 100

μm. Image from Kim and Kim (2014).

Xiao et al. (2004), in their review of the Weng'an algae, considered three characters phylogenetically significant when attempting to reconcile their affinity as florideophytes: their possession of structures interpreted as carposporangia, pseudoparenchymatous thallus construction, and apical growth. Apical growth is a primitive feature of multicellular rhodophytes, observed in both the bangiophyceae and the compsopogonophyceae, and is not unique to florideophyceae. Possession of pseudoparenchyma is a feature that the florideophyceae do not share with other red algae. Bangiales are generally considered parenchymatous (at least in their gametophyte life phase) (Saunders and Hommersand 2004), and the other non-florideophyte red algae are generally filamentous. If the Weng'an fossils could be definitively proven to have pseudoparenchyma, this would be grounds for placing them within the florideophyceae, however the fossil evidence is not enough to distinguish whether the Weng'an algae were parenchymatous or pseudoparenchymatous.

The strongest evidence for a florideophyte interpretation would undoubtedly be possession of carposporangia, which are unique to the florideophyceae. Xiao et al. (2004) interpret the cell islands found in some specimens as carposporangia, and this is consequently the main basis for assigning the Weng'an algae to this clade. However, there are problems with this interpretation, namely that carposporangia and the carposporophytes that bear them, are complex structures, and the fossils are missing a lot of this complexity. The majority of cell islands observed do not have the general morphology of a carposporophyte, and lack any evidence of possessing gonimoblasts - the filaments on which the carposporangia form. The cell islands of the Weng'an algae more closely resemble zygotosporangia, making a Bangiophyceae interpretation more probable, though this has problems of its own - in particular, a given bangiophyte thallus will produce a

112

great many zygotosporangia along its periphery, whereas the Weng'an algae produce comparatively few cell islands, in some specimens only one or two. Further, of the two taxa of Weng'an algae, only one shows evidence of cell islands - the other lacks any definitive features that would place it in either Bangiophyceae or Florideophyceae.

It is possible that the Weng'an algae do not fall within Rhodophyta at all. Both Phaeophyta (brown algae) and Chlorophyta (green algae), possess organised multicellular thalli and sporangia, and although Xiao et al. (2004), rejected a brown algal hypothesis for the Weng'an algae partially on the basis of their lacking true parenchyma, as discussed above the fossil evidence is not strong enough to distinguish whether the Weng'an algae were parenchymatous or pseudoparenchymatous. However, the Weng'an algae lack common phaeophyte features such as plurilocular sporangia (in which the sporangia are divided into chambers), and conceptacles - although the cell islands have in some cases a conceptacle-like morphology, their placement within the thallus is not compatible with a conceptacle interpretation. Xiao et al. (2004) also reject a green algal affinity on the basis of differences in thallus organisation - in particular, the Weng'an algae lack the nodal-internodal construction characteristic of charophycean green algae. Additionally, although green algae produce sporangia, those produced by non-charophycean multicellular green algae (e.g. ulvophyceans) are little differentiated from the vegetative cells (Maggs and Callow, 2003), unlike the cell islands of the Weng'an algae. Although both the carposporangial and zygotosporangial interpretations of the cell islands are problematic, they do bear resemblance to vegetative propagules produced by certain rhodophytes such as *Hildenbrandia* (figure 1-10 in Sherwood and Sheath, 2000).

We therefore place the Weng'an algae in total group Rhodophyta, as they do not possess features that tie them unequivocally to any modern rhodophyte group, but do show evidence of features that tie them to Rhodophyta rather than Chlorophyta or Phaeophyta.

3.4.4 Evolutionary significance

Given the life cycle that certain of the Weng'an algae seem to exhibit, they clearly have an extended period of embryonic development, reflecting the adverse conditions in the Ediacaran, both temporally and spatially. This is similar to the pattern we see in other Ediacaran organisms (Cohen et al. 2009, Yin et al. 2018, Landon et al. 2019) of having encysted developmental stages to ride out periods of adverse conditions.

Various molecular divergence time analyses have used the Weng'an algae to calibrate the bangiales/florideophyte divergence, on the basis of their being the first appearance of florideophyte algae in the fossil record (Yoon et al. 2004, 2006, 2010; Yang et al. 2016; Parfrey et al. 2011; Sharpe et al. 2015). However, none of the Weng'an algae can be described as crown group florideophyceae with any certainty; at best they fall into total-group Rhodophyta, and therefore cannot be used to calibrate the appearance of the florideophyte clade. As a consequence, it is likely that the bangiales/florideophyte divergence is younger than current molecular divergence time analyses predict, and the florideophyte clade is younger than thought. With the removal of the Weng'an algae to total-group Rhodophyta, the oldest known examples of florideophyceans are the solenoporacean algae, which have been reported from the Cambrian, but are known more definitively from the Ordovician through to the Miocene (Brooke and Riding, 1998).

3.5 Conclusions

Our observations show that our specimens can only be assigned to existing taxa if their histology and external morphology are considered separately. Considered together, these taxonomic assignments are not compatible. We consider the Weng'an algae *Thallophyca, Wengania, Thallophycoides, Paramecia* and *Gremiphyca* to be different parts of a single developmental cycle rather than separate taxa, and accordingly we synonymise them as *Thallophyca.* This life cycle involves the alga growing daughter 'cell islands' within itself and then ejecting them into the environment, and may also include a spore producing phase. The biota also includes one unnamed algal taxa different to any previously described. The Weng'an algae cannot definitively be placed in either crown Florideophyceae or crown Bangiophyceae, and we instead place them in total-group Rhodophyta.

3.6 Systematic Palaeontology

Genus *Thallophyca* Zhang Y., 1989, emend.

Thallophyca Zhang Y. 1989, p. 125

Wengania Zhang Y. 1989, p. 129

Thallophycoides Zhang Y. and Yuan X., 1992, p. 16-17

Gremiphyca Zhang et al. 1998, p. 46

Paramecia Zhang Y. and Yuan X., 1992, p. 18

Type species. *Thallophyca ramosa* Zhang Y., 1989, emend.

115

Emended diagnosis. The juvenile form has a lobate or spheroidal thallus, with spheroidal cells either regularly arranged in cell rows or irregularly arranged. The adult form has a lobate, spheroidal or nodular thallus differentiated into distinct cortical and medullary tissues distinguished by differences in cell size and orientation, with cortical cells being smaller and oriented parallel to the thallus surface. Medullary cells are larger and more variable in shape. Spheroidal clusters of morphologically distinct cells appear within medullary or cortical regions of the thallus in some specimens.

Discussion. Generic diagnosis emended to embrace *Wengania, Thallophycoides, Gremiphyca* and *Paramecia*, which we consider synonymous. Variation is considered developmental rather than taxonomic.

Thallophyca ramosa Zhang Y., 1989, emend.

Thallophyca ramosa Zhang Y., 1989, p.125, fig. 6-8, 11A-C, 12

Thallophyca corrugata Zhang Y. and Yuan X., 1992, p.16, fig. 8A-D

Wengania globosa Zhang Y., 1989, p.129, fig. 13A-C

Wengania exquisita Zhang et al. 1998, p. 45, fig. 15.1-15.4

Thallophycoides phloeatus Zhang Y. and Yuan X., 1992 p.16-17, fig. 9B, D, F

Gremiphyca corymbiata Zhang et al. 1998, p. 46, fig. 20.1-20.3

Paramecia incognata Zhang Y. and Yuan X. 1992, p.18, fig. 21, 23

Emended diagnosis. As for the genus.

Chapter 4: Experimental and comparative taphonomy of Weng'an embryoids and Kuanchuanpu animal embryos

Project design: E. Landon, P. Donoghue, E. Raff, R. Raff, R. Turner; Materials: E. Landon, P. Donoghue, E. Raff, R. Raff, R. Turner; Data collection: E. Landon (fossil data), E. Raff, R. Raff, R. Turner (decay experiments); Analysis: E. Landon (fossils and decay experiments), E. Raff, R. Raff, R. Turner (decay experiments); Interpretation: E. Landon with contributions from P. Donoghue; Writing: E. Landon wrote the text to which P. Donoghue contributed edits, with the exception of sections 4.2.2, 4.3.2, and 4.4.2, in which the first drafts were written by E. Raff, R. Raff and R. Turner, to which E. Landon contributed edits.

4.1 Introduction

Molecular clocks estimate that metazoans originated in the early Neoproterozoic, well before the first definitive fossil evidence of metazoans in the Cambrian and potentially the late Neoproterozoic. dos Reis et al. (2015) estimate metazoans to have diverged sometime within a Tonian-Cryogenian interval, and bilaterians within a Cryogenian-Ediacaran interval. However, there are no definitive fossil metazoans until late in the Ediacaran, and no definitive fossil bilaterians until the Cambrian (Cunningham et al. 2017a). It remains unclear whether molecular clock estimates are unrealistically old or else the fossil record grossly underestimates the age of these fundamental metazoan clades (Cunningham et al. 2017a). The Ediacaran Weng'an biota has elicited considerable interest because this site of exceptional fossil preservation provides a window onto marine biodiversity during this critical interval. The age of the biota is uncertain,

certainly older than ~555 Ma (Condon et al. 2005) but it is not clear whether it pre-dates (Zhou et al. 2017) or post-dates (Condon et al. 2005) the Gaskier's glaciation with the oldest estimates suggesting that it is older than ~609 Ma (Zhou et al. 2017). In either instance, these dates place the Weng'an biota within a critical temporal window - postdating molecular clock estimates for the origin of animals but prior to the late Ediacaran-Phanerozoic fossil record of animal evolution. As such, it provides a basis for testing between these two scenarios for timescale of early animal evolution.

Unfortunately, the phylogenetic interpretation of almost every component of the Weng'an biota is the subject of controversy (Cunningham et al. 2017b). This is especially true of the millimetre scale embryo-like fossils that dominate the biota - so much so that in some localities and horizons, they are rock-forming. The most common of these fossils, attributed to the taxa *Megasphaera, Megaclonophycus, Parapandorina* and *Tianzhushania*, resemble the early cleavage stages of animal embryonic development, preserving sequences of binary reductive cell division from one to perhaps thousands of cells (Xiao et al. 1998; Hagadorn et al. 2006; Huldtgren et al. 2011). Preservation extends beyond cell membranes, to nuclei, some fossilized in the process of nuclear division (Hagadorn et al. 2006; Huldtgren et al. 2011; Yin et al. 2017; Sun et al. 2020). Similarity to animal embryos inspired interpretation as such, apparently evidencing the presence of animals in the early Ediacaran (Xiao et al. 1998), perhaps attributable to bilaterian and non-bilaterian animal phyla (Chen J. et al. 2000; 2002; 2009a; 2009b). However, absence of evidence of gastrulation has also been used to argue for a stem-metazoan affinity (Hagadorn et al. 2006; Chen L. et al. 2014) or a non-metazoan holozoan affinity (Huldtgren et al. 2011). They have also been compared to giant sulfur bacteria (Bailey et al.

2007; refuted by Cunningham et al. 2012b) and volvocalean green algae (Xue et al. 1999; Chen L. et al. 2014). Since these fossil remains are limited to early developmental stages comprised of simple geometric arrangements of cells, it is difficult to discriminate between these competing interpretations in the absence of the later adult stages predicted by the animal-embryo interpretation (though see Raff et al. 2006; Gostling et al. 2009).

Here I try to test the hypothesis of the animal embryo interpretation of the Weng'an embryoid fossils through comparative taphonomy. I do this in two main ways: (i) by comparison to the taphonomy of undoubted animal embryos from the Kuanchuanpu Formation, an early Cambrian lagerstatten that occurs higher in the same stratigraphic sequences in South China, preserving a variety of developmental stages attributed to cnidarians, including cleavage stages (Steiner et al. 2004b, 2014; Donoghue et al. 2006; Dong et al. 2013, 2016; Duan et al. 2017); (ii) by comparison to decay experiments of animal embryos. Animal embryos have been the subject of taphonomy experiments previously (Raff et al. 2006, 2008; Gostling et al. 2008, 2009), however, these have focussed on the very earliest stages of cleavage (1-8 cells) or larvae. Here I focus on later cleavage stage embryos composed of tens of cells, more comparable to the (potentially) most informative developmental stages from Weng'an, as well as the early Cambrian cleavage stage embryos from the Kuanchuanpu biota.

4.2 Methods

4.2.1 Comparative taphonomy of Kuanchuanpu animal embryo fossils

I used a combination of backscattered electron imaging (BSE), electron probe microanalysis (EPMA) and synchrotron radiation X-ray tomographic microscopy (SRXTM) to characterise the preservation of the Kuanchuanpu embryos, in order to compare them to the results of a study of the Weng'an embryoids by Cunningham et al. (2012a).

BSE allows high resolution examination of texture and some aspects of chemistry, and so BSE can be used to characterise texture, general chemistry, and patterns of crystal growth. SRXTM also allows high resolution examination of texture, and also allows me to characterise internal structures of the fossils in three dimensions, providing information on morphology and structure. EPMA allows me to map the distribution of elements across specimens, and provides detailed chemical information, allowing us to distinguish between different phases of the same mineral.

I used these techniques to determine: the number of mineral phases present in the Kuanchuanpu embryos, and the chemistry of each phase; whether a given phase preserves original biological structure or is void filling; whether the phases present in Kuanchuanpu are the same as those present in Weng'an, and if so, was the order of mineralisation the same in both biotas, and do these phases preserve the same sorts of structures in both biotas? Given the similar diagenetic histories of the two formations, I would expect the Kuanchuanpu embryos and the Weng'an embryoids to preserve the same or similar structures and features, in the same mineral phases.

The specimens were recovered from phosphoritic dolomite from the early Cambrian Kuanchuanpu Formation at the Shizhonggou Section in Ningqiang County, Shaanxi Province, China. The samples were processed through acid digestion using 10% technical grade acetic acid (following Müller 1985) and manually picked from the residue under a binocular microscope.

For BSE and EPMA analyses, specimens were embedded in epoxy resin and ground down to the level of interest using decreasing grades of silicon carbide paper before being polished using first 6μm then 1μm diamond paste. The samples were then carbon coated, and EPMA analyses were carried out on a JEOL JXA8530F hyperprobe with a typical voltage of 15-20kV and dwell time of 100ms. BSE analyses were carried out on a Hitachi S-3500N SEM at a voltage of 15-20kV.

SRXTM experiments were carried out at the X02DA (TOMCAT) beamline of the Swiss Light Source at the Paul Scherrer Institute, Villigen, Switzerland. SRXTM data were obtained using a 20X objective lens, yielding reconstructed tomographic data with voxel dimensions of 0.325 μm, at energy levels of 14-18 keV, exposure times of 200-220 ms, and scintillators composed of lutetium, aluminium and garnet. 1501 projections were taken through 180° of rotation within the beam, which were then post-processed and rearranged with flat and dark-field-corrected sinograms. Reconstruction was done on a 60 core Linux PC farm, using a routine based on the Fourier transform method and a regridding procedure (Marone et al. 2017). Slice data were analysed using AVIZO (www.thermofisher.com).

4.2.2 Experimental Taphonomy

Embryos of the sea urchin *Heliocidaris erythrogramma* were used as a model because they are direct developers with large, yolky eggs, comparable in size to the Weng'an embryoids and Kuanchuanpu embryos. This organism was used in previous embryo taphonomy experiments for this reason (Raff et al. 2006, 2008). This study focuses on later developmental stages, with 16 to 64 cells (Figure 4.3, b-l) (as opposed to previous studies by Raff et al. (2006, 2008), which focussed on earlier developmental stages), in order to determine whether they exhibit a different taphonomy to the earliest cleavage stages.

The embryos were killed by treatment with 100 mM beta-mercaptoethanol (BME) in seawater at the desired cell stage. BME was used because it produces strong reducing conditions, as a stand-in for the high H_2S levels that are considered to have produced reducing conditions in the marine environment in which the Weng'an embryoids fossilised (Raff et al. 2006). In these conditions, autolysis is inhibited, and dead autolysis-inhibited embryos are subsequently stable for months.

The BME-treated embryos were washed into sterile seawater and incubated with the bacterium *Pseudoalteromonus tunicata* in 150 μm mesh-bottomed baskets in 6-well plastic cell culture plates, in order to produce a pseudomorph. The experiments were carried out aerobically at 23°C, as previous experiments have shown that the pattern of decay is the same regardless of aerobic/anaerobic conditions and temperature, but experiments in aerobic and higher temperature regimes run faster (Raff et al. 2013). Samples for scanning electron microscopy were fixed in

2.5% glutaraldehyde in seawater. To display internal structure, specimens were frozen and fractured after fixation.

4.3 Results

4.3.1 Comparative taphonomy of Kuanchuanpu animal embryo fossils

The Kuanchuanpu embryos generally consist of hundreds of cells, and all specimens show cells on the surface (Figure 4.1A-C). No specimens preserve the fertilisation envelope. The embryos exhibit a range of preservational states, but the actual biological structure preserved is limited to cell membranes, and that only in a few specimens. The embryos do not preserve any intracellular structures - the interiors are either a homogenous mass of crystals or a hollow space (Figure 4.1D), and any cellular structure is preserved only at the exterior of the fossils, the interior having either coalesced, or rotted away entirely (Figure 4.1A-D). Where the component blastomeres are preserved, they often have hollow spaces running between them, left after the degradation of the cell membrane (Figure 4.1E).

Preservation of the component blastomeres ranges from complete through to just the outlines of adjacent cells being preserved at the surface of the specimen. In most cases, the blastomeres are preserved incompletely such that they do not extend to the centre of the embryo, so the boundaries between cells degrade away from the exterior (Figure 4.1F-I). The cells can either be infilled (Figure 4.1E) or hollow (Figure 4.1F-I).

In the infilled specimens, the infill consists of relatively large, blocky crystals 5-10μm across, with no preferred orientation. These crystals have high x-ray attenuation, appearing pale in SRXTM images (Figure 4.1E; centre of Figure 4.1F). Elemental analysis shows that this phase is relatively depleted in carbon, sulphur and sodium, and enriched in calcium, phosphorus and fluorine (Figure 4.2). Some specimens also preserve a smaller (3-5μm) needle shaped mineral phase with the same chemistry, oriented in bands.

Some specimens preserve a second pale phase that surrounds the infilling crystals. The crystals of this second phase are square shaped and align along the blastomere edges (Figure 4.1H-I). They thin outwards in orientation, suggesting they likely grew from another structure. Although this phase appears similar to the phase described above in SRXTM images, elemental analysis shows it has a different chemistry, being depleted in calcium, phosphorus and fluorine, and enriched in carbon, sulphur and sodium.

The final mineral phase exhibited by the specimens has small (less than 2μm across) crystals that have low x-ray attenuation (they appear dark in SRXTM images). This phase is located along putative cell boundaries between the bands of oriented square crystals (Figure 4.1H-I). The phase is relatively enriched in sulphur and carbon compared to the bright phase, and depleted in fluorine, phosphorus and calcium.
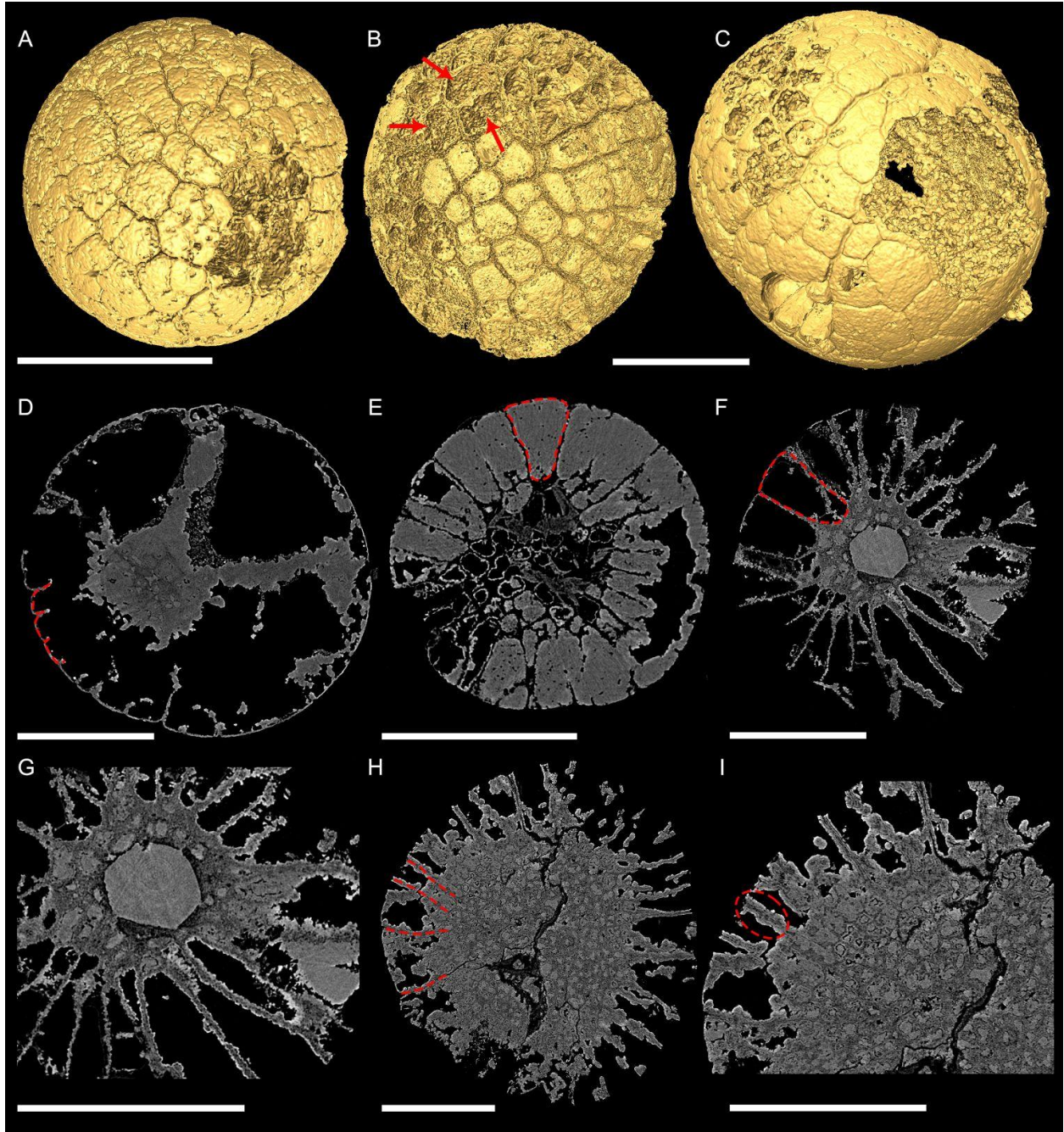
Figure 4.1. 3D surface renderings and orthoslices of Kuanchuanpu cleavage embryos. (A) 3D surface rendering of DXP18E10_4, showing surface preservation of cells. (B) 3D surface rendering of DXP18F8_1, showing surface preservation of cells. In the upper part of the specimen, the cell surface has not been preserved at all, and the hollow interior can be seen (red arrows). (C) 3D surface rendering of DXP18F8_3, showing surface preservation of cells. (D)

Orthoslice of DXP18F8_3, showing a mostly hollow interior with some void fill. Cell boundaries are visible only on the surface of the specimen (bottom left of image, blastomere boundaries traced in red; see 4.1C for corresponding surface rendering). (E) Orthoslice of DXP18E10_4, showing infilled cells with the membrane position preserved as a void (example blastomere highlighted in red). (F) Orthoslice of DXP18F8_1, showing hollow cells (example blastomere highlighted in red), with the membrane preserved by void fill. (G) Close-up of (F). (H) Orthoslice of DXP18E8_1, showing hollow cells that are only preserved at the edges of the specimen blastomere boundaries traced in red), and a coalesced centre with a compacted morphology. (I) Close-up of (H) The red dashed ellipse indicates a region where the darker membrane replicating phase can be seen, between layers of paler void fill. All scale bars equal 200 μm.
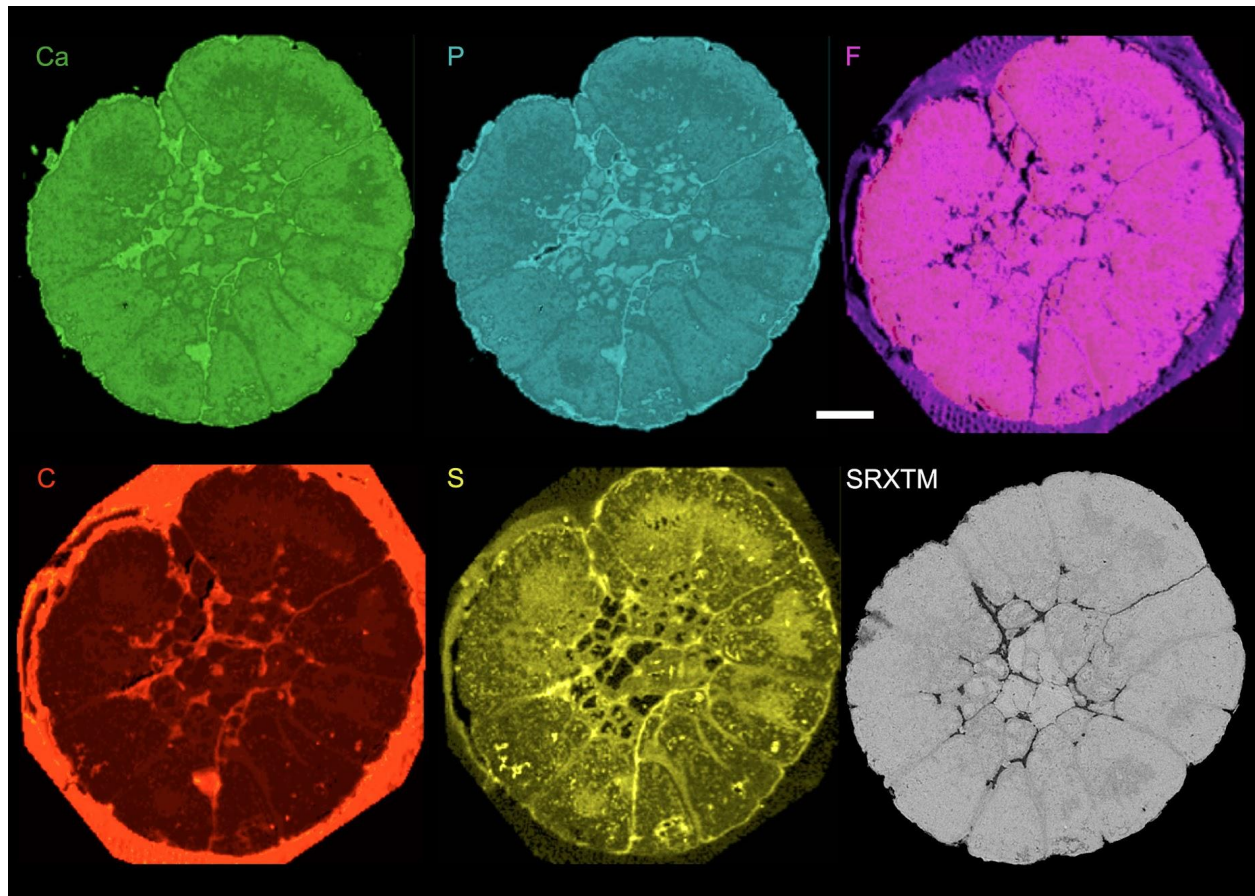
Figure 4.2. Elemental maps of a Kuanchuanpu cleavage stage embryo, showing the relative abundance of Calcium (Ca), Phosphorus (P), Fluorine (F), Carbon (C), and Sulphur (S), along with an SRXTM image of the same specimen. Brighter tones represent greater abundance; in the SRXTM image, brighter tones represent higher X-ray attenuation. Scale bar is 50 μm.

4.3.2 Experimental Taphonomy

At the time of cleavage in late stage embryos, the blastomeres are distinct (Figure 4.3, b-e). Unlike in early cleavage stages, however, the blastomeres of later cleavage stages are not closely adherent, and the central internal cavity that will be present at the later blastula stage is beginning to form (Figure 4.3, f). The cellular preservation characteristic of embryos from 2-cell to 8-cell (less well at 16-cell stage; Figure 4.3, h) includes both outer cell surfaces and internal cell boundaries. The internal cell boundaries begin to become obviated by the 32 to 64-cell stage (Figure 4.3, h and i). Comparison of Figure 4.3, f and i shows that after death, autolysis-inhibited multi-cell embryos do not retain the original loose packing of cells, nor the clear cell boundaries of the live embryo. Instead, although the outermost blastomere boundaries are distinct, the internal blastomere boundaries become tightly packed and the cell boundaries are obscured. Pseudomorphing with *P. tunicata* gives excellent preservation of surface features (Figure 4.3, j), but reflects the more compressed internal morphology (Figure 4.3, k and l).
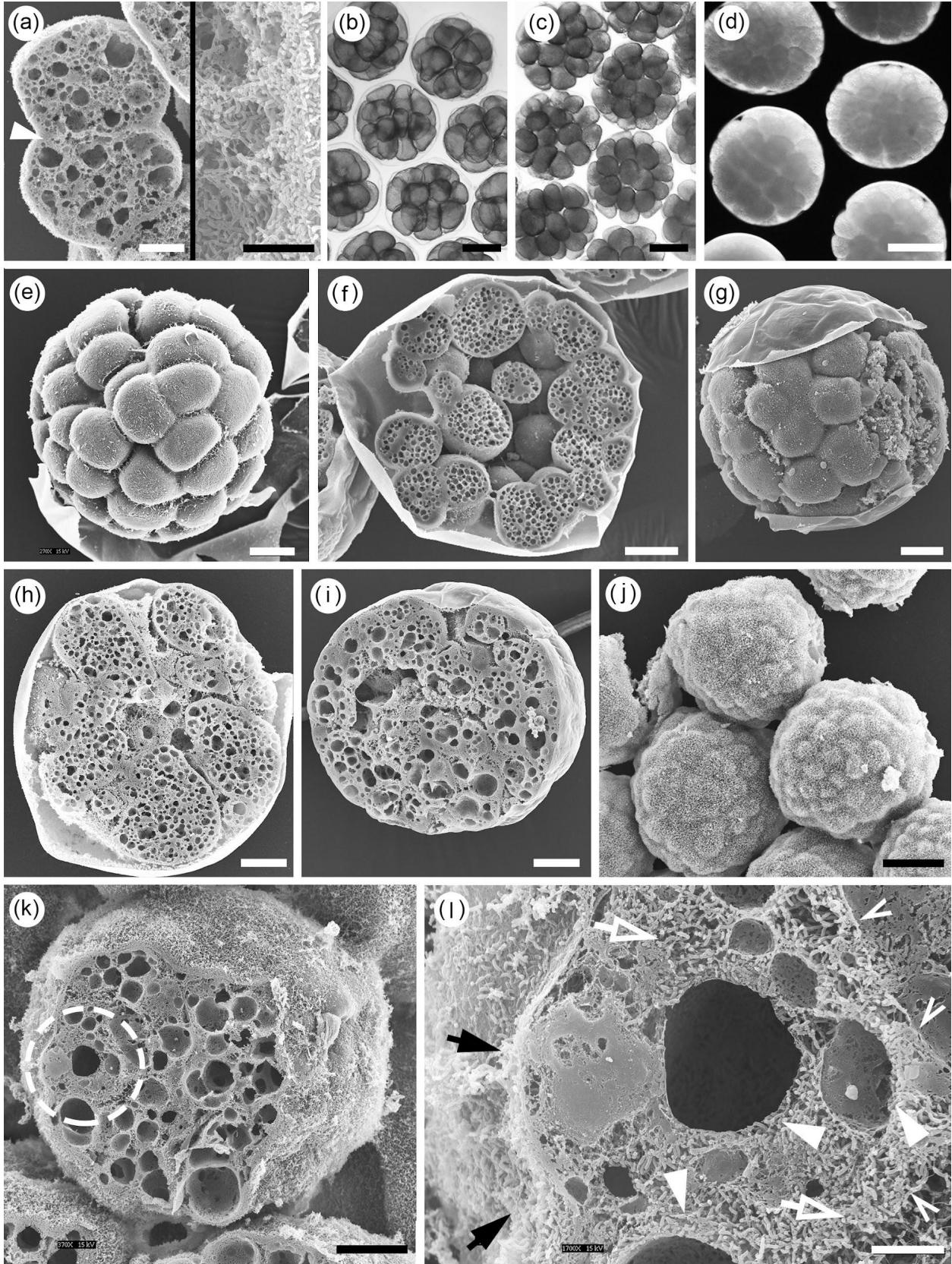
Figure 4.3. Autolysis inhibition and taphonomy of late-stage embryos. (*a*) Scanning electron microscopy images (SEMs) of pseudomorphs of killed autolysis-inhibited 2-cell embryos. Embryos in this preparation had been stored for two years after autolysis inhibition by treatment with 100 mM beta-mercaptoethanol (BME), and then treated with *Pseudoalteromonas tunicata* for four days. Left: Pseudomorph of a 2 cell embryo, fractured to show internal structure. Arrowhead indicates the boundary between blastomeres, which is clearly preserved. Right: high magnification view of the dense internal bacterial biofilm in another pseudomorphed embryo in this preparation. (*b-d*) Light microscopic views of live multi-cell stage embryos of the sea urchin *Heliocidaris erythrogramma*. These embryos undergo equal cleavage, and individual blastomeres are clearly distinct. (*b*) 16-cell; (*c*) 32-cell; (*d*) 64-cell. Fertilization envelopes surrounding the embryos are visible in *a* and *c*. Micrographs are bright field images in *b, c*; dark field optics in d. (e, f) SEMs of 64-cell embryos at time of cleavage. (*e*) Whole embryo with fertilization envelope peeled off, showing the arrangement of blastomeres. (f) 64-cell embryo fractured to show internal structure. The blastomeres are only loosely associated, and the central cavity present at the later blastula stage is beginning to form. (*g-i*) SEMs of dead autolysis-inhibited multi-cell embryos, fixed for SEM after about a month in BME. (*g*) 32 to 64-cell embryo. The fertilization envelope is partly peeled back, revealing the blastomeres. The external morphology is like that in the newly cleaved embryo in panel e. (*h, i*) Embryos fractured to reveal internal structure. (*h*) 16-cell embryo; internal blastomere boundaries remain relatively distinct. (*i*) 64-cell embryo; outermost blastomere boundaries are distinct, but internal blastomere boundaries have become tightly packed and cell bounderies are obscured. (*j-l*) SEM images showing taphonomy of dead autolysis inhibited multi-cell embryos that had been in BME for about a month and then incubated with *P. tunicata*. (*j*) Whole 64-cell embryos after four days

130

incubation with *P. tunicata*. The 'fuzzy' bacterial biofilm on the surface of the embryos

preserves and displays the external morphology of the multi-celled embryo. (*k*) 64-cell embryo

after seven days incubation with *P. tunicata*; fractured to reveal internal structure. A bacterial

pseudomorph has formed, as in panel j. Internal blastomere boundaries are difficult to discern;

the region circled is interpreted as a blastomere. (*l*) Higher magnification view of the region

circled in panel *k*. A three-dimensional bacterial biofilm has replaced the embryo cytoplasm,

generating a pseudomorph. Black arrows show the external bacterial biofilm on the surface of

the embryo. Within the embryo, bacterial assemblages demarcate lipid vacuole margins (white

arrowheads), and have formed dense biofilms in the cytoplasm (open white arrows). The

presumptive original blastomere boundary is indicated by the open white arrowheads.

Scale bars: b-d: 200 μm; j, 100 μm; a (left), e-i, k: 50 μm; a (right), l: 10μm.

4.4.1 Preservation of the Kuanchuanpu embryos

In the Kuanchuanpu embryos, the cell membranes have been replicated by a microcrystalline low-attenuation mineral phase, with the blastomere spaces being infilled with a high attenuation diagenetic mineral phase consisting of large geoidal crystals (Figure 4.1E). Some of the fossils preserve the blastomeres well in their entirety, but most preserve blastomere morphology well at the surface of the fossil and poorly in the interior (e.g. Figure 4.1H), suggesting mineralisation occurred from the outside in.

All phases of mineralisation rely on the presence of cell membranes, as they provided the template for the void filling phase to grow from. The pattern of mineralisation is centripetal, with layers being added away from the membranes. The position of the membranes themselves is often preserved as a hollow space, with the void fill preserving an endocast of the original morphology. This suggests that either the membrane persisted long enough for the void fill to start forming, or that the membranes did mineralise but that phase was subsequently lost either during diagenesis or extraction of the fossils. The membranes can also be preserved via infilling by a later phase of mineralisation. Where the blastomere structure is preserved incompletely or only on the exterior of the specimen, the membraneless region is either a hollow space or entirely infilled, as without the membranes to act as a scaffold there was no structure for the void fill to grow from.

132

Rarely, the membranes are preserved in a fine, cryptocrystalline phase that greatly resembles the cryptocrystalline phase in the Doushantuo that replicates original biology (Figure 4.1H-I). It is possible that more of the specimens had their membranes preserved in this way, and it has subsequently degraded to leave the hollow space observed in most specimens. Alternatively, the membranes may have initially been preserved in a phase that degraded entirely during diagenesis, either being replaced by the later mineralisation, or leaving voids.

The general pattern of decay and preservation seen in the Kuanchuanpu embryos starts with the decay of the cell contents, while the cell membrane persists. This membrane is mineralised, and the cell interiors are then infilled using the membranes as a template (Figure 4.4A). Rarely, the early mineralised membrane is preserved (Figure 4.4A, 3.1-3.2), but more commonly the mineralised membrane is degraded away, leaving a void that preserves an endocast of the cell (Figure 4A, 1.1-1.2). This void either remains empty, or is infilled by a third generation of mineralisation (Figure 4A, 2.1-2.3).
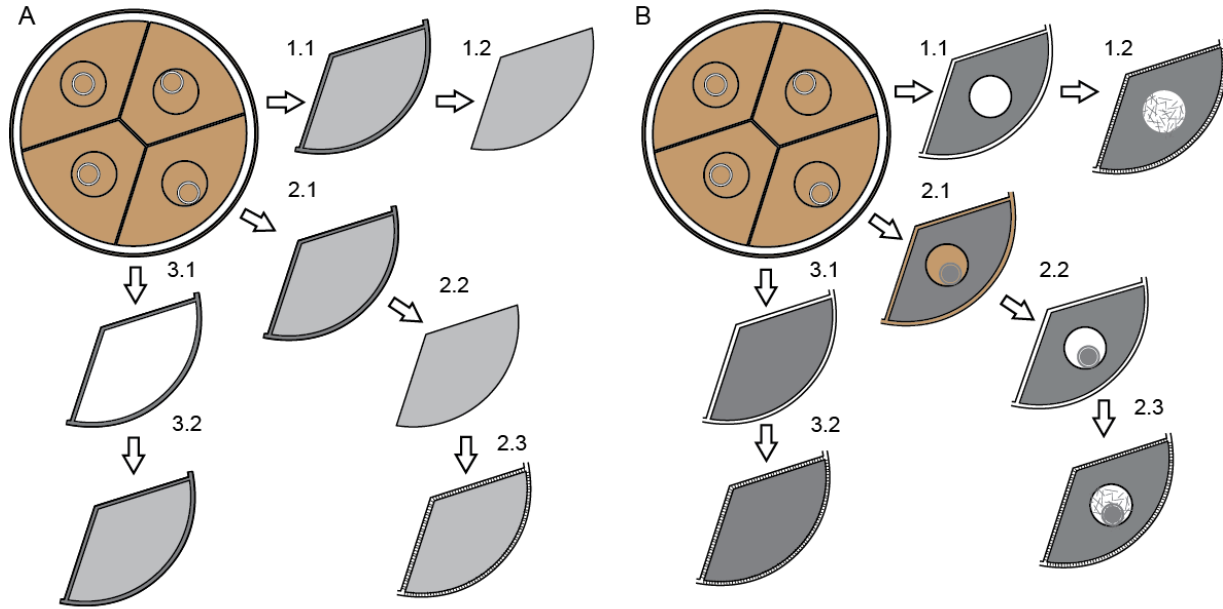
Figure 4.4. Taphonomic Pathways of (A) Kuanchuanpu embryos, and (B) Weng'an embryoids. (A1.1-1.2) The membrane is mineralised (dark grey) while the cell contents decay, and the interior of the cell is infilled (light grey) before the membrane degrades, leaving an endocast of the cell. (A2.1-2.3) The membrane is mineralised (dark grey) while the cell contents decay and the interior of the cell is infilled (light grey). The membrane degrades, leaving an endocast of the cell, and the resulting void is then infilled. (A3.1-3.2) The membrane is mineralised (dark grey), while cell contents decay and the interior of the cell is infilled (light grey). (B1.1-1.2) The cytoplasm mineralises first (dark grey), before the nucleus later decays leaving a void (white) that is filled by diagenetic cement (slashes within the white void). (B2.1-2.3) Cytoplasm and nucleoli mineralise first (dark grey) before the nucleus later decays leaving a void (white) that is filled by diagenetic cement (slashes within the white void). (B3.1-3.2) Cell mineralises as a homogenous structure due to decay of the nucleus and cytoplasm. Modified from Yin et al. (2017).

4.4.2 Decay experiments

Decay experiments on early cleavage stage embryos (2- to 8-cell stage) have shown that, provided autolysis is inhibited, both external and internal morphology can be well preserved (Raff et al. 2013, 2014). When incubated with rapidly killed autolysis-blocked early cleavage stage embryos, the marine bacterium *Pseudoalteromonas tunicata* generates pseudomorphs of the embryos that faithfully model both external and internal embryo structure, including subcellular structures (Figure 4.3, a; Raff et al. 2006, 2008, 2013). When autolysis is inhibited immediately post-death, blastomere numbers and shape can be preserved, but when decay is allowed to progress, lipid granules coalesce, cell membranes degrade, and blastomere morphology cannot be preserved (Raff et al. 2006, 2008). However, whether internal structure is preserved during taphonomy of cleavage-stage embryos depends on environmental conditions and on what bacteria species were present (Raff et al. 2013, 2014), as well as autolysis inhibition. For example, some bacteria generate pseudomorphs that preserve external morphology but not internal structure (Raff et al. 2013).

The experiments reported here examined the taphonomy of late-stage multi-celled embryos, using 16 to 64 cell *H. erythrogramma* embryos (Figure 4.3, b-l). The initial step towards long-term preservation, autolysis inhibition, is the same in later stage embryos as in early cleavage embryos. However, in subsequent steps of preservation, the later stage embryos behave differently (figure 4.3, g-l). The overall external morphology of late stage embryos can be preserved, but the internal morphology is much less likely to be preserved, even in optimal pseudomorphing conditions.

Morphologically the late-stage embryos are different to the early stages, which may account for why they decay differently - in late stage embryos, the blastomeres are not closely adherent, and the central internal cavity of the blastula stage is beginning to form (Figure 4.3, f). Post-death, autolysis-inhibited late-stage embryos do not retain the original loose packing of cells, nor the clear cell boundaries of the live embryo (Figure 4.3, i). Instead, their internal morphology is compressed, and the cell boundaries start to become obviated (Figure 4.3, h and i). Pseudomorphing with *P. tunicata* gives excellent preservation of surface features (Figure 4.3, j), but reflects the more compressed internal morphology (Figure 4.3, k and l). This suggests that by the time a pseudomorph of a late stage cleavage embryo becomes mineralised, only surface features are available for replacement. I am not able to explain the loss of clear cell boundaries in autolysis-inhibited late stage cleavage embryos versus their retention in early cleavage stages, but it does appear to have a biological basis in the properties of blastomeres at different stages in living embryos. This could be due to membrane composition or organisation, perhaps to do with blastula formation, but exploring this is beyond the scope of this study.

4.4.3 Comparison of Kuanchuanpu embryos to decay experiments

The decay pattern of modern early stage cleavage embryos shows a number of differences when compared to the Kuanchuanpu embryos. The fossil embryos do not have any preservation of internal morphology beyond the shape of the component blastomeres, which does not match what is observed in early stage cleavage embryos in which autolysis is inhibited immediately post-death, as these preserve internal morphology very well. However, the Kuanchuanpu embryos do not fit the pattern shown by more decayed early stage embryos either. The shape of

the blastomeres in the fossils tends to be well defined; they do not exhibit the warped shape shown in decay experiments where the embryos have decayed prior to pseudomorphing.

The Kuanchuanpu embryos are a better match for the decay pattern shown in late stage cleavage embryos. In particular, their excellent preservation of surface features and poor preservation of internal features is exactly what the decay experiments show, with some specimens preserving a similar compaction of cell contents (Figure 4.1H-I). Even here there are differences, however. In the late-stage decay experiments cell boundaries are obscured and cell contents compressed, and even in optimal pseudomorphing conditions they do not preserve well defined blastomeres, unlike what is generally seen in the Kuanchuanpu embryos. The decay experiments represent our best approximation of the conditions the fossils were preserved in, but they cannot be an exact reproduction. Consequently the differences seen between what the decay experiments show and what the fossils preserve could be down to some quirk of environment that the decay experiments do not capture. Alternatively, it could be due to biology - the experiments assume the modern embryos have a very similar biology and development as the fossil embryos, which is not necessarily the case.

4.4.4 Are the Weng'an embryoids animal embryos?

The Doushantuo fossils are preserved by two mineral phases, both fluorapatite of varying compositions (Cunningham et al. 2012a). Preserved soft tissue is replicated in a cryptocrystalline low attenuation C-rich phase with relatively low abundances of Ca, P and F (Cunningham et al. 2012a). This phase also appears as void fill, which can replicate the overall morphology of the fossil's biological features, but structures within the void fill cannot be interpreted as biological.

137

The void fill can be distinguished from preserved soft tissue by its texture, as the void fill has a geoidal texture with relatively large (greater than 1μm) crystals, the long axes of which are perpendicular to the surface on which they formed (Cunningham et al. 2012a). Latest void filling and encrusting mineralisation is typically preserved in a high attenuation C-poor fluorapatite phase that has a relatively high abundance of Ca, P and F (Cunningham et al. 2012a).

The best preserved of the embryoids preserve the fertilisation envelope and intracellular structures (Yin et al. 2017; Sun et al. 2020). Some of these structures have been previously interpreted as lipid granules (Cunningham et al. 2012a; Hagadorn et al. 2006; Huldtgren et al. 2011; Schiffbauer et al. 2012), and some specimens include structures interpreted as nuclei (Cunningham et al. 2012a; Yin et al. 2017; Sun et al. 2020). The embryos almost always have distinct cells, but the cell membrane is not preserved. There are two general pathways of preservation in the Doushantuo. In the first and most common, the cell mineralises as a homogenous structure after the decay of the cytoplasm and intracellular structures (Figure 4.4B 3.1-3.2; Yin et al. 2017). In cases of best preservation, the cytoplasm is mineralised early, before the intracellular structures (such as nuclei) decay. After the mineralisation of the cytoplasm, the intracellular structures then decay away, leaving a void that is later infilled with diagenetic cement (Figure 4.4B 1.1-1.2, 2.1-2.3; Yin et al. 2017; Sun et al. 2020).

The Kuanchuanpu embryos do not preserve any intracellular structures. Their interior consists either of a homogeneous mass of crystals or a hollow void. This space is sometimes surrounded by a rim of small blocky crystals, and some of the embryos preserve their original cell membrane structure, unlike the Weng'an embryoids. However, the Kuanchuanpu embryos rarely have

distinct cells - in most specimens the cells have begun to coalesce, as the boundaries between them have been broken down. These features are preserved in two different mineral phases - an early forming low attenuation phase that replicates the original biological structure of the cell membranes, and a late forming highly attenuating phase that is void-filling.

Despite the great similarity between the mineral phases present at each site, they preserve entirely different structures. In the Doushantuo, there is early mineralisation of cell contents and cytoplasm, with late void infill where the cell membranes would have been, whereas in the Kuanchuanpu, there is early mineralisation of cell membranes, and the cell contents are lost to later be replaced by void fill, or to simply remain a hollow space (Figure 4.4).

With regard to the decay experiments, the spectrum of preservation that is seen in the Weng'an embryoids matches the pattern of decay seen in modern early-stage cleavage embryos, often preserving sub-cellular structures and cell boundaries, even if the membranes themselves are not preserved.

The spectrum of preservation exhibited by the Kuanchuanpu embryos compares better to the pattern of decay seen in modern late-stage cleavage embryos than in early-stage cleavage embryos, but they also show some clear differences: in particular, the decay experiments suggest that cell boundaries are lost early in late-stage cleavage embryos even in optimal preservation conditions, whereas the best preserved Kuanchuanpu embryos consistently display well defined blastomeres.

The decay experiments therefore suggest that the Weng'an embryoids represent early-stage cleavage embryos, while the Kuanchuanpu embryos bear far more resemblance to late-stage cleavage embryos, allowing for some differences in decay pathways, as some Kuanchuanpu embryo specimens preserve features that do not persist in the decay of modern embryos.

It is clear that early-stage and late-stage cleavage embryos decay in fundamentally different ways, even under the same taphonomic conditions, which may be responsible for the differences in internal preservation exhibited by the Weng'an embryoids and Kuanchuanpu embryos. This would account for the absence of internal structures in the Kuanchuanpu embryos, versus the high fidelity internal structures preserved in the Weng'an embryoids. The difference in the structures the fossils preserve, and the mineral phases that preserve them, could be reflective simply of differences in their decay pathways due to local conditions at each site, or it could be due to differences in biology. Regardless, the taphonomic evidence seems to corroborate the interpretation that the Weng'an embryoids are comparable to animal embryos, and the differences when comparing them to the unequivocal embryos of the Kuanchuanpu Formation come down to the different preservational pathways of embryos at different stages of their developmental cycle.

4.5 Conclusion

Experimental taphonomy shows that early- and late-stage cleavage embryos display fundamentally different preservation pathways that could account for the differences in preservation between the Weng'an embryoids and the Kuanchuanpu embryos, from two deposits

that are otherwise very similar. The Weng'an fossils and the Kuanchuanpu fossils are preserved in the same suite of mineral phases, but these phases consistently preserve very different structures in the embryoids and embryos. This could either reflect the biological differences between the fossils, or it could reflect differences in local conditions at the time of their preservation, despite their broadly similar diagenetic histories. Regardless, decay experiments suggest that the effect biology has had on the taphonomy of the embryoids and embryos appears to be due to their respective cleavage stages, and an animal affinity for the Weng'an embryoids cannot be ruled out on this basis.

Chapter 5: Conclusions

The aims of this thesis were to develop a better understanding of the taxonomy, systematics and taphonomy of the Weng'an Biota. I have done this principally by describing new elements of the biota, elucidating the biology, taxonomy, systematics and affinity of the algae preserved within the biota, and undertaking a comparative taphonomy study of the embryoid fossils and unequivocal animal embryos with the same diagenetic history, from an overlying Cambrian succession. Together, these provide fundamental new insights into debate over the palaeobiology of the Weng'an Biota.

In Chapter 2 I described a new eukaryote from the biota, which represents part of a developmental cycle that is compatible with the vegetative phases in the life cycle of various unicellular eukaryotes, but not with any metazoan affinity. This organism, *Sporosphaera guizhouensis,* is preserved in the act of encystment, a strategy that was likely a response to the

spatially and temporally variable nature of Ediacaran marine environments and the widespread anoxic conditions in continental shelf bottom waters at the time, adding to evidence that this was a common strategy in Ediacaran acritarchs.

In Chapter 3 I undertook a critical evaluation of the algae from the Weng'an biota, using SRXTM to reconcile their external morphology, histology and variation. I used the resulting data to test their taxonomy and phylogenetic interpretations. I found that several of the Weng'an algal taxa are different stages of a single developmental cycle, providing both insights into their biological affinity and their taxonomy. Indeed, most of the Weng'an algae can be synonymised as *Thallophyca ramosa* and perhaps ironically, the additional insights into biology that synonymy provides, diminish certainty as to their affinity. Absence of key characters, including carposporangia, preclude assignment to Florideophyceae where they have previously served as calibrations in molecular clock analyses. Affinity cannot be constrained beyond total-group Rhodophyta.

In Chapter 4 I aimed to test the animal-embryo interpretation of the Weng'an embryoids by comparing their taphonomy to living embryos and unequivocal animal embryos from the Kuanchuanpu biota. I found that comparing the taphonomy of the Weng'an embryoids and the Kuanchuanpu embryos showed that the fossils at both sites are preserved by the same mineral phases, however those phases preserve different structures at each site. Comparing the embryoids and embryos to the decay patterns of living embryos showed that the embryoids compare well to the decay pattern exhibited by early stage cleavage embryos, and the Kuanchaunpu embryos compare somewhat well to the decay pattern exhibited by late stage cleavage embryos. The

142

differences between the Doushantuo and the Kuanchuanpu could suggest that the Weng'an embryoids are not animal embryos, but it could equally be that the differences are due to variations in local conditions during their phosphatisation, or due to the fundamentally different preservation potential of early stage cleavage embryos versus late-stage cleavage embryos.

This thesis adds to a growing body of evidence that many Weng'an fossils have either resting stages in their life cycles or undergo an extended period of embryonic development, in response to the variability of Ediacaran shallow marine environments. Further, I have shown that while elements of the Weng'an Biota (particularly the algae) are widely used as calibrations in molecular divergence time analyses, this is in error, as the fossils cannot definitively be placed in the clades whose emergence they are used to date.

5.1 Concluding remarks

The Doushantuo microfossils are valuable tools for elucidating the biology of early Ediacaran organisms, and the variable nature of the environments in which they lived, and the Weng'an is frequently pitched as a window for testing clock estimates for the origin of animals.

Despite the enigmatic nature of the fossils, it is possible to tease out some details of their affinity. In particular, while the embryoid fossils do not possess the unique characteristics that would place them definitively in crown-group Metazoa, they could represent a stem lineage, and future discoveries may yet strengthen this interpretation. However, there are no convincing crown-group metazoans in the biota. At best, fossils like *Caveasphaera* could perhaps be

143

interpreted as cnidarians, and there are no hints of any bilaterians. This lack of metazoans fits with the absence of metazoans in other early Ediacaran fossils assemblages, such as the Lantian Biota (Yuan et al. 1999) and the Miaohe Biota (Xiao et al. 2002), and with the absence of metazoan trace fossils prior to the late Ediacaran and the appearance of the Ediacaran macrofauna (Jensen 2003). Clock estimates that predict bilaterians in the Late Cryogenian or Early Ediacaran (e.g. dos Reis et al. 2015; Erwin et al. 2011; Erwin 2015), can perhaps, therefore, be rejected, and new clock studies recalibrated in this light, as the absence of unambiguous metazoan fossils in the Early Ediacaran suggests a younger divergence age of Metazoa than molecular clocks currently suggest.

Likewise, although the algae are not, as previously described, crown-group florideophytes, they still fall within total group Rhodophyta, and their unusual developmental cycle, with its extended period of embryonic development, suggests that like many other Weng'an organisms, they were adapted to allow them to ride out periods of adverse conditions that fossil evidence suggests were all to frequent in Ediacaran oceans.

5.2 Future work

Further analysis of the developmental biology of the embryoids could give further clarity as to their affinities - in particular, it would be worth teasing out whether the link between *Megasphaera/Tianzhushania* and *Megaclonophycus* is demonstrable rather than inferred, and whether there is any evidence of cell sorting or unequal cell division in the late-stage embryoids.

Spiralicellula would also be a good target for this, as its developmental biology is not well constrained.

Other taphonomic models could be considered for the Weng'an embryoids as well - we know they compare well to the decay pathway of early-stage animal embryos, but how do they compare to the embryos of mesomycetozoans, or red algae? The Weng'an embryoids, particularly *Parapandorina* and *Megaclonophycus,* have comparable morphologies to mesomycetozoans, so a comparison of their taphonomy could offer a credible alternative to their stem metazoan interpretation. As to the algae, red algae are already known from the biota, and an exploration as to whether the embryoids could instead be part of an algal developmental cycle would also be beneficial in constraining their affinities.

Bibliography

Bailey, J.V., Joye, S.B., Kalanetra, K.M., Flood, B.E., Corsetti, F.A. 2007. Evidence of giant sulphur bacteria in Neoproterozoic phosphorites. Nature 445, 198-201.

Barfod, G.H., Albaréde, F., Knoll, A.H., Xiao, S.,Télouk, P., Frei, R. & Baker, J. 2002. New Lu-Hf and Pb-Pb age constraints on the earliest animal fossils. Earth and Planetary Science Letters 201, 203–12.

Bengtson, S. and Budd, G. 2004. Comment on "Small Bilaterian Fossils from 40 to 55 Million Years Before the Cambrian". Science 306, 1291a–1291a.

Bengtson, S., Cunningham, J. A., Yin, C. and Donoghue, P. C. J. 2012. A merciful death for the "earliest bilaterian," *Vernanimalcula*. Evolution & Development 14, 421-427

Bengtson, S., Sallstedt, T., Belivanova, V., and Whitehouse, M. 2017. Three-dimensional preservation of cellular and subcellular structures suggests
1.6 billion-year-old crown-group red algae. PLoS Biol 15 (3), e2000735.

Bengtson, S., and Yue, Z. 1997. Fossilized metazoan embryos from the earliest Cambrian. Science 277, 1645–1648.

Betts, H.C., Puttick, M.N., Clark, J.W., Williams, T.A., Donoghue, P.C.J., Pisani, D. 2018. Integrated genomic and fossil evidence illuminates life's early evolution and eukaryote origin. Nature Ecology and Evolution 2, 1556–1562.

de Bettignies, T., Wernberg, T., Gurgel, C.F.D. 2018. Exploring the influences of temperature on aspects of the reproductive phenology of temperate seaweeds. Frontiers in Marine Science 5, 218.

Bottjer, D. J., Yin, Z., Zhao, F. and Zhu, M. 2020. Comparative taphonomy and phylogenetic signal of phosphatized Weng'an and Kuanchuanpu Biotas. Precambrian Research 349, 105408.

Bowyer, F., Wood, R.A., Poulton, S.W. 2017. Controls on the evolution of Ediacaran metazoan ecosystems: a redox perspective. Geobiology 15, 516-551.

Brodie, J., Bartsch, I., Neefus, C., Orfanidis, S., Bray, T., Mathieson, A.C. 2007. New insights into the cryptic diversity of the North Atlantic-Mediterranean 'Porphyra leucosticta' complex: P. olivii sp. nov. and P. rosengurttii (Bangiales, Rhodophyta). European Journal of Phycology 42, 3-28.

Brooke, C., Riding, R. 1998. Ordovician and Silurian coralline red algae. Lethaia 31, 185-195.

Budd, G.E. 2013. At the origin of animals: the revolutionary Cambrian fossil record. Current Genomics 14 (6), 344-354.

Budd, G.E., Mann, R.P. 2020. Survival and selection biases in early animal evolution and a source of systematic overestimation in molecular clocks. Interface Focus 10, 20190110.

Butterfield, N.J. 2000. *Bangiomorpha pubescens* n. gen., n. sp.: implications for the evolution of sex, multicellularity, and the Mesoproterozoic/Neoproterozoic radiation of eukaryotes. Paleobiology 26 (3), p. 386-404.

Carlisle, E.M., Jobbins, M., Pankhania, V., Cunningham, J.A., Donoghue, P.C.J. 2021. Experimental taphonomy of organelles and the fossil record of early eukaryote evolution. Science Advances 7 (5), eabe9487.

Chen, J. Y., Bottjer, D. J., Davidson, E. H., Dornbos, S. Q., Gao, X., Yang, Y. H., Li, C. W., Li, G., Wang, X. Q., Xian, D. C., Wu, H. J., Hwu, Y. K. and Tafforeau, P. 2006. Phosphatized polar lobe-forming embryos from the Precambrian of Southwest China. Science 312, 1644-1646.

Chen, J.-Y., Bottjer, D. J., Davidson, E. H., Li, G., Gao, F., Cameron, R. A., Hadfield, M. G., Xian, D.-C., Tafforeau, P., Jia, Q.-J., Sugiyama, H. and Tang, R. 2009a. Phase contrast synchrotron X-ray microtomography of Ediacaran (Doushantuo) metazoan microfossils: phylogenetic diversity and evolutionary implications. Precambrian Research 173, 191-200.

Chen, J.-Y., Bottjer, D.J., Li, G., Hadfield, M.G., Gao, F., Cameron, R.A., Zhang, C.-Y., Xian, D.-C., Tafforeau, P., Liao, X., Yin, Z.-J. 2009b. Complex embryos displaying bilaterian

characters from Precambrian Doushantuo phosphate deposits, Weng'an, Guizhou, China. Proceedings of the National Academy of Sciences USA 106, 19056-19060.

Chen, J.-Y., Bottjer, D. J., Oliveri, P., Dornbos, S. Q., Gao, F., Ruffins, S., Chi, H., Li, C. W. and Davidson, E. 2004. Small bilaterian fossils from 40 and 55 million years before the Cambrian. Science 305, 218-222.

Chen, J., Oliveri, P., Gao, F., Dornbos, S. Q., Li, C. W., Bottjer, D. J. and Davidson, E. H. 2002. Precambrian animal life: Probable developmental and adult cnidarian forms from Southwest China. Developmental Biology 248, 182-196.

Chen, J., Oliveri, P., Li, C.-W., Zhou, G.-Q., Gao, F., Hagadorn, J. W., Peterson, K. J. and Davidson, E. H. 2000. Precambrian animal diversity: putative phosphatised embryos from the Doushantuo Formation of China. Proceedings of the National Academy of Sciences USA 97, 4457-4462.

Chen. M. and Liu, K. 1986. The geological significance of newly discovered microfossils from the upper Sinian (Doushantuo age) phosphorites. Chinese Journal of Geology 1986 (1), 46-53.

Chen, L., Xiao, S., Pang, K., Zhou, C., Yuan, X. 2014. Cell differentiation and germ-soma separation in Ediacaran animal embryo-like fossils. Nature 516, 238-240.

Chen, Y.-Q., Jiang, S.-Y., Ling, H.-F. & Yang, J.-H. 2009. Pb–Pb dating of black shales from the Lower Cambrian and Neoproterozoic strata, South China. Chemie der Erde - Geochemistry 69 (2), 183–9.

Cock J., Collén J. 2015. 'Independent Emergence of Complex Multicellularity in the Brown and Red Algae' in Ruiz-Trillo, I., Nedelcu, A.M. (eds) Evolutionary Transitions to Multicellular Life, Advances in Marine Genomics, vol 2. Springer, Dordrecht, p. 335-361.

Cohen, P.A., Knoll, A.H., Kodner, R.B. 2009. Large spinose microfossils in Ediacaran rocks as resting stages of early animals. Proceedings of the National Academy of Sciences 106, 6519-6524.

Condon, D., Zhu, M., Bowring, S., Wang, W., Yang, A., Jin, Y. 2005. U-Pb ages from the Neoproterozoic Doushantuo Formation, China. Science 308, 95–98.

Cunningham, J.A., Donoghue, P.C.J., Bengtson, S. 2014. 'Distinguishing biology from geology in soft-tissue preservation' in Laflamme, M., Schiffbauer, J.D., Darroch, S.A.F. (Eds.) Reading and Writing of the Fossil Record: Preservational Pathways to Exceptional Fossilization. The Palaeontological Society Papers 20, 275-288.

Cunningham, J.A., Liu, A.G., Bengtson, S., Donoghue, P.C.J. 2017a. The origin of animals: can molecular clocks and the fossil record be reconciled? Bioessays 39, 1600120.

Cunningham, J.A., Thomas, C.-W., Bengtson, S., Kearns, S.L., Xiao, S., Marone, F., Stampanoni, M., Donoghue, P.C.J. 2012a. Distinguishing geology from biology in the Ediacaran Doushantuo biota relaxes constraints on the timing of the origin of bilaterians. Proceedings of the Royal Society B 279, 2369-2376.

Cunningham, J.A., Thomas, C.-W., Bengtson, S., Marone, F., Stampanoni, M., Turner, F.R., Bailey, J.V., Raff, R.A., Raff, E.C., Donoghue, P.C.J. 2012b. Experimental taphonomy of giant sulphur bacteria: implications for the interpretation of the embryo-like Ediacaran Doushantuo fossils. Proceedings of the Royal Society B 279, 1857-1864.

Cunningham, J.A., Vargas, K., Liu, P., Belivanova, V., Marone, F., Martínez-Pérez, C., Guizar-Sicairos, M., Holler, M., Bengtson, S., Donoghue, P.C.J. 2015. Critical appraisal of tubular putative eumetazoans from the Ediacaran Weng'an Doushantuo biota. Proceedings of the Royal Society B 282, 20151169.

Cunningham, J.A., Vargas, K., Marone, F., Bengtson, S., and Donoghue, P.C.J. 2016. A multicellular organism with embedded cell clusters from the Ediacaran Weng'an biota (Doushantuo Formation, South China). Evolution and Development 18, 308-316.

Cunningham, J.A., Vargas, K., Yin, Z., Bengtson, S., Donoghue, P.C.J. 2017b. The Weng'an Biota (Doushantuo Formation): an Ediacaran window on soft-bodied and multicellular microorganisms. Journal of the Geological Society 174, 793-802.

Davies, T. G., Rahman, I. A., Lautenschlager, S., Cunningham, J. A., Asher, R. J., Barrett, P. M., Bates, K. T., Bengtson, S., Benson, R. B. J., Boyer, D. M., Braga, J., Bright, J. A., Claessens, L. P. A. M., Cox, P. G., Dong, X.-P., Evans, A. R., Falkingham, P. L., Friedman, M., Garwood, R. J., Goswami, A., Hutchinson, J. R., Jeffery, N. S., Johanson, Z., Lebrun, R., Martínez-Pérez, C., Marugán-Lobón, J., O'Higgins, P. M., Metscher, B., Orliac, M., Rowe, T. B., Rücklin, M., Sánchez-Villagra, M. R., Shubin, N. H., Smith, S. Y., Starck, J. M., Stringer, C., Summers, A. P., Sutton, M. D., Walsh, S. A., Weisbecker, V., Witmer, L. M., Wroe, S., Yin, Z., Rayfield, E. J. and Donoghue, P. C. J. 2017. Open data and digital morphology. Proceedings of the Royal Society B: Biological Sciences, 284.

Degnan, B.M., Adamska, M., Richards, G.S., Larroux, C., Leininger, S., Bergum, B., Calcino, A., Taylor, K., Nakanishi, N., Degnan, S.M. 2015. 'Porifera' in Wanninger A. (Ed.) Evolutionary Developmental Biology of Invertebrates 1: Introduction, Non-Bilateria, Acoelomorpha, Xenoturbella, Chaetognatha. Springer-Verlag, Wien, pp. 65-106.

Dong, X.-P., Cunningham, J.A., Bengtson, S., Thomas, C.-W., Liu, J., Stampanoni, M., Donoghue, P.C.J. 2013. Embryos, polyps and medusae of the Early Cambrian scyphozoan *Olivooides*. Proceedings of the Royal Society B 280, 20130071.

Dong, X.-P., Vargas, K., Cunningham, J.A., Zhang, H., Liu, T., Chen, F., Liu, J., Bengtson, S., Donoghue, P.C.J. 2016. Developmental biology of the Early Cambrian cnidarian *Olivooides*. Palaeontology 59, 1-21.

Dong, L., Xiao, S., Shen, B., Zhou, C., Li, G., Yao, J. 2009. Basal Cambrian microfossils from the Yangtze Gorges area (South China) and the Aksu area (Tarim block, Northwestern China). Journal of Paleontology 83, 30-44.

Donoghue, P.C.J., Bengtson, S., Dong, X.-P., Gostling, N.J., Huldtgren, T., Cunningham, J.A., Yin, C., Yue, Z., Peng, F., Stampanoni, M. 2006. Synchrotron X-ray tomographic microscopy of fossil embryos. Nature 442, 680-683.

dos Reis, M., Thawornwattana, Y., Angelis, K., Telford, M.J., Donoghue, P.C.J., Yang, Z. 2015. Uncertainty in the timing of origin of animals and the limits of precision in molecular timescales. Current Biology 25, 1-12.

Duan, B., Dong, X.-P., Porras, L., Vargas, K., Cunningham, J.A., Donoghue, P.C.J. 2017. The early Cambrian fossil embryo *Pseudooides* is a direct-developing cnidarian, not an early ecdysozoan. Proceedings of the Royal Society B 284, 20172188.

Dunn, F.S., Liu, A.G., Gehling, J.G. 2019. Anatomical and ontogenetic reassessment of the Ediacaran frond *Arborea arborea* and its placement within total group Eumetazoa. Palaeontology 62 (5), 851-865.

Dunn, F.S., Liu, A.G., Grazhdankin, D.V., Vixseboxse, P., Flannery-Sutherland, J., Green, E., Harris, S., Wilby, P.R., Donoghue, P.C.J. 2021. The developmental biology of *Charnia* and the eumetazoan affinity of the Ediacaran rangeomorphs. Science Advances 7, eabe0291.

Eme, L., Sharpe, S.C., Brown, M.W., Roger, A.J. 2014. On the age of eukaryotes: evaluating evidence from fossils and molecular clocks. Cold Spring Harbour Perspectives in Biology 6 (8), a016139.

Erwin, D.H. 2015. Early metazoan life: divergence, environment and ecology. Philosophical Transactions of the Royal Society B 370, 20150036

Erwin, D.H., Laflamme, M., Tweedt, S.M., Sperling, E.A., Pisani, D., Peterson, K.J. 2011. The Cambrian conundrum: early divergence and later ecological success in the early history of animals. Science 334, 1091-1097.

Gabrielson, P. W., Garbary, D. J., and Scagel, R. F., 1985. The nature of the ancestral red alga: inferences from a cladistic analysis. Biosystems, 18, 335-346.

Gibson, T.M., Shih, P.M., Cumming, V.M., Fischer, W.W., Crockford, P.W., Hodgskiss, M.S.W., Wörndle, S., Creaser, R.A., Rainbird, R.H., Skulski, T.M., Halverson, G.P. 2018. Precise age of *Bangiomorpha pubescens* dates the origin of eukaryotic photosynthesis. Geology 46 (2), 135-138.

Gostling, N.J., Dong, X.-P., Donoghue, P.C.J. 2009. Ontogeny and taphonomy: an experimental taphonomy study of the development of the brine shrimp *Artemia salina*. Palaeontology 52, 169–186.

Gostling, N.J., Thomas, C.-W., Greenwood, J.M., Dong, X., Bengtson, S., Raff, E.C., Raff, R.A., Degnan, B.M., Stampanoni, M., Donoghue, P.C.J. 2008. Deciphering the fossil record of early bilaterian embryonic development in light of experimental taphonomy. Evolution and Development 10, 339-349.

Green, K.J., Viamontes, G.I., Kirk, D.L. 1981. Mechanism of formation, ultrastructure, and function of the cytoplasmic bridge system during morphogenesis in Volvox. Journal of Cell Biology 91, 756-769.

Guiry, M.D. 1990. 'Sporangia and Spores' in Cole, K.M. and Sheath, R.G. (eds.) *Biology of the red algae.* New York: Cambridge University Press, pp. 347.

Hagadorn, J. W., Xiao, S., Donoghue, P. C., Bengtson, S., Gostling, N. J., Pawlowska, M., Raff, E. C., Raff, R. A., Turner, F. R., Chongyu, Y., Zhou, C., Yuan, X., McFeely, M. B., Stampanoni, M., and Nealson, K. H., 2006. Cellular and subcellular structure of Neoproterozoic animal embryos. Science 314, 291-294.

Han, J., Conway Morris, S., Ou, Q., Shu, D., Huang, H. 2017. Meiofaunal deuterostomes from the basal Cambrian of Shaanxi (China). Nature 542, 228-232.

Han, J., Kubota, S., Li, G., Yao, X., Yang, X., Shu, D., Li, Y., Kinoshita, S., Sasaki, O., Komiya, T., Yan, G. 2013 Early Cambrian Pentamerous Cubozoan Embryos from South China. PLoS ONE 8 (8): e70741

Han, J., Kubota, S., Li, G., Ou, Q., Wang, X., Yao, X., Shu, D., Li, Y., Uesugi, K., Hoshino, M., Sasaki, O., Kano, H., Sato, T., Komiya, T. 2016. Divergent evolution of medusozoan symmetric patterns: evidence from the microanatomy of Cambrian tetramerous cubozoans from South China. Gondwana Research 31, 150-163.

Harden, L.K., Morales, K.M., Hughey, J.R. 2016. Identification of a new marine algal species *Pyropia nitida* sp. nov. (Bangiales: Rhodophyta) from Monterey, California. Mitochondrial DNA Part A 27 (4), 3058-3062.

Hoekzema, R.S., Brasier, M.D., Dunn, F.S., Liu, A.G. 2017. Quantitative study of developmental biology confirms *Dickinsonia* as a metazoan. Proceedings of the Royal Society B 284, 20171348.

Hommersand, M.H. and Fredericq, S. 1990. 'Sexual reproduction and cystocarp development' in Cole, K.M. and Sheath, R.G. (eds.) *Biology of the red algae.* New York: Cambridge University Press, pp. 306.

Huldtgren, T., Cunningham, J.A., Yin, C., Stampanoni, M., Marone, F., Donoghue, P.C.J., Bengtson, S. 2011. Fossilized nuclei and germination structures identify Ediacaran "embryos" as encysting protists. Science 334, 1696-1699.

Jensen, S. 2003. The Proterozoic and Earliest Cambrian Trace Fossil Record; Patterns, Problems and Perspectives. Integrative and Comparative Biology 43 (1), 219–228

Jeppsson, L., Anehus, R., Fredholm, D., 1999. The optimal acetate buffered acetic acid technique for extracting phosphatic fossils. Journal of Paleontology 73, 964-972.

Jiang, G., Shi, X., Zhang, S., Wang, Y., Xiao, S. 2011. Stratigraphy and paleogeography of the Ediacaran Doushantuo Formation (ca. 635-551 Ma) in South China. Gondwana Research 19, 831-849.

Kim, B., Kim, M.S. 2014. Three new species of *Polysiphonia sensu lato* (Rhodophyta) based on the morphology and molecular evidence. Algae 29, 183-195.

Landon, E.N.U., Liu, P., Yin, Z., Sun, W., Shang, X., Donoghue, P.C.J. 2019. Cellular preservation of excysting developmental stages of new eukaryotes from the early Ediacaran Weng'an Biota. Palaeoworld 28, 461-468.

Le Gall, L., Saunders, G. W. 2007. A nuclear phylogeny of the Florideophyceae (Rhodophyta) inferred from combined EF2, small subunit and large subunit ribosomal DNA: Establishing the

new red algal subclass Corallinophycidae. Molecular Phylogenetics and Evolution 43, 1118–1130.

Li, C.-W., Chen, J.-Y., Hua, T.-E. 1998. Precambrian sponges with cellular structures. Science 279, 879-882.

Li, G., Xue, Y., Zhou, C. 1997. Late Proterozoic tubular fossils from the Doushantuo Formation of Weng'an, Guizhou, China. Palaeoworld 7, 29-37.

Li, Y. 1986. Proterozoic and Cambrian phosphorites – regional review: China. In Phosphate Deposits of the World: Volume 1 (Eds. Cook, P., and Shergold, J.), Cambridge University Press, Cambridge, pp. 42-62.

Li, Z. 1984. The discovery and its significance of small shelly fossils in Hexi area, Xixiang, Shaanxi. Geology of Shaanxi 2, 73–77.

Liu, P., Xiao, S., Yin, C., Zhou, C., Gao, L., Tang, F. 2008. Systematic description and phylogenetic affinity of tubular microfossils from the Ediacaran Doushantuo Formation at Weng'an, South China. Palaeontology 51, 339-366.

Liu, Y., Shao, T., Zhang, H., Wang, Q., Zhang, Y., Chen, C., Liang, Y., Xue, J. 2017. A new scyphozoan from the Cambrian Fortunian Stage of South China. Palaeontology 60 (4), 511-518.

Liu, Y., Xiao, S., Shao, T., Broce, J., Zhang, H. 2014. The oldest priapulid-like scalidophoran animal and its implications for the early evolution of cycloneuralians and ecdysozoans. Evolution and Development 16, 155-165.

Love, G.D., Grosjean, E., Stalvies, C., Fike, D.A., Grotzinger, J.P., Bradley, A.S., Kelly, A.E., Bhatia, M., Meredith, W., Snape, C.E., Bowring, S.A., Condon, D.J., Summons, R.E. 2009. Fossil steroids record the appearance of Demospongiae during the Cryogenian period. Nature 457, 718-721.

Lücking, R., and Nelsen, M.P. 2018. 'Ediacarans, Protolichens and Lichen-Derived *Penicillium*: A Critical Reassessment of the Evolution of Lichenization in Fungi' in Krings, M. Harper, C.J., Cúneo, N.R., Rothwell, G.W. (Eds.) Transformative Paleobotany, Academic Press, pp. 551-590.

Maddison, W.P., and Maddison, D.R. 2019. Mesquite: a modular system for evolutionary analysis. Version 3.61 http://www.mesquiteproject.org

Maggs, C. A., and Callow, M. E. 2003. 'Algal spores' in Encyclopedia of Life Sciences, Nature Publishing Group, pp. 1–6.

Margaritondo, G., 2002. Elements of synchrotron light for biology, chemistry, and medical research, New York, Oxford University Press, pp. 260.

Marone, F., Münch, B., Stampanoni, M., 2010. Fast reconstruction algorithm dealing with tomography artifacts. Proceedings of SPIE 7804, 780410

Marone, F., Studer, A., Billich, H., Sala, L., and Stampanoni, M., 2017. Towards on-the-fly data post-processing for real-time tomographic imaging at TOMCAT. Advanced Structural and Chemical Imaging 3, 1.

Mendoza, L., Taylor, J.W., Ajello, L. 2002. The class Mesomycetozoa: a heterogeneous group of microorganisms at the animal-fungal boundary. Annual Review of Microbiology 56, 315-344.

Müller, K.J. 1985. Exceptional preservation in calcereous nodules. Philosophical Transactions of the Royal Society of London B 311, 67-73.

Muscente, A.D., Hawkins, A.D., Xiao, S. 2015. Fossil preservation through phosphatization and silicification in the Ediacaran Doushantuo Formation (South China): A comparative synthesis. Palaeogeography, Palaeoclimatology, Palaeoecology 434, 46-62.

Nettersheim, B.J., Brocks, J.J., Schwelm, A., Hope, J.M., Not, F., Lomas, M., Schmidt, C., Schiebel, R., Nowack, E.C.M., De Deckker, P., Pawlowski, J., Bowser, S.S., Bobrovskiy, I., Zonneveld, K., Kucera, M., Stuhr, M., Hallmann, C. 2019. Putative sponge biomarkers in unicellular Rhizaria question an early rise of animals. Nature Ecology and Evolution 3, 577-581.

Pang, K., Tang, Q., Schiffbauer, J.D., Yao, J., Yuan, X.L., Wan, B., Chen, L., Ou, Z.J., Xiao, S.H. 2013. The nature and origin of nucleus-like intracellular inclusions in Paleoproterozoic eukaryote microfossils. Geobiology 11, 499-510.

Parfrey, L.W., Lahr, D.J.G., Knoll, A.H., Katz, L.A. 2011. Estimating the timing of early eukaryotic diversification with multigene molecular clocks. Proceedings of the National Academy of Sciences USA 108, p. 13624-13629.

Porter, S. 2020. Insights into eukaryogenesis from the fossil record. Interface Focus 10, 20190105.

Porter, S., Meisterfeld, R., Knoll, A.H. 2003. Vase-shaped microfossils from the Neoproterozoic Chuar Group, Grand Canyon: A classification guided by modern testate amoebae. Journal of Paleontology 77 (3), 409-429.

Pueschel, C.M., Cole, K.M. 1982. Rhodophycean pit plugs: an ultrastructural survey with taxonomic implications. American Journal of Botany 69, 703-720.

Qian, Y. 1977. Hyolitha and some problematica from the Lower Cambrian Meischucunian stage in central and southwestern China. Acta Palaeontologica Sinica 16, 255–275.

Raff, E.C., Andrews, M.E., Turner, F.R., Toh, E., Nelson, D.E., Raff, R.A. 2013. Contingent interactions among biofilm-forming bacteria determine preservation or decay in the first steps toward fossilization of marine embryos. Evolution and Development 15, 243-256.

Raff, E.C., Schollaert, K.L., Nelson, D.E., Donoghue, P.C.J., Thomas, C.-W., Turner, F.R., Stein, B.D., Dong, X., Bengtson, S., Huldtgren, T., Stampanoni, M., Yin, C., Raff, R.A. 2008. Embryo fossilization is a biological process mediated by microbial films. Proceedings of the National Academy of Sciences USA 105, 19360-19365.

Raff, E.C., Villinski, J.T., Turner, F.R., Donoghue, P.C.J., Raff, R.A. 2006. Experimental taphonomy shows the feasibility of fossil embryos. Proceedings of the National Academy of Science USA 103, 5846-5851.

Raff, R.A., Andrews, M.E., Pearson, R.L., Turner, F.R., Saur, S.T., Thomas, D.C., Eagan, J.L., Raff, E.C. 2014. Microbial ecology and biofilms in the taphonomy of soft tissues. Palaios 29, 560-569.

Rensing, S.A. 2016. (Why) Does evolution favour embryogenesis? Trends in Plant Science 21 (7), 562-573.

Saunders, G.W., Hommersand, M.H. 2004. Assessing red algal supraordinal diversity and taxonomy in the context of contemporary systematic data. American Journal of Botany 91, 1494-1507.

Schaap, P. 2012. Evolutionary crossroads in developmental biology: *Dictyostelium discoideum.* Development 138, 387-396.

Schiffbauer, J. D., Xiao, S. H., Sen Sharma, K., and Wang, G., 2012. The origin of intracellular structures in Ediacaran metazoan embryos. Geology 40 (3), 223-226.

Shao, T., Liu, Y., Duan, B., Zhang, H., Zhang, H., Wang, Q., Zhang, Y., Qin, J. 2018. The Fortunian (lowermost Cambrian) *Qinscyphus necopinus* (Cnidaria, Scyphozoa, Coronatae) underwent direct development. Neues Jahrbuch für Geologie und Paläontologie - Abhandlungen 289 (2), 149-159.

Sharpe, S.C., Eme, L., Brown, M.W., Roger, A.J. 2015. 'Timing the Origins of Multicellular Eukaryotes Through Phylogenomics and Relaxed Molecular Clock Analyses' in Ruiz-Trillo, I., Nedelcu, A.M. (eds) Evolutionary Transitions to Multicellular Life, Advances in Marine Genomics, vol 2. Springer, Dordrecht, pp. 3-29.

Sherwood, A.R., Sheath, R.G. 2000. Microscopic analysis and seasonality of gemma reproduction in the freshwater red alga *Hildenbrandia angolensis* (Hildenbrandiales, Rhodophyta). Phycological Research 48, 241-249.

Steiner, M., Qian, Y., Li, G., Hagadorn, J.W., Zhu, M. 2014. The developmental cycles of early Cambrian Olivooidae fam. nov. (?Cycloneuralia) from the Yangtze Platform (China). Palaeogeography, Palaeoclimatology, Palaeoecology 398, 97-124.

Steiner, M., Li, G., Qian, Y., Zhu, M. 2004a. Lower Cambrian Small Shelly Fossils of northern Sichuan and southern Shaanxi (China), and their biostratigraphic importance. Geobios 37, 259-275.

Steiner, M., Zhu, M., Li, G., Qian, Y., Erdtmann, B.-D. 2004b. New Early Cambrian bilaterian embryos and larvae from China. Geology 32 (10), 833-836.

Sun, W., Yin, Z., Cunningham, J.A., Liu, P., Zhu, M., Donoghue, P.C.J. 2020. Nucleus preservation in early Ediacaran Weng'an embryo-like fossils, experimental taphonomy of nuclei and implications for reading the eukaryote fossil record. Interface Focus 10, 20200015.

Sun, W.-C., Yin, Z.-J., Donoghue, P.C.J., Liu, P.-J., Shang, X.-D. and Zhu, M.-Y. 2019. Tubular microfossils from the Ediacaran Weng'an Biota (Doushantuo Formation, South China) are not early animals. Palaeoworld 28, 469-477.

Tsekos, I. 1982. Tumour-like growths induced by bacteria in the thallus of a red alga, *Gigartina teedii* (Roth) Lamour. Annals of Botany 49, 123-126.

Wang, F., Zhang, X., Guo, R. 1983. The Sinian microfossils from Jinning, Yunnan, south west China. Precambrian Research 23, 133-175.

Wang, X., Han, J., Vannier, J., Ou, Q., Yang, X., Uesugi, K., Sasaki, O., Komiya, T. 2017. Anatomy and affinities of a new 535-million-year-old medusozoan from the Kuanchuanpu Formation, South China. Palaeontology 60 (6), 853-867.

Wang, X., Vannier, J., Yang, X., Kubota, S., Ou, Q., Yao, X., Uesugi, K., Sasaki, O., Komiya, T., Han, J. 2020. An intermediate type of medusa from the Early Cambrian Kuanchuanpu Formation South China. Palaeontology 63 (5), 775-789.

Weatherbee, R. 1980. Postfertilization development in the red alga *Polysiphonia.* Journal of Ultrastructure Research 70, 259-274.

West, J.A. and Hommersand, M.H. 1981. 'Rhodophyta: life histories' in Lobban, C.S. and Wynne, M.J. (eds.) *The biology of seaweeds.* Berkeley: University of California Press, pp. 137-141.

Xian, X.-F., Zhang, H.-Q., Liu, Y.-H., Zhang, Y.-N. 2019. Diverse radial symmetry among the Cambrian Fortunian fossil embryos from northern Sichuan and southern Shaanxi provinces, South China. Palaeoworld 28, 225-233.

Xiao, S.H., Hagadorn, J.W., Zhou, C.M., Yuan, X.L. 2007. Rare helical spheroidal fossils from the Doushantuo Lagerstatte: Ediacaran animal embryos come of age? Geology 35 (2), 115-118.

Xiao, S., and Knoll, A.H. 1999. Fossil preservation in the Neoproterozoic Doushantuo phosphorite Lagerstätte, South China. Lethaia 32, 219-240.

Xiao, S., and Knoll, A.H. 2000. Phosphatized animal embryos from the Neoproterozoic Doushantuo Formation at Weng'an, Guizhou, South China. Journal of Paleontology 74, 767-788.

Xiao, S.H., Knoll, A.H., Schiffbauer, J.D., Zhou, C.M., Yuan, X.L. 2012. Comment on "Fossilized nuclei and germination structures identify Ediacaran 'animal embryos' as encysting protists". Science 335, 1169-c.

Xiao, S., Knoll, A.H., Yuan, X., Pueschel, C.M. 2004. Phosphatized multicellular algae in the Neoproterozoic Doushantuo Formation, China, and the early evolution of florideophyte red algae. American Journal of Botany 91, 214-227.

Xiao, S., Muscente, A.D., Chen, L., Zhou, C., Schiffbauer, J.D., Wood, A.D., Polys, N.F., Yuan, X. 2014a. The Weng'an biota and the Ediacaran radiation of multicellular eukaryotes. National Science Review 1, 498-520.

Xiao, S., Yuan, X., Knoll, A.H. 2000. Eumetazoan fossils in terminal Proterozoic phosphorites? PNAS 97, 13684-13689.

Xiao, S., Yuan, X., Steiner, M., Knoll, A.H. 2002. Macroscopic carbonaceous compressions in a terminal Proterozoic shale: a systematic reassessment of the Miaohe Biota, South China. Journal of Paleontology 76, 347-376.

Xiao, S., Zhang, Y., and Knoll, A.H. 1998. Three-dimensional preservation of algae and animal embryos in a Neoproterozoic phosphorite. Nature 391, 553-558.

Xiao, S., Zhou, C., Liu, P., Wang, D., Yuan, X. 2014b. Phosphatized Acanthomorphic Acritarchs and Related Microfossils from the Ediacaran Doushantuo Formation at Weng'an (South China) and their Implications for Biostratigraphic Correlation. Journal of Paleontology 88 (1), 1–67.

Xing, Y., Ding, Q., Luo, H., He, T.,Wang, Y. 1984. The Sinian–Cambrian boundary of China. Bulletin of the Institute of Geology, Chinese Academy of Geological Sciences 10, 1-262.

Xue, Y., Zhou, C., Tang, T. 1999. "Animal embryos" a misinterpretation of Neoproterozoic microfossils, Acta Micropalaeontologica Sinica 16, 1-4.

Yang, E.C., Boo, S.M., Bhattacharya, D., Saunders, G.W., Knoll, A.H., Fredericq, S., Graf, L., Yoon, H.S. 2016. Divergence time estimates and the evolution of major lineages in the florideophyte red algae. Scientific Reports 6, 21361.

Yin, C., Bengtson, S., Yue, Z. 2004. Silicified and phosphatized *Tianzhushania*, spheroidal

microfossils of possible animal origin from the Neoproterozoic of South China. Acta

Palaeontologica Polonica 49, 1–12.

Yin, C., Gao, L., Yue, Z. 2003. New advances in the study of the Sinian Doushantuo acritarch

genus *Tianzhushania*. Geological Bulletin of China 22, 87–94.

Yin, L., Li, Z. 1978. Precambrian microfloras of southwest China with reference to their

stratigraphic significance. Memoir Nanjing Institute of Geology and Palaeontology, Academia

Sinica 10, 41-108.

Yin, L., Zhu, M., Knoll, A.H., Yuan, X., Zhang, J., Hu, J. 2007. Doushantuo embryos preserved

inside diapause egg cysts. Nature 446, 661-663.

Yin, Z., Cunningham, J.A., Vargas, K., Bengtson, S., Zhu, M., Donoghue, P.C.J. 2017. Nuclei

and nucleoli in embryo-like fossils from the Ediacaran Weng'an Biota. Precambrian Research

301, 145-151.

Yin, Z.J., Liu, P.J., Li, G., Tafforeau, P., Zhu, M.Y. 2014. Biological and taphonomic implications

of Ediacaran fossil embryos undergoing cytokinesis. Gondwana Research 25, 1019-1026.

Yin, Z., Sun, W., Liu, P., Zhu, M., Donoghue, P.C.J. 2020. Developmental biology of

Helicoforamina reveals holozoan affinity, cryptic diversity, and adaptation to heterogeneous

environments in the early Ediacaran Weng'an biota (Doushantuo Formation, South China). Science Advances 6 (24), eabb0083.

Yin, Z., Vargas, K., Cunningham, J.A., Bengtson, S., Zhu, M., Marone, F., Donoghue, P.C.J. 2019. The early Ediacaran *Caveasphaera* foreshadows the evolutionary origin of animal-like embryology. Current Biology 29 (24), 4307–4314.e2.

Yin, Z., Zhao, D., Pan, B., Zhao, F., Zeng, H. Li, G., Bottjer, D.J., Zhu, M. 2018. Early Cambrian animal diapause embryos revealed by X-ray tomography. Geology 46, 387-390.

Yin, Z.J., Zhu, M.Y., Bottjer, D.J., Zhao, F.C., Tafforeau, P. 2016. Meroblastic cleavage identifies some Ediacaran Doushantuo (China) embryo-like fossils as metazoans. Geology 44, 735-738.

Yin, Z., Zhu, M., Davidson, E.H., Bottjer, D.J., Zhao, F., Tafforeau, P. 2015. Sponge grade body fossil with cellular resolution dating 60 Myr before the Cambrian. Proceedings of the National Academy of Sciences USA 112, E1453-E1460.

Yin, Z., Zhu, M., Tafforeau, P., Chen, J., Liu, P., Li, G. 2013. Early embryogenesis of potential bilaterian animals with polar lobe formation from the Ediacaran Weng'an Biota, South China. Precambrian Research 225, 44-57.

Yoon, H.S., Hackett, J.D., Ciniglia, C., Pinto, G., Bhattacharya, D. 2004. A molecular timeline for the origin of photosynthetic eukaryotes. Molecular Biology and Evolution 21 (5), 809-818.

Yoon, H., Muller, K.M., Sheath, R.G., Ott, F.D., Bhattacharya, D. 2006. Defining the major lineages of red algae (Rhodophyta). Journal of Phycology 42, 482–492.

Yoon, H.S., Zuccarello, G.C., Bhattacharya, D. 2010. 'Evolutionary history and taxonomy of red algae' in Seckbach, J., Chapman, D.J. (eds) Red algae in the genomic age. Springer, Dordrecht, pp. 25–42

Yuan, X., Li, J., Cao, R. 1999. A diverse metaphyte assemblage from the Neoproterozoic black shales of South China. Lethaia 32, 143-155.

Yuan, X., Xiao, S., Taylor, T.N. 2005. Lichen-like symbiosis 600 million years ago. Science 308, 1017-1020.

Yue, Z., and Bengtson, S. 1999. Embryonic and post-embryonic development of the Early Cambrian cnidarian Olivooides. Lethaia 32, 181–195.

Zhang, H., Xiao, S., Liu, Y., Yuan, X., Wan, B., Muscente, A.D., Shao, T., Gong, H., Cao, G. 2015. Armored kinorhynch-like scalidophoran animals from the early Cambrian. Scientific Reports 5, 16521.

Zhang, X.G., Pratt, B.R. 2014. Possible algal origin and life cycle of Ediacaran Doushantuo microfossils with dextral spiral structure. Journal of Paleontology 88, 92-98.

Zhang, Y. 1989. Multicellular thallophytes with differentiated tissues from Late Proterozoic phosphate rocks of South China. Lethaia 22 (2), 113-132.

Zhang, Y. and Yuan, X. 1992. New data on multicellular thallophytes and fragments of cellular tissues from Late Proterozoic phosphate rocks, South China. Lethaia 26, 1-18.

Zhang, Y. and Yuan, X. 1996. Sexual reproductive structures of Latest Proterozoic multicellular rhodophytes (red algae) from South China. Science in China Series C – Life Sciences 39, 28-36.

Zhang, Y., Yin, L., Xiao, S., Knoll, A.H. 1998.
Permineralized Fossils from the Terminal Proterozoic Doushantuo Formation,
South China. Memoir (The Paleontological Society), Vol. 50, Supplement to Vol.
72, no. 4 of the Journal of Paleontology, pp. 1-52.

Zhang, Z. 1985. Coccoid microfossils from the Doushantuo Formation (Late Sinian) of South China. Precambrian Research 28, 163-173.

Zhao, D. 1986. The discovery of phosphatic red algae in the Sinian Doushantuo Formation. Acta Sedimentologica Sinica 4, 126–127.

Zhou, C., Li, X., Xiao, S., Lan, Z., Ouyang, Q., Guan, C., Chen, Z. 2017. A new SIMS zircon U–Pb date from the Ediacaran Doushantuo Formation: age constraint on the Weng'an biota. Geological Magazine 154, 1193-1201.

Zhu, R.-X., Li, X.-H., Hou, X.-G., Pan, Y.-X., Wang, F., Deng, C.-L., He, H.-Y. 2009. SIMS U-Pb zircon age of a tuff layer in the Meishucun section, Yunnan, southwest China: constraint on the age of the Precambrian-Cambrian boundary. Science in China Series D: Earth Sciences 52 (9), 1385-1392.

Zhu, S. and Wang, Y. 1984. Phosphatic stromatolites and microfossils from the Doushantuo age in the central Guizhou. In: Wang, Y., Yin, G. and Zheng, S. et al. (eds). The Upper Precambrian and Sinian-Cambrian Boundary in Guizhou. Guiyang: The People's Publishing House of Guizhou, 1984, 93–105.

Zhu, S., Wang, Y. and Zhang, L. 1984. Formation of the Kaiyang phosphorites in China as relates to ancient microorganisms. In: Symposium of 5th International Field Workshop and Seminar on Phosphorite. Beijing: Geological Publishing House, pp. 165–93.

Zimorski, V., Ku, C., Martin, W.F., Gould, S.B. 2014. Endosymbiotic theory for organelle origins. Current Opinion in Microbiology 22, 38-48.